Rapid #: -19150648

CROSS REF ID: **872517**

LENDER: **LHL4CRLRM :: Main Library**

BORROWER: **ORU :: Main Library**

TYPE:	Article CC:CCL
JOURNAL TITLE:	Journal of petrology
USER JOURNAL TITLE:	Journal of petrology.
ARTICLE TITLE:	Internally-Consistent Thermodynamic data for minerals in the system Na2O-K2O-CaO-MgO-FeO-Fe2O3-Al2O3-SiO2-TiO2-H2O-CO2
ARTICLE AUTHOR:	Berman, R. G.
VOLUME:	29
ISSUE:	
MONTH:	
YEAR:	1988
PAGES:	445-522
ISSN:	0022-3530
OCLC #:	1782966

Processed by RapidX: 6/8/2022 12:54:16 PM

Internally-Consistent Thermodynamic Data for Minerals in the System Na_2O–K_2O–CaO–MgO–FeO–Fe_2O_3–Al_2O_3–SiO_2–TiO_2–H_2O–CO_2

by R. G. BERMAN*

Department of Geological Sciences, University of British Columbia, Vancouver, B. C. Canada V6T 2B4

(*Received 16 March 1987; revised typescript accepted 7 October 1987*)

ABSTRACT

Internally consistent standard state thermodynamic data are presented for 67 minerals in the system Na_2O–K_2O–CaO–MgO–FeO–Fe_2O_3–Al_2O_3–SiO_2–TiO_2–H_2O–CO_2. The method of mathematical programming was used to achieve consistency of derived properties with phase equilibrium, calorimetric, and volumetric data, utilizing equations that account for the thermodynamic consequences of first and second order phase transitions, and temperature-dependent disorder. Tabulated properties are in good agreement with thermophysical data, as well as being consistent with the bulk of phase equilibrium data obtained in solubility studies, weight change experiments, and reversals involving both single and mixed volatile species. The reliability of the thermodynamic data set is documented by extensive comparisons (Figs. 4–45) between computed equilibria and phase equilibrium data. The high degree of consistency obtained with these diverse experimental data gives confidence that the refined thermodynamic properties should allow accurate prediction of phase relationships among stoichiometric minerals in complex chemical systems, and provide a reasonable basis from which activity models for minerals may be derived.

INTRODUCTION

Thermodynamics provides a fundamental tool for gaining insight into and quantifying diverse processes which span most geologic disciplines. One of the most important applications of thermodynamics is the prediction of stable phase relationships, and software is now available for quick and accurate calculation of stable phase relationships of any complexity among phases of geologic interest (e.g., Ghiorso *et al.*, 1983; Perkins *et al.*, 1986; Berman *et al.*, 1987). The only limitation on the accuracy of calculated phase relationships is that imposed by our knowledge of the thermodynamic parameters describing the state functions of each phase, component, or species in the databases utilized by these software.

Over the past several decades, considerable effort has been directed towards formulating thermodynamic databases, starting with compilations which drew heavily upon calorimetric data (e.g., Kelley, 1960; Kelley & King, 1961; Robie *et al.*, 1979). More recent efforts have made use of phase equilibrium data to verify and refine these calorimetric data, an important step in the light of conclusions that enthalpies of formation have not in general been determined calorimetrically with the accuracy necessary to reproduce phase equilibrium data (Helgeson *et al.*, 1978; Berman *et al.*, 1985). The most extensive compilation of

*Present address: Geological Survey of Canada, 588 Broth St., Ottawa, Ontario, Canada K2P ϕE4

refined thermodynamic data remains that of Helgeson *et al.* (1978), who presented standard state properties for some 70 common rock-forming minerals, including many that exhibit considerable non-stoichiometry and complications due, for example, to temperature-dependent disordering. Since completion of this pioneering work, many additional experimental data have been gathered, but recent studies (e.g., Robinson *et al.*, 1982; Halbach & Chatterjee, 1984; Holland & Powell, 1985; Berman *et al.*, 1986) have focussed on stoichiometric minerals in smaller chemical subsystems, and can be viewed primarily as efforts to explore the results of using different mathematical techniques for extracting thermodynamic parameters from diverse sets of experimental observations (see below).

In this paper internally consistent thermodynamic data are presented for 67 minerals (Table 1) in the system Na_2O–K_2O–CaO–MgO–FeO–Fe_2O_3–Al_2O_3–SiO_2–TiO_2–H_2O–CO_2. This database has been derived through consideration of the most recent experimental data, using equations that take into account important effects such as temperature-dependent disordering and lambda transitions, without which it is impossible to reproduce the experimental data faithfully, or to apply them confidently to geological problems. For the most part, this work considers minerals that are stoichiometric in restricted portions of this chemical system. Solid solution effects have been evaluated only when sufficient data are available to allow reasonable confidence in derived activity models *and* when treatment of such data allows access to experimental data which contribute to significant refinement in the thermodynamic properties of other phases in the database (e.g., hydrous cordierite and aluminous enstatite). By refining thermodynamic parameters with experimental data involving stoichiometric phases, analysis of solution properties and more complex experimental data is avoided and greater accuracy is achieved in derived standard state properties. Although it is anticipated that some adjustments may be necessary, particularly in enthalpies of formation that are used as reference values (see discussion of reference values below), these standard state properties can then be used as a starting point to constrain activity models for the same minerals in chemically more complex systems.

The main purpose of this paper is to document fully the results of this thermodynamic analysis, showing which experimental data are reproduced well, which are not, and discussing sources of discrepancies. This detailed documentation is important not only to help define a reliable set of experimental data, but also because it offers the only means to assess the overall accuracy of derived thermodynamic parameters. The underlying premise of this work is that it is only possible to evaluate the validity of thermodynamic properties by comparison with all available data, because subsets of preferred experimental data are never sufficiently precise to define fully all thermodynamic parameters. This conclusion stems from the nature of phase equilibrium data which bracket the position of, but do not indicate the exact location of an equilibrium (see discussion of phase equilibrium data below).

THERMODYNAMIC RELATIONS

At a pressure P (b) and temperature T (K), the apparent free energy of formation of a pure phase from the elements*, $\Delta_a G^{P,T}$, is defined by

$$\Delta_a G^{P,T} = \Delta_a H^{P,T} - T \cdot S^{P,T} \quad (1)$$

* In this paper, the IUPAC recommendation (Cox, 1979) is followed whereby a subscript modifying the Δ is used to denote a specific process. For simplicity, the convention of denoting standard state thermodynamic properties with a $^\circ$ has not been adopted because this paper deals in entirety with standard state properties.

where

$$\Delta_a H^{P,T} = \Delta_f H^{P_r,T_r} + \int_{T_r}^{T} Cp\,dT + \int_{P_r}^{P} \left\{ V^{P_r,T_r} - T\left(\frac{\partial V}{\partial T}\right)_P \right\} dP \quad (2)$$

and

$$S^{P,T} = S^{P_r,T_r} + \int_{T_r}^{T} \left(\frac{Cp}{T}\right) dT - \int_{P_r}^{P} \left(\frac{\partial V}{\partial T}\right)_P dP. \quad (3)$$

$\Delta_a H^{P,T}$ is the apparent enthalpy of formation of the pure phase from the elements at P and T, $\Delta_f H^{P_r,T_r}$, S^{P_r,T_r}, and V^{P_r,T_r} are the enthalpy of formation from the elements, third law entropy, and molar volume, respectively, at the reference pressure ($P_r = 1$ b $= 10^5$ Pa) and temperature ($T_r = 298{\cdot}15$ K), and Cp is the heat capacity at constant pressure. Note that in eqns (1–3) the properties of the elements are used only to define the standard state enthalpy of formation $\Delta_f H^{P_r,T_r}$. In this regard, the apparent free energy function expressed through eqns (1–3) differs from that defined by Benson (1968) and used by Helgeson *et al.* (1978) which incorporates the entropies of the elements at 298·15 K and 1 b.

Heat capacity of minerals that do not undergo lambda transitions is parameterized with the function (Berman & Brown, 1985)

$$Cp = k_0 + k_1 T^{-0.5} + k_2 T^{-2} + k_3 T^{-3} \quad (4)$$

where k_1 and k_2 are constrained to be less than or equal to zero. These constraints ensure that no inflections occur in the $Cp(T)$ function above 298·15 K, and it has been demonstrated (Berman & Brown, 1985) that the heat capacity of minerals can be reliably extrapolated to higher temperatures than available calorimetric data. This latter point is extremely important in that many important rock-forming minerals have stabilities far in excess of the temperatures of present calorimetric measurements. Because the k_3 term can be positive, inflections can occur at temperatures below the lowest temperature data point used in deriving the thermal functions (usually 250 K), and caution should be exercised not to use the Cp functions below these temperatures (Table 3).

In a previous study (Berman *et al.*, 1985) it was found that adequate representation of phase equilibrium data was possible using the assumption that mineral volumes are independent of pressure and temperature. In spite of the fact that the requisite data are incomplete with respect to many important minerals, this simplication has not been made in this work because expansivity and compressibility terms make significant contributions to low entropy (notably solid–solid) reactions and to reactions in which the reactant and product mineral assemblages have highly contrasting volumetric properties (e.g., muscovite dehydration equilibria). The pressure and temperature dependence of mineral volumes is represented with the following equation:

$$\frac{V^{P,T}}{V^{P_r,T_r}} = 1 + v_1(P - P_r) + v_2(P - P_r)^2 + v_3(T - T_r) + v_4(T - T_r)^2. \quad (5)$$

This equation was chosen over alternate representations for two reasons. First, it is linear in the fit parameters v_1–v_4, a feature which greatly simplifies the refinement process of these terms (see below). Second, use of a more complex equation that allows accurate extrapolations to high pressures is unwarranted because the emphasis in this paper is on deriving standard state thermodynamic properties for minerals from phase equilibrium data that for the most part are restricted to pressures less than 10 kb. Although the parameterization of eqn (5) gives smooth extrapolations to high pressure and temperature, this equation has no

theoretical basis and caution should therefore be exercised in using it at conditions beyond those of the volumetric data listed in Table 4 or the phase equilibrium data shown in Figs. 4–45.

Substitution of eqns (2–5) into (1), and rearrangement, yields:

$$\begin{aligned}\Delta_a G^{P,T} = \Delta_f H^{P_r,T_r} - TS^{P_r,T_r} + k_0\{(T-T_r) - T(\ln T - \ln T_r)\} \\ + 2k_1\{(T^{0.5} - T_r^{0.5}) + T(T^{-0.5} - T_r^{-0.5})\} \\ - k_2\{(T^{-1} - T_r^{-1}) - T/2(T^{-2} - T_r^{-2})\} \\ - k_3\{(T^{-2} - T_r^{-2})/2 - T/3(T^{-3} - T_r^{-3})\} \\ + V^{P_r,T_r}[(v_1/2 - v_2)(P^2 - P_r^2) + v_2/3(P^3 - P_r^3) \\ + \{1 - v_1 + v_2 + v_3(T-T_r) + v_4(T-T_r)^2\}(P-P_r)]. \end{aligned} \quad (6)$$

For gases, the explicit volume integrations in eqn (6) are replaced by:

$$\int_{P_r}^{P} V_{gas}\, dP = G^{P,T} - G^{P_r,T} \quad (7)$$

where the right hand side of eqn (7) has been evaluated using the equations of state of Haar *et al.* (1984) for H_2O below 10 kb, Delany & Helgeson (1978) for H_2O above 10 kb, and Kerrick & Jacobs (1981) for CO_2.

Polymorphic transitions

For accurate representation of the thermodynamic properties of minerals it is necessary to account for the consequences of both first- and second-order (lambda) polymorphic transitions, although in practice the exact nature of a phase transition may be ambiguous. Treatment of the former is the easier task because the temperature dependence of thermodynamic properties is quite similar above and below the transition temperature. Heat content measurements spanning the transition are sufficient to define the enthalpy of transition, $\Delta_t H$, and because the change in Gibbs free energy of the reaction $\Delta_r G = 0$ at the transition temperature (T_t), these data also define the entropy of transition, $\Delta_t S (\Delta_t S = \Delta_t H / T_t)$. Volumetric data are needed to define the volume of transition $\Delta_t V$, as well as changes in expansivity and compressibility. The internal consistency of these various data may be assessed (and refined) with use of the Clapeyron equation, $(dP/dT)_{\Delta_r G = 0} = (\Delta_r S / \Delta_r V)$, if the P–T slope of the transition is known.

Treatment of lambda transitions is more complicated because of the marked difference in the temperature dependence of thermodynamic properties above and below the lambda point (T_λ). In this paper, lambda transitions are modelled with the function proposed by Berman & Brown (1985), wherein heat capacity is separated into two components: a 'lattice' heat capacity that is represented by the same $k_0 - k_3$ coefficients (eqn 4) for both polymorphs, and a 'lambda' component (Cp_λ) that, for $T_{ref} < T < T_\lambda$ is computed at 1 b pressure by:

$$Cp_\lambda^{1\,bar} = T(l_1 + l_2 T)^2. \quad (8)$$

The parameters l_1, l_2, T_{ref} (usually 298·15 K), and T_λ are defined by Cp or heat content data at 1 b, and for the most part have been taken from Berman & Brown (1985). Equation (8) allows reasonable representation of calorimetric data usually to within about 30° of the lambda point. The simple form of the equation does not allow more accurate representation

closer to the lambda point, nor does it account for the decrease in Cp (relative to the 'lattice' Cp) commonly observed just above the lambda point.

Heat capacity measurements at elevated pressure are not presently available, necessitating an assumption regarding the pressure dependence of Cp_λ. Here it is assumed that the magnitude of Cp_λ is independent of P, and that the position of onset and width of the lambda transition remains fixed in relation to the lambda point at all pressures (Fig. 1b and c). Most phase equilibrium data are broadly consistent with modelling polymorphic transitions as straight lines in P–T, such that:

$$T_\lambda^P = T_\lambda^{1\,\mathrm{bar}} + k(P-1). \tag{9}$$

By defining $T_\mathrm{d} = T_\lambda^{1\,\mathrm{bar}} - T_\lambda^P$, and $T' = T + T_\mathrm{d}$, $C_{P\lambda}^P$ is computed at any pressure for $T_\mathrm{ref} < T' < T_\lambda^{1\,\mathrm{bar}}$ by:

$$Cp_\lambda^P = T'(l_1 + l_2 T')^2. \tag{8a}$$

In order to calculate the effect of the lambda transition on other thermodynamic variables, Cp_λ^P is integrated between a reference temperature defined by $t_\mathrm{r} = T_\mathrm{ref} - T_\mathrm{d}$ and $T(T \leqslant T_\lambda^P)$, giving:

$$\Delta_\lambda H^{P,T} = \int_{t_\mathrm{r}}^{T} Cp_\lambda \mathrm{d}T = x_1(T - t_\mathrm{r}) + \frac{x_2}{2}(T^2 - t_\mathrm{r}^2) + \frac{x_3}{3}(T^3 - t_\mathrm{r}^3) + \frac{x_4}{4}(T^4 - t_\mathrm{r}^4) \tag{10}$$

$$\Delta_\lambda S^{P,T} = \int_{t_\mathrm{r}}^{T} (Cp_\lambda / T)\,\mathrm{d}T = x_1(\ln T - \ln t_\mathrm{r}) + x_2(T - t_\mathrm{r}) + \frac{x_3}{2}(T^2 - t_\mathrm{r}^2) + \frac{x_4}{3}(T^3 - t_\mathrm{r}^3) \tag{11}$$

where

$$x_1 = l_1^2 T_\mathrm{d} + 2l_1 l_2 T_\mathrm{d}^2 + l_2^2 T_\mathrm{d}^3$$

$$x_2 = l_1^2 + 4l_1 l_2 T_\mathrm{d} + 3l_2^2 T_\mathrm{d}^2$$

$$x_3 = 2l_1 l_2 + 3l_2^2 T_\mathrm{d}$$

$$x_4 = l_2^2.$$

By performing the integrations in this manner, $\Delta_\lambda H$ remains constant at the lambda point at all pressures, while $\Delta_\lambda S$ decreases with increasing pressure if $k > 0$ (Fig. 2). Note that if T is greater than the transition temperature, T_λ^P, the integrations in (10) and (11) are performed between t_r and T_λ^P. The change in Gibbs free energy contributed by the increase in heat capacity associated with the lambda transition is calculated from

$$\Delta_\lambda G^{P,T} = \Delta_\lambda H^{P,T} - T \cdot \Delta_\lambda S^{P,T} \tag{12}$$

and $\Delta_\lambda G$ is added to the free energy function given by eqn (1).

It is important to note that, although the magnitude of Cp_λ is independent of P, the fact that the onset of the lambda transition does change with pressure (Figs. 1b, 1c) implies that $(\partial Cp/\partial P)_T \neq 0$, $(\partial S/\partial P)_T \neq 0$, and therefore that $(\partial V/\partial T)_P = -(\partial S/\partial P)_T$ is also non-zero. These relationships are most easily illustrated with reference to a particular lambda transition. Cp data for the α–β quartz transition are shown in Fig. 1b along with the computed Cp function using Eqns (4) and (8). The dotted curve in Fig. 1a shows volumes at 1 b for α-quartz computed from finite difference derivatives of $(\partial G_\lambda/\partial P)_T = V_\lambda$, with the assumption that the slope of this transition is constant ($k = (\mathrm{d}T/\mathrm{d}P) = 0{\cdot}0237$ K/b). In order

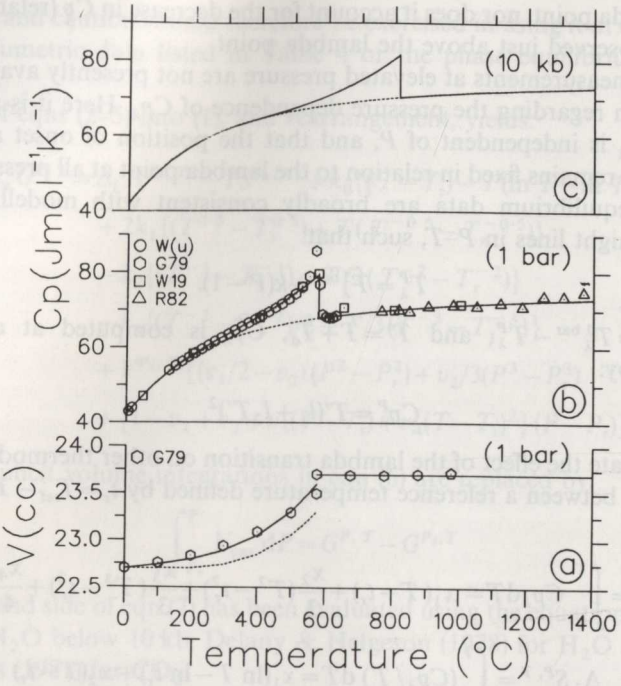

FIG. 1. Effect of the lambda transition on the heat capacity and volume of quartz. (a) Solid lines show the computed volume of quartz compared to Ghiorso *et al.*'s (1979) representation of experimental data. The dotted line shows that portion of the volume which results from the lambda transition (see text). (b) Heat capacity of quartz at 1 b compared to experimental data: W(u)—E. F. Westrum, Jr. (unpublished data); G79—Ghiorso *et al.* (1979); W19—White (1919); R82—Richet *et al.* (1982). The dotted line represents the 'lattice' heat capacity. (c) Heat capacity of quartz at 10 kb. Note that the magnitude of Cp_λ remains constant at elevated pressure, while the position of the onset of the transition moves to higher temperature.

to fit the measured volumes of α-quartz at 1 b, the *explicit* expansivity terms, v_3 and v_4 were fitted to the differences between the measured data and the volumes resulting from the lambda function. The same procedure was followed for other phases that undergo lambda transitions, and where there is information regarding the P–T slope of the transition. Where this information is lacking, or where the data suggest a near-vertical slope (see the discussion of tridymite), it has been assumed that $(dT/dP)=0$, so that $T_d=0$, and therefore $V_\lambda=0$.

The following points should be kept in mind in using the above equations and data presented below for calculation of the thermodynamic properties of polymorphic transitions. For those phases which undergo lambda transitions which are dependent on pressure, thermodynamic properties calculated for the low temperature polymorph with the above equations are valid up to T_λ^P. Thermodynamic properties at temperatures above the lambda point are computed using the standard state properties and 'lattice' Cp of the high temperature polymorph. The latter properties were derived from phase equilibrium constraints on the P–T position of the transition. That such properties can be extracted is a necessary and crucial test of the consistency of the thermodynamic properties of both polymorphs, because most polymorph transitions involve very small entropy changes and thus small inconsistencies between the Gibbs free energy functions of both polymorphs result in large displacements or pronounced curvature of the computed transitions.

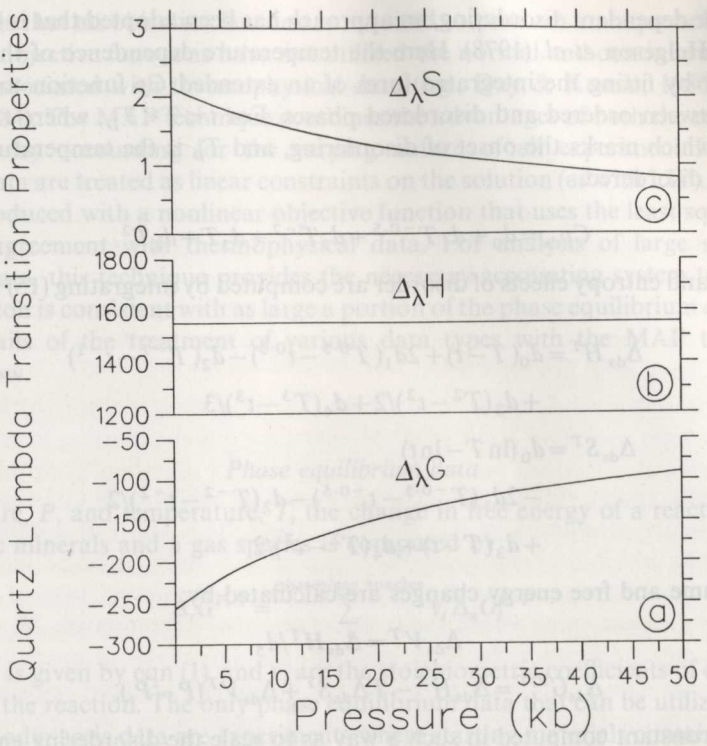

FIG. 2. Integral lambda transition properties ($Jmol^{-1}$) of quartz, calculated at the lambda points at each pressure.

For those phases that undergo lambda transitions which are assumed to be independent of P, standard state properties are provided only for the low temperature polymorph. The free energy function at temperatures above T_λ^P can be computed with

$$\Delta_a G^{P,T} = \Delta_a G^{P,T_\lambda} - (T - T_\lambda^P)\Delta_\lambda S^{P,T_\lambda} \tag{13}$$

where $\Delta_\lambda S^{P,T_\lambda}$ is given by eqn (11). Commonly, the best representation of Cp and heat content data for lambda transition phases is achieved if a first-order transition is assumed to be superimposed on the lambda transition. In such cases $\Delta_t H$ (over and above $\Delta_\lambda H$) is non-zero (499 $Jmol^{-1}$ results from Berman & Brown's (1985) analysis of the α–β quartz transition), and the free energy function for the high temperature polymorph is computed from:

$$\Delta_a G^{P,T} = \Delta_a G^{P,T_\lambda} - (T - T_\lambda^P)(\Delta_t S + \Delta_\lambda S^{P,T_\lambda}). \tag{14}$$

Order–disorder

A number of important rock-forming minerals have disordered cation distributions, but the extent and temperature dependence of the disordering process are presently not well known for most phases. This problem has been treated here in two ways. Where the temperature dependence of this process is not constrained by available data, allowance has been made for a constant 'zero-point' contribution to the third law entropy. Where such data exist, or where representation of phase equilibrium data is improved by consideration

of temperature dependent disordering, an approach has been adopted that is similar to that proposed by Helgeson *et al.* (1978). Here the temperature dependence of this process are accounted for by fitting the integrated form of an extended Cp function to the enthalpy differences between ordered and disordered phases. For $t < T < T_D$, where t is a reference temperature which marks the onset of disordering, and T_D is the temperature at which a phase is fully disordered,

$$Cp_{ds} = d_0 + d_1 T^{-0.5} + d_2 T^{-2} + d_3 T + d_4 T^2. \tag{15}$$

The enthalpy and entropy effects of disorder are computed by integrating (15) between t and $T(T < T_D)$:

$$\begin{aligned} \Delta_{ds} H^T = {} & d_0(T-t) + 2d_1(T^{0.5} - t^{0.5}) - d_2(T^{-1} - t^{-1}) \\ & + d_3(T^2 - t^2)/2 + d_4(T^3 - t^3)/3 \end{aligned} \tag{16}$$

$$\begin{aligned} \Delta_{ds} S^T = {} & d_0(\ln T - \ln t) \\ & - 2d_1(T^{-0.5} - t^{-0.5}) - d_2(T^{-2} - t^{-2})/2 \\ & + d_3(T-t) + d_4(T^2 - t^2)/2 \end{aligned} \tag{17}$$

while the volume and free energy changes are calculated by:

$$\Delta_{ds} V^T = \Delta_{ds} H^T / d_5 \tag{18}$$

$$\Delta_{ds} G^{P,T} = \Delta_{ds} H^T - T\Delta_{ds} S^T + \Delta_{ds} V^T (P - P_r). \tag{19}$$

where d_5 is a constant computed in such a way as to scale the disordering enthalpy to the volume of disorder. The apparent Gibbs free energy of the disordered phase is computed by adding the $\Delta_{ds} G^T$ values to the free energy function given by eqn (1). At temperatures above T_D, eqns (16) and (17) are integrated between t and T_D, and the free energy function is computed from

$$\Delta_a G^{P,T} = \Delta_a G^{P,T_D} - (T - T_D)\Delta_{ds} S^{T_D}. \tag{20}$$

TREATMENT OF EXPERIMENTAL DATA

Derivation of an optimized set of standard state thermodynamic properties based on phase equilibrium, volumetric, and calorimetric data was accomplished using the technique of mathematical programming (MAP). Application of this technique, which is an extension of the linear programming (LIP) method (Gordon, 1973), is described in detail by Berman *et al.* (1986), and only the most essential points are reiterated here.

Two methods have been used extensively to extract thermodynamic information from diverse sets of experimental data. Analysis by multiple linear regression (Haas & Fisher, 1976; Robinson *et al.*, 1982; Powell & Holland, 1985) produces a unique solution weighted by the uncertainties in all data. It is ideally suited to thermophysical data that are characterized by a normal probability distribution about the mean experimentally determined value. Application of this technique to phase equilibrium data is hampered because these data provide brackets on the position of an equilibrium without a 'best' estimate of its location, and solutions are produced that, while minimizing the global sum of the squared residuals, can be inconsistent with some phase equilibrium brackets.

The technique of LIP accounts for the nature of phase equilibrium data by treating them as linear inequalities in the change in Gibbs free energy of a reaction (see below). Its

disadvantage is that an objective function is required to produce a unique solution, and in the past such objective functions have not utilized the normal and continuous probability distribution associated with thermophysical data (e.g., Day & Kumin, 1980; Halbach & Chatterjee, 1984). The MAP technique combines the advantages of both the regression and LIP methods by accounting for the varying nature of all experimental data. Phase equilibrium data are treated as linear constraints on the solution (as with LIP), and a unique solution is produced with a nonlinear objective function that uses the least squares criteria to optimize agreement with thermophysical data. For analysis of large sets of phase equilibrium data, this technique provides the necessary accounting system to ensure that the final solution is consistent with as large a portion of the phase equilibrium constraints as possible. Details of the treatment of various data types with the MAP technique are discussed below.

Phase equilibrium data

At a pressure, P, and temperature, T, the change in free energy of a reaction involving stoichiometric minerals and a gas species is computed by

$$\Delta_r G^{P,T} = \sum_i^{\text{phases/gas species}} v_i \Delta_a G_i^{P,T} \tag{21}$$

where $\Delta_a G^{P,T}$ is given by eqn (1), and v_i are the stoichiometric coefficients of each phase or gas species in the reaction. The only phase equilibrium data that can be utilized to retrieve reliable thermodynamic data are experiments where starting materials contain reactants or products or a mixture of both, and one assemblage is observed to increase (be stable) at the expense of the other assemblage. Each such experiment specifies the sign of the free energy change of the reaction, yielding a linear inequality constraint:

$$\Delta_r G^{P,T} \lesseqgtr 0 \tag{22}$$

where use of the 'less than' and 'greater than' inequality signs is determined by whether the products or reactants are stable, respectively. Substitution of eqns (1)–(3) yields

$$\sum_i^{\text{phases/gas species}} v_i \left\{ \Delta_f H_i^{P_r,T_r} - T \cdot S_i^{P_r,T_r} + \int_{T_r}^{T} Cp_i \mathrm{d}T - T \cdot \int_{T_r}^{T} \left(\frac{Cp_i}{T} \right) \mathrm{d}T \right\}$$
$$+ \sum_i^{\text{minerals}} v_i \left\{ V_i^{P_r,T_r}(P - P_r) + \int_{P_r}^{P} (V_i - V_i^{P_r,T_r}) \mathrm{d}P \right\}$$
$$\lesseqgtr \sum_i^{\text{gas species}} -v_i \int_{P_r}^{P} V_i \mathrm{d}P. \tag{23}$$

Each experimental datum is cast in terms of relation 23, and a matrix of coefficients for the variables and the right hand side of these constraint rows is constructed from phase equilibrium brackets for all reactions studied. Relation (23) is expanded (see eqn (6)) such that all thermodynamic variables of minerals are linear in the fit parameters ($\Delta_f H_i^{P_r,T_r}$, $S_i^{P_r,T_r}$, $V_i^{P_r,T_r}$, $k_0 - k_3$ heat capacity terms, and $v_1 - v_4$ volume terms).

A major advantage of the LIP/MAP technique is that experimental uncertainties can be accounted for explicitly. Prior to writing relation 23, the P, T, X coordinates of each experimental datum are adjusted away from the estimated position of equilibrium by an amount equal to the experimental uncertainties in pressure, temperature, and composition of a given phase. This procedure provides a conservative way to analyze a large body of

experimental data that have been determined in many different laboratories using a variety of techniques. In all cases, the errors used in these calculations are a combination of precision (variation of P, T, X during an experiment), and accuracy (incorporating P, T calibrations and temperature gradients across the sample). In most recent work, experimentalists have attempted to assess the different sources of error, and their quoted estimates have been adopted. In many earlier studies in which only precision has been reported, 3° was added in order to account for absolute uncertainties in reported temperatures. In studies where no experimental errors are reported, conservative estimates of 10° and 5% in pressure were adopted.

For those data collected in piston-cylinder or internally heated gas apparatus, reported temperatures have been corrected for the effect of pressure on thermocouple EMFs using the data of Cheng *et al.* (1975).

Thermophysical data

Standard state molar volumes and third law entropies have been accurately determined for most minerals considered in this analysis. These data add direct constraints to the variables of the MAP problem imposing bounds such that variables lie within the 2σ uncertainties of the measurements. For many phases, however, two or more volume determinations do not agree within the limits of reported uncertainties. In some cases, the discrepancies reflect differences between imprecise and inaccurate measurements, but many of these discrepancies are probably due to real differences between natural samples and those which have been synthesized over a range of pressures and temperatures. In treating these data, the volume of a given phase has been allowed to vary between the outside limits of all determinations in which the samples are well characterized. In the final optimization of the problem (discussed below) the solution was weighted towards the value corresponding to the sample judged to be most representative of those used in the phase equilibrium and calorimetric studies.

Third law entropies are determined from low temperature Cp data, and yield minimum values for those minerals with frozen-in disorder that does not contribute to measured Cp at low temperature. For minerals with potential for disorder but for which data are not available to evaluate explicitly the temperature dependence of this process (with eqns (15)–(20)), only lower bounds were placed on S^{P_r, T_r}, and phase equilibrium data were used to derive optimized third law entropies.

All enthalpies of formation given in this paper are referenced to the elements in their stable states at 1 b and 298·15 K. In order to use this convention for all minerals, reference values for $\Delta_f H^{P_r, T_r}$ must be selected for one phase for each component in the chemical system, because elements do not participate in any of the equilibria utilized in this study. The selected reference values, noted in Table 2, are oxide minerals which were for the most part taken from the CODATA recommendations (CODATA, 1978). The exceptions are the values for muscovite (K component), albite (Na component), and fayalite (Fe component), chosen because the oxides of these components are not involved in the analyzed phase equilibria. An independent source of experimental data (e.g., solubility data) must be used to check the validity of these reference values, but a comprehensive evaluation of such data is beyond the scope of this study. The choices of muscovite over potassium feldspar, and albite over jadeite were made on the basis of a preliminary analysis (Berman *et al.*, 1985) of unpublished solubility data (reported by Helgeson *et al.*, 1978) involving Na–K phases. It should be noted that, in order to preserve the internal consistency of the thermodynamic data set presented in this paper, changes in the $\Delta_f H^{P_r, T_r}$ of any reference phase must be

accompanied by equal changes in the $\Delta_f H^{P_r, T_r}$ of all minerals consisting of the component for which this phase was the reference.

Enthalpies of formation have been determined through heat of solution measurements for most of the minerals considered in this study. Previous work (Helgeson *et al.*, 1978; Berman *et al.*, 1985) indicate, however, that these data are not generally of sufficient accuracy to permit agreement (within their quoted uncertainties) with phase equilibrium data. Consequently, the calorimetric data have not been used to place bounds on these variables (with the exception of reference values noted above), and agreement with these data is maximized in the final optimization of the MAP problem.

Heat capacity, expansivity, and compressibility data

Thermal and volume functions (eqns (4) and (5)) for all minerals were derived by weighted linear regression of pertinent data prior to the MAP analysis, and these regressed functions were retained for most minerals. In cases where preliminary analysis indicated inconsistencies among the various experimental data, or where Cp and volume data had to be estimated (see below), these functions were modified and optimized using the MAP objective function described below. Although the coefficients of eqns (4) and (5) could be obtained for all minerals with this objective function, this procedure was not adopted because of the greatly increased computational complexity and expense.

Where heat capacity data are lacking, Cp was estimated using the predictive model presented by Berman & Brown (1985):

$$Cp = \sum_{i}^{\text{components}} v_i c_{ij} \tag{24}$$

where the v_i and c_{ij} are the number of moles and the j Cp coefficients, respectively, of the ith oxide component of a mineral. The values of the c_{ij} were determined by regression analysis of the Cp data of minerals in the system Na_2O–K_2O–CaO–MgO–FeO–Fe_2O_3–Al_2O_3–SiO_2–TiO_2–H_2O–CO_2. Predicted heat capacities with this model reproduce most data for minerals within 2% (Berman & Brown, 1985).

Estimation of mineral expansivities and compressibilities is more problematic. Most recent work (e.g., Hazen & Finger, 1985) indicates that polyhedral volumes show similar expansivity and compressibility within, and to some extent, between mineral groups. A more important factor, and one which leads to differences in expansivity and compressibility of minerals within the same structural group is the varied response to temperature and pressure of bond angles between polyhedra of different minerals. Presently there is no model that predicts mineral expansivities and compressibilities with complete success. Those presented for instance by Wang (1978) and Powell & Holland (1985) reproduce much of the available experimental data, but exceptions for specific minerals are numerous. Although it may be possible to develop a model that utilizes measured Cp data and the thermodynamic relationship

$$Cp = C_v + \alpha^2 VT/\beta \tag{25}$$

to help predict α and β (T. H. Brown, in prep.), in this study the methods presented by Powell & Holland (1985) were used as first approximations. Optimized expansivity and compressibility coefficients were subsequently derived during the MAP analysis of combined phase equilibrium and thermophysical data.

Final optimization

The technique of linear programming solves systems of linear inequalities (relation 23) for the values of variables which are consistent with all experimental constraints. If some of the constraints on the problem are contradictory, the problem is infeasible, and the source of the discrepancies must be analyzed and removed. This case may arise when two studies on the same equilibrium provide brackets which do not overlap, but more commonly inconsistencies are produced during analysis of different equilibria which are linearly dependent. In either case, all experimental results must be scrutinized and questionable data either removed or adjusted (if uncertainties in T, P, X are poorly documented). The rejection criteria most often invoked are inadequate phase characterization, and questionable demonstration of reaction progress. These factors are addressed below in relation to specific experimental results.

Once inconsistencies are removed, there are an infinite number of solutions to any given problem within this so-called 'feasible region'. A solution is unique only in conjunction with optimization of some objective function. In this study standard mathematical programming methods have been used to optimize the nonlinear objective function given by:

$$\sum_{i}^{n}(X_i - M_i)^2/W_i \tag{26}$$

where the M_i are measured $\Delta_f H_i^{P_r, T_r}$, $S_i^{P_r, T_r}$, and $V_i^{P_r, T_r}$ data with associated variances, W_i, the X_i are calculated values, and n is the number of experimentally determined thermodynamic parameters of phases considered in the problem. When necessary this objective function can be modified and extended in order to optimize Cp $(k_0 - k_3)$ and expansivity/-compressibility $(v_1 - v_4)$ coefficients. It seems worthwhile to emphasize that while final optimization with (26) proceeds, consistency is maintained with all linear inequality constraints (phase equilibrium constraints) as well as with all bounds (2σ uncertainties of thermophysical data) on the thermodynamic parameters of all minerals.

RESULTS

Minerals considered in this study (Table 1) were those for which phase equilibrium data are available, and for which complications due to solid solution in restricted chemical systems are minimal. Refined standard state properties ($\Delta_f G^{P_r, T_r}$, $\Delta_f H^{P_r, T_r}$, S^{P_r, T_r}, V^{P_r, T_r} are presented in Table 2. Coefficients for Cp and volume functions are given in Tables 3a, 3b (Cp_λ), and 4, along with comparisons with selected experimental data. Table 5 presents the coefficients for calculation of temperature-dependent disordering.

Derived standard state properties can be compared with thermophysical data that are compiled in the Appendix. The agreement is excellent for volumes and entropies, but notably poorer for enthalpies of formation (Fig. 3), especially those based on heat of solution measurements of natural samples in HF at room temperature. The degree of consistency with enthalpies of formation derived from high temperature heats of solution is acceptable, however, when one compares the overall results with the scatter between different measurements for given minerals (e.g., forsterite in Fig. 3 and the Appendix). The poorer agreement among these data relative to enthalpies of formation derived from phase equilibrium studies (see below) may stem from the difficulty of maintaining the strict stoichiometry of oxide phases analysed by solution calorimetry or from the 'infinite dilution' assumption that is employed in high temperature solution calorimetry.

The phase equilibrium data (approximately 1200 half-brackets involving 180 different equilibria) used to refine all thermodynamic parameters are presented in Figs. 4–45, and discussed below. Overall agreement with these data is excellent with approximately 1% of the data inconsistent with the tabulated thermodynamic properties. The remaining portion of this paper presents details of the refinement process, addressing in particular the inconsistencies that were found among the experimental data. For ease of presentation, minerals are discussed in groups based on mutual participation

TABLE 1

Abbreviations and chemical formulae

Phase	*Abbreviation*	*Formula*
Akermanite	Ak	$Ca_2MgSi_2O_7$
Albite	Ab	$NaAlSi_3O_8$
Albite (high)	hAb	$NaAlSi_3O_8$
Albite (low)	lAb	$NaAlSi_3O_8$
Almandine	Alm	$Fe_3Al_2Si_3O_{12}$
Andalusite	And	Al_2SiO_5
Anorthite	An	$CaAl_2Si_2O_8$
Anthophyllite	Ath	$Mg_7Si_8O_{22}(OH)_2$
Antigorite	Atg	$Mg_{48}Si_{34}O_{85}(OH)_{62}$
Brucite	Br	$Mg(OH)_2$
Ca-Al pyroxene	CTs	$CaAl_2SiO_6$
Calcite	Cc	$CaCO_3$
Chrysotile	Chr	$Mg_3Si_2O_5(OH)_4$
Clinochlore	Cln	$Mg_5Al(AlSi_3O_{10})(OH)_8$
Coesite	Cs	SiO_2
Cordierite	Cd	$Mg_2Al_4Si_5O_{18}$
Corundum	Co	Al_2O_3
Cristobalite (alpha)	aCr	SiO_2
Cristobaite (beta)	bCr	SiO_2
Diaspore	Dsp	$AlO(OH)$
Diopside	Di	$CaMgSi_2O_6$
Dolomite	Do	$CaMg(CO_3)_2$
Enstatite (clino)	cEn	$MgSiO_3$
Enstatite (ortho)	En	$MgSiO_3$
Enstatite (proto)	pEn	$MgSiO_3$
Fayalite	Fa	Fe_2SiO_4
Ferrosilite	Fsl	$FeSiO_3$
Forsterite	Fo	Mg_2SiO_4
Gehlenite	Ge	$Ca_2Al_2SiO_7$
Grossular	Gr	$Ca_3Al_2Si_3O_{12}$
Hematite	Hm	Fe_2O_3
Ilmenite	Ilm	$FeTiO_3$
Jadeite	Jd	$NaAlSi_2O_6$
Kaolinite	Kln	$Al_2Si_2O_5(OH)_4$
Kyanite	Ky	Al_2SiO_5
Lawsonite	Lw	$CaAl_2Si_2O_7(OH)_2 \cdot H_2O$
Lime	Lm	CaO
Magnesite	Mst	$MgCO_3$
Magnetite	Mt	Fe_3O_4
Margarite	Mrg	$CaAl_4Si_2O_{10}(OH)_2$
Meionite	Me	$Ca_4Al_6Si_6O_{25}(CO_2)$
Merwinite	Mw	$Ca_3MgSi_2O_8$
Monticellite	Mo	$CaMgSiO_4$
Muscovite	Ms	$KAl_3Si_3O_{10}(OH)_2$
Paragonite	Pg	$NaAl_3Si_3O_{10}(OH)_2$
Periclase	Pe	MgO
Phlogopite	Phl	$KMg_3(AlSi_3O_{10})(OH)_2$
Potassium feldspar	Kfs	$KAlSi_3O_8$
Sanidine	Sa	$KAlSi_3O_8$
Microcline	Mcr	$KAlSi_3O_8$
Prehnite	Prh	$Ca_2Al_2Si_3O_{10}(OH)_2$
Pyrope	Py	$Mg_3Al_2Si_3O_{12}$
Pyrophyllite	Prl	$Al_2Si_4O_{10}(OH)_2$
Quartz (alpha)	aQz	SiO_2
Quartz (beta)	bQz	SiO_2
Rutile	Rt	TiO_2
Sillimanite	Si	Al_2SiO_5
Sphene	Sph	$CaTiSiO_5$

TABLE 1 (*Continued*)

Phase	*Abbreviation*	*Formula*
Spinel	Sp	$MgAl_2O_4$
Talc	Tc	$Mg_3Si_4O_{10}(OH)_2$
Tremolite	Tr	$Ca_2Mg_5Si_8O_{22}(OH)_2$
Tridymite (low)	lTr	SiO_2
Tridymite (high)	hTr	SiO_2
Wollastonite	Wo	$CaSiO_3$
Pseudowollastonite	pWo	$CaSiO_3$
Zoisite (ortho)	Zo	$Ca_2Al_3Si_3O_{12}(OH)$
Zoisite (clino)	cZo	$Ca_2Al_3Si_3O_{12}(OH)$
Carbon dioxide	CO_2	CO_2
Water	W	H_2O
Aqueous silica	S	SiO_2

TABLE 2

Refined standard state thermodynamic properties at 1 b, 298·15 K

Phase	$\Delta_f G^{P_r, T_r}$	$\Delta_f H^{P_r, T_r}$	S^{P_r, T_r}	V^{P_r, T_r}
Akermanite	−3663·786	−3860·441	212·000	9·252
Albite	−3703·293	−3921·618	224·412	10·083
Albite (high)	−3703·293	−3921·618	224·412	10·083
Albite (low)*	−3711·715	−3935·100	207·443	10·043
Almandine	−4941·728	−5265·502	339·927	11·511
Andalusite	−2441·806	−2589·972	91·434	5·147
Anorthite	−4003·221	−4228·730	200·186	10·075
Anthophyllite	−11342·582	−12069·032	535·195	26·560
Antigorite	−66076·529	−71364·156	3602·996	174·246
Brucite	−834·868	−925·937	63·064	2·468
Ca-Al pyroxene	−3122·310	−3298·767	140·751	6·356
Calcite	−1128·295	−1206·819	91·725	3·690
Chrysotile	−4035·373	−4363·356	220·134	10·720
Clinochlore	−8250·546	−8909·590	435·154	21·147
Coesite	−852·585	−907·604	39·424	2·064
Cordierite	−8651·517	−9158·727	417·970	23·311
Corundum*	−1582·199	−1675·700	50·820	2·558
Cristobalite (alpha)	−853·918	−907·753	43·394	2·587
Cristobalite (beta)	−853·327	−906·377	46·029	2·730
Diaspore	−920·806	−999·378	35·308	1·776
Diopside	−3026·202	−3200·583	142·500	6·620
Dolomite	−2162·354	−2325·248	154·890	6·432
Enstatite (clino)	−1458·601	−1545·926	66·325	3·131
Enstatite (ortho)	−1458·181	−1545·552	66·170	3·133
Enstatite (proto)	−1456·965	−1543·959	67·438	3·242
Fayalite*	−1380·154	−1479·360	150·930	4·630
Ferrosilite	−1117·472	−1194·375	95·882	3·296
Forsterite	−2055·023	−2174·420	94·010	4·366
Gehlenite	−3785·954	−3988·158	198·600	9·033
Grossular	−6270·974	−6632·859	255·150	12·538
Hematite	−743·681	−825·627	87·437	3·027
Ilmenite	−1155·320	−1231·947	108·628	3·170
Jadeite	−2846·482	−3025·118	133·574	6·034
Kaolinite	−3799·770	−4120·327	203·700	9·952
Kyanite	−2443·370	−2594·220	82·430	4·412
Lawsonite	−4509·709	−4865·666	229·176	10·144
Lime*	−603·350	−635·090	37·750	1·676
Magnesite	−1029·875	−1113·636	65·210	2·803
Magnetite	−1014·235	−1117·403	146·114	4·452

TABLE 2 (*Continued*)

Phase	$\Delta_f G^{P_r, T_r}$	$\Delta_f H^{P_r, T_r}$	S^{P_r, T_r}	V^{P_r, T_r}
Margarite	−5852·244	−6236·603	265·084	12·958
Meionite	−13105·915	−13849·723	730·000	34·036
Merwinite	−4309·707	−4537·497	251·777	9·847
Monticellite	−2132·222	−2250·027	108·300	5·148
Muscovite*	−5596·723	−5976·740	293·157	14·087
Paragonite	−5563·572	−5944·208	277·699	13·216
Periclase*	−569·209	−601·500	26·951	1·125
Phlogopite	−5827·224	−6207·342	334·158	14·977
Potassium feldspar	−3745·415	−3970·791	214·145	10·869
Sanidine	−3738·804	−3959·704	229·157	10·896
Microcline	−3745·415	−3970·791	214·145	10·869
Prehnite	−5820·154	−6198·606	288·634	14·016
Pyrope	−5936·009	−6286·548	266·359	11·316
Pyrophyllite	−5266·865	−5640·781	239·400	12·760
Quartz (alpha)*	−856·288	−910·700	41·460	2·269
Quartz (beta)	−855·033	−908·627	44·207	2·370
Rutile*	−889·497	−944·750	50·460	1·882
Sillimanite	−2439·265	−2586·091	95·930	4·983
Sphene	−2455·134	−2596·652	129·290	5·565
Spinel	−2176·537	−2300·313	84·535	3·977
Talc	−5517·657	−5897·387	261·240	13·610
Tremolite	−11578·548	−12305·578	551·150	27·268
Tridymite (low)	−854·026	−907·750	43·770	2·675
Tridymite (high)	−853·844	−907·045	45·524	2·737
Wollastonite	−1546·123	−1631·500	81·810	3·983
Pseudowollastonite	−1543·085	−1627·427	85·279	4·016
Zoisite (ortho)	−6494·148	−6889·488	297·576	13·588
Zoisite (clino)	−6496·497	−6894·968	287·076	13·673
Carbon dioxide (gas)*	−394·341	−393·510	213·677	0·0
Water (liquid)*	−237·130	−285·830	69·915	0·0
Water (gas)	−228·538	−241·816	188·72	0·0
Aqueous silica	−833·258	−881·359	62·630	0·0

$\Delta_f G^{P_r, T_r}$ = Gibbs free energy of formation from the elements (kJ/mol), calculated using entropies for the elements taken from Robie *et al.* (1979)

$\Delta_f H^{P_r, T_r}$ = Enthalpy of formation from the elements (kJ/mol)

S^{P_r, T_r} = Third law entropy (J/mol/K)

V^{P_r, T_r} = Molar volume (J/b)

* indicates enthalpy of formation of this phase was chosen as a reference value (see text)

in experimentally studied phase equilibria. Although the following discussion focusses on these minerals and the data that constrain their thermodynamic properties separately, the reader should be aware that thermodynamic parameters for all minerals were derived simultaneously so that every phase equilibrium experiment had the potential to contribute to the refinement of the thermodynamic properties of each mineral.

Silica polymorphs

Refinement of the thermodynamic properties of the silica polymorphs is complicated by the lambda transitions exhibited in quartz, cristobalite, and tridymite. The α–β quartz transition has been discussed above, and the use of eqns (8)–(14) to represent the thermodynamic consequences of this transition permits excellent consistency among the calorimetric, volumetric, and phase equilibrium data (Fig. 4a). The properties of coesite were derived primarily from the data of Bohlen & Boettcher (1982) on the α-quartz-coesite equilibrium (Fig. 4a). The computed position of the β-quartz-coesite boundary is within the uncertainties of the high temperature brackets reported by Mirwald & Massonne (1980).

TABLE 3a

Coefficients for calculation of heat capacity (J/mol/K)*

Phase	k_0	$k_1(\times 10^{-2})$	$k_2(\times 10^{-5})$	$k_3(\times 10^{-7})$	*Range(K)*	*AAD†*	*Reference*
Akermanite	387·06	−29·388	0·0	−4·079	295–374	0·36	Hemingway *et al.* (1986)
					332–995	0·78	Hemingway *et al.* (1986)
					432–1605	0·47	Pankratz & Kelley (1964*b*)
Albite	393·64	−24·155	−78·928	107·064			(same as low albite)
Albite (high)	393·64	−24·155	−78·928	107·064			(same as low albite)
Albite (low)	393·64	−24·155	−78·928	107·064	250–370	0·11	Openshaw *et al.* (1976)
					339–997	0·65	Hemingway *et al.* (1981)
					472–1270	0·47	Kelley *et al.* (1953)
					373–1373	0·26	White (1919)
Almandine	573·96	−14·831	−292·920	502·208	420–997	0·18	L. Anovitz (unpublished data)
Andalusite	236·48	−11·029	−75·268	93·644	254–377	0·08	Robie & Hemingway (1984*a*)
					397–1601	0·21	Pankratz & Kelley (1964*a*)
Anorthite	439·37	−37·341	0·0	−31·702	292–381	0·08	Robie *et al.* (1978)
					349–986	0·40	Krupka *et al.* (1979)
					373–1373	0·21	White (1919)
Anthophyllite	1219·31	−57·665	−347.661	440·090	250–385	0·07	Krupka *et al.* (1985*a*)
					344–697	0·46	Krupka *et al.* (1985*b*)
Antigorite§	7394·51	0·0	−5483·630	8728·412	279–296	0·37	King *et al.* (1967)
					405–847	0·18	King *et al.* (1967)
Brucite	136·84	−5·371	−43·619	55·269	253–299	0·32	Giauque & Archibald (1937)
					350–666	0·14	King *et al.* (1975)
Ca–Al pyroxene	310·70	−16·716	−74·553	94·878	253–379	0·13	Haselton *et al.* (1984)
					350–859	0·40	D. Perkins III (unpublished data)
Calcite	178·19	−16·577	−4·827	16·660	257–286	0·11	Staveley & Linford (1969)
					345–780	0·95	Jacobs *et al.* (1981)
					400–1200	0·75	Kelley (1960)
Chrysotile	610·02	−55·812	−18·573	19·547	256–296	0·08	King *et al.* (1967)
					400–1000	0·52	Estimated (Berman & Brown, 1985)
Clinochlore	1214·28	−112·171	0·0	−125·625	300–800	0·73	Henderson *et al.* (1983)
Coesite	94·907	−7·673	−5·279	2·627	254–846	0·21	Holm *et al.* (1967)
					577–1072	0·38	Holm *et al.* (1967)
					350–650	2·66	Watanabe (1982)
Cordierite	954·39	−79·623	−23·173	−37·021	256–296	0·06	Weller & Kelley (1963)
					400–1652	0·13	Pankratz & Kelley (1964*b*)
Corundum	155·02	−8·284	−38·614	40·908	250–290	0·03	Ditmars & Douglas (1971)
					300–2300	0·11	Ditmars & Douglas (1971)

Cristobalite‡	83·51	−3·747	−24·554	28·007	272–297	0·72	Anderson (1936)
					360–524	1·21	Thompson & Wennemer (1979)
					373–1673	0·07	White (1919)
					1007–1834	0·12	Richet *et al.* (1982)
Diaspore	143·24	−15·404	−3·231	6·463	256–295	0·07	King & Weller (1961*a*)
					340–509	0·18	Perkins III *et al.* (1979)
Diopside	305·41	−16·049	−71·660	92·184	256–295	0·18	King (1957)
					254–381	0·09	Krupka *et al.* (1985*a*)
					344–999	0·53	Krupka *et al.* (1985*b*)
					373–1523	0·12	White (1919)
					573–1573	0·43	Wagner (1932)
Dolomite	328·48	−25·544	−46·885	79·038	250–300	0·08	Stout & Robie (1963)
					349–650	0·41	Krupka *et al.* (1985*b*)
Enstatite (clino)	139·96	−4·970	−44·002	53·571	256–295	0·20	Kelley (1943)
					373–773	0·73	White (1919)
					573–1573	0·77	Wagner (1932)
Enstatite (ortho)	166·58	−12·006	−22·706	27·915	254–385	0·06	Krupka *et al.* (1985*a*)
					344–999	0·37	Krupka *et al.* (1985*b*)
					973–1273	0·84	Haselton (1979)
Enstatite (proto)	166·58	−12·006	−22·706	27·915			Assumed equal to orthoenstatite
Fayalite	248·93	−19·239	0·0	−13·910	255–362	0·19	Robie *et al.* (1982*a*)
					492–1370	0·16	Orr (1953)
Ferrosilite	169·06	−11·930	−20·971	29·253	250–300	0·46	Estimated (Berman & Brown, 1985)
					420–997	0·29	L. Anovitz (unpublished data)
Forsterite	238·64	−20·013	0·0	−11·624	253–299	0·08	Robie *et al.* (1982*b*)
					304–380	0·89	Robie *et al.* (1982*b*)
					398–1807	0·21	Orr (1953)
Gehlenite	373·09	−22·768	−47·785	47·791	276–296	0·07	Weller & Kelley (1963)
					402–1801	0·09	Pankratz & Kelley (1964*b*)
Grossular	573·43	−20·394	−188·872	231·931	255–574	0·12	Westrum *et al.* (1979)
					600–1000	0·02	Perkins III *et al.* (1977)
Hematite‡	146·86	0·0	−55·768	52·563	258–345	0·30	Gronvold & Westrum (1959)
					301–936	0·61	Gronvold & Samuelsen (1975)
					374–1757	0·36	Coughlin *et al.* (1951)
Ilmenite	150·00	−4·416	−33·237	34·815	256–296	0·02	Shomate (1946)
					260–332	0·62	Anovitz *et al.* (1985)
					340–997	0·63	Anvoitz *et al.* (1985)
					375–1237	1·16	Naylor & Cook (1946)
Jadeite	311·29	−20·051	−53·503	66·257	266–296	0·07	Kelley *et al.* (1953)
					393–1189	0·11	Kelley *et al.* (1953)
Kaolinite	523·23	−44·267	−22·443	9·231	256–296	0·11	King & Weller (1961*a*)
					340–560	0·43	Hemingway *et al.* (1978)

TABLE 3a (*continued*)

Phase	k_0	$k_1(\times 10^{-2})$	$k_2(\times 10^{-5})$	$k_3(\times 10^{-7})$	*Range(K)*	*AAD*†	*Reference*
Kyanite	262·68	−20·014	−19·997	−6·318	252–370	0·09	Robie & Hemingway (1984*a*)
					390–1503	0·15	Pankratz & Kelley (1964*a*)
Lawsonite	728·67	−82·481	0·0	85·056	259–320	0·38	Perkins III *et al.* (1980)
					319–600	0·30	Perkins III *et al.* (1980)
Lime	58·79	−1·339	−11·471	10·298	250–300	0·10	Gmelin (1969)
					563–1176	0·71	Lander (1951)
Magnesite	162·30	−11·093	−48·826	87·466	288–383	0·09	Hemingway *et al.* (1977)
					500–750	0·16	Kelley (1960)
Magnetite‡	207·93	0·0	−72·433	66·436	257–347	0·53	Westrum & Gronvold (1969)
					329–818	1·04	Gronvold & Sveen (1974)
Margarite	699·80	−55·871	−68·077	73·432	351–1825	0·40	Coughlin *et al.* (1951)
					255–345	0·08	Perkins III *et al.* (1980)
Meionite	1511·35	−132·433	0·0	−75·161	319–996	0·49	Perkins III *et al.* (1980)
Merwinite	453·62	−32·500	0·0	−34·423			Estimated (calcite + 3 anorthite)
					286–296	0·05	Weller & Kelley (1963)
Monticellite	226·34	−15·427	−11·797	−2·329	397–1601	0·13	Pankratz & Kelley (1964b)
Muscovite	651·49	−38·732	−185·232	274·247	300–1000	0·01	Sharp *et al.* (1986)
					257–377	0·15	Robie *et al.* (1976)
Paragonite	577·57	−14·728	−322·144	505·008	362–967	0·40	Krupka *et al.* (1979)
Periclase	61·11	−2·962	−6·212	0·584	337–719	0·42	Holland (1979; unpublished data)
					250–269	0·10	Barron *et al.* (1959)
					250–320	0·16	Gmelin (1969)
					350–679	0·41	Krupka *et al.* (1979)
					373–1173	0·15	Victor & Douglas (1963)
					402–1798	0·23	Pankratz & Kelley (1963)
Phlogopite	610·38	−20·838	−215·330	284·104	260–380	0·15	Robie & Hemingway (1984*b*)
					300–1000	0·47	Robie & Hemingway (1984*b*)
Potassium feldspar	381·37	−19·410	−120·373	183·643			(same as microcline)
Sanidine	381·37	−19·410	−120·373	183·643			(same as microcline)
Microcline	381·37	−19·410	−120·373	183·643	250–370	0·11	Openshaw *et al.* (1976)
					339–997	0·60	Hemingway *et al.* (1981)
Prehnite	716·05	−64·046	−21·825	26·850	260–347	0·29	Perkins III *et al.* (1980)
					319–790	0·68	Perkins III *et al.* (1980)
Pyrope	640·72	−45·421	−47·019	0·0	297–345	0·14	Haselton & Westrum (1980)
					350–1000	1·38	Newton *et al.* (1979)
					973–1273	0·67	Haselton (1979)
Pyrophyllite	665·93	−58·974	−49·799	66·181	254–304	0·02	Robie *et al.* (1976)
					332–679	0·37	Krupka *et al.* (1979)

Quartz‡	80·01	−2·403	−35·467	49·157	250–290	0·17	E. F. Westrum (unpublished data)
					400–820	0·32	Ghiorso *et al.* (1979)
					340–990	0·80	Hemingway (1987)
					373–1373	0·17	White (1919)
					1001–1676	0·08	Richet *et al.* (1982)
Rutile	77·84	0·0	−33·678	40·294	251–297	0·10	Shomate (1947)
					762–1746	0·35	Naylor (1946)
Sillimanite	256·73	−18·872	−29·774	25·096	253–378	0·33	Robie & Hemingway (1984*a*)
					401–1496	0·33	Pankratz & Kelley (1964*a*)
Sphene	234·62	−10·403	−51·183	59·146	255–296	0·08	King *et al.* (1954)
					375–1495	0·21	King *et al.* (1954)
Spinel	235·90	−17·666	−17·104	4·062	256–296	0·13	King (1955)
					421–1805	0·33	Bonnickson (1955)
Talc	664·11	−51·872	−21·472	−32·737	250–290	0·62	Robie & Stout (1963)
					349–639	0·23	Krupka *et al.* (1985*b*)
Tremolite	1229·36	−64·019	−320·899	420·881	250–300	0·11	Robie & Stout (1963)
					350–680	0·45	Krupka *et al.* (1985*b*)
Tridymite‡	75·37	0·0	−59·581	95·825	272–294	0·38	Anderson (1936)
					360–839	1·31	Thompson & Wennemer (1979)
					366–818	0·69	Mosesman & Pitzer (1941)
Wollastonite	149·07	−6·903	−36·593	48·435	251–386	0·13	Krupka *et al.* (1985*a*)
					344–999	0·50	Krupka *et al.* (1985*b*)
					566–1383	0·48	Wagner (1932)
					573–1373	0·52	Elsner von Gronow & Schwiete (1933)
					484–1423	0·26	Southard (1941)
					973–1433	0·21	White (1919)
Pseudowollastonite	141·16	−4·172	−58·576	94·074	275–295	0·35	Wagner (1932)
					576–1558	0·44	Wagner (1932)
					373–1673	0·25	White (1919)
Zoisite (ortho)	749·17	−65·093	−23·805	12·486	257–317	0·09	Perkins III *et al.* (1980)
					344–729	0·25	Perkins III *et al.* (1980)
Zoisite (clino)	749·17	−65·093	−23·805	12·486			Assumed equal to zoisite
Carbon Dioxide‖	93·00	−13·409	1·238		298–3000	0·15	Stull & Prophet (1971)
Water (gas)¶	115·45	−37·999	−28·713		298–2273	0·21	Haar *et al.* (1984)

* The tabulated k_1–k_3 coefficients (Eqn. 4) are to be multiplied by 10^2, 10^5, and 10^7, respectively.
† Average absolute per cent deviation of data from adopted function.
‡ Polymorphic transition properties are given in Table 3b.
§ Heat content data corrected for antigorite formula of King *et al.* (1967).
‖ Equation (4) extended to include the terms: $-0{\cdot}002876\ T+6336{\cdot}20\ T^{-1}$.
¶ For all calculations presented in this paper, the Cp of water was calculated with the Haar *et al.* (1984) equation of state. In the alternate representation given here, eqn (4) is extended to include the terms: $-0{\cdot}002062\ T+51055{\cdot}16\ T^{-1}$.

TABLE 3b

Thermodynamic parameters describing polymorph transitions with eqns (8)–(14)*

Mineral	T_λ	T_{ref}	dT/dP	$l_1(\times 10^2)$	$l_2(\times 10^5)$	$\Delta_t H$
Akermanite	358	298	0·0	0·0	0·0	452
Alpha cristobalite	535	298	0·0480	−14·216	44·142	0
Hematite	955	298	0·0	−7·403	27·921	1287
Magnetite	848	298	0·0	−19·502	61·037	1565
Alpha quartz	848	373	0·0237	−9·187	24·607	0
Low tridymite	383	298	0·0	42·670	−144·575	130

*Temperature (K), dT/dP (K/b), l_1 and l_2 parameters in $(J/mol)^{0.5}\,K^{-1}$ and $(J/mol)^{0.5}\,K^{-2}$, respectively, and $\Delta_t H$(J/mol)

Of the numerous low temperature transitions reported in tridymite (e.g., Moseman & Pitzer, 1941; Austin, 1954; Cohen & Klement, 1980; Raz, 1983), acceptable consensus has been obtained only for the 'low-middle' transition at 1 b and 110 °C (Raz, 1983) and the 'middle–high' transition at 1 b and 159 °C (Cohen & Klement, 1980). The 'low–middle' transition, modelled as a lambda transition (Thompson & Wennemer, 1979), has a P–T slope of approximately 0·001 K/b (Fig. 4b); little error is introduced by assuming that it is vertical. In order to reproduce the measured volume difference (Austin, 1954) of the 'middle–high' transition (assumed to be first order), $\Delta_t H$ was fixed at 355 $Jmol^{-1}$, which is the sum of the heats of transition measured by Moseman & Pitzer (1941) at 163 and 225 °C.

In contrast to the overall agreement among all experimental data obtained for α- and β-quartz, the P–T positions of the polymorph transitions in tridymite (Fig. 4b) and cristobalite (Fig. 4c) could not be fitted without adopting much lower expansivities for α-tridymite and α-cristobalite than indicated by measurements. In order to compensate for the smaller expansivities of the low temperature polymorphs and because accurate thermodynamic properties are most important for the high temperature polymorphs due to their much wider stability fields, the standard state volumes were adjusted upwards so as to lead to agreement with the measured volumes at high temperature.

The heat capacity of tridymite and to a lesser extent cristobalite are poorly constrained by existing data, with heat content data (Table 3) yielding heat capacities which differ considerably from the Cp data of Thompson & Wennemmer (1979). The adopted Cp functions permit the standard state properties of quartz, cristobalite, and tridymite to be in accord with measured third law entropies as well as the data constraining the phase relationships among these phases (Fig. 4d). The calculated position of the quartz-tridymite-cristobalite invariant point is 1·51 kb and 1167 °C, while the position at 1 b of the metastable quartz–cristobalite transition is 895 °C, in good agreement with the limited experimental constraints (summarized by Hosieni *et al.*, 1985).

The refined data are in excellent agreement with several recent studies aimed at resolving inconsistencies in the thermodynamic properties of the silica polymorphs. The calculated value of $H^{1000}-H^{298}$ for quartz is 45501 $Jmol^{-1}$, compared to 45579 ± 150, 45452 ± 70, and 45520 derived by Richet *et al.* (1982), Hosieni *et al.* (1985), and Hemingway (1987), respectively. The entropy of β-quartz at 1000 K is 116·24 $Jmol^{-1}\,K^{-1}$, compared to 116·259, 116·215, and 116·25 by the same authors. For cristobalite, S^{1000}, and $H^{1000}-H^{298}$ are 118.24 $Jmol^{-1}\,K^{-1}$ and 44887 $Jmol^{-1}$, compared to 118·17 and 44859 (Richet *et al.*, 1982), and 118·216 and 44985 (Hosieni *et al.*, 1985).

Kyanite, sillimanite, andalusite, corundum

The recent work of Robie & Hemingway (1984*a*) places tight constraints of the entropies of the three aluminosilicate polymorphs. In view of the fact that these determinations yield third law entropies outside of the range of uncertainties reported by Todd (1950) for sillimanite and andalusite, it is encouraging that the new measurements are in excellent agreement with phase equilibrium data among these phases (Fig. 5), and also with the enthalpy of solution data which constrain the differences in heats of formation between sillimanite and kyanite (Anderson & Kleppa, 1969), and between sillimanite and andalusite (Anderson *et al.*, 1977). It is worthwhile to note, however, that the calorimetric data cannot discriminate between the positions of the andalusite–sillimanite equilibria

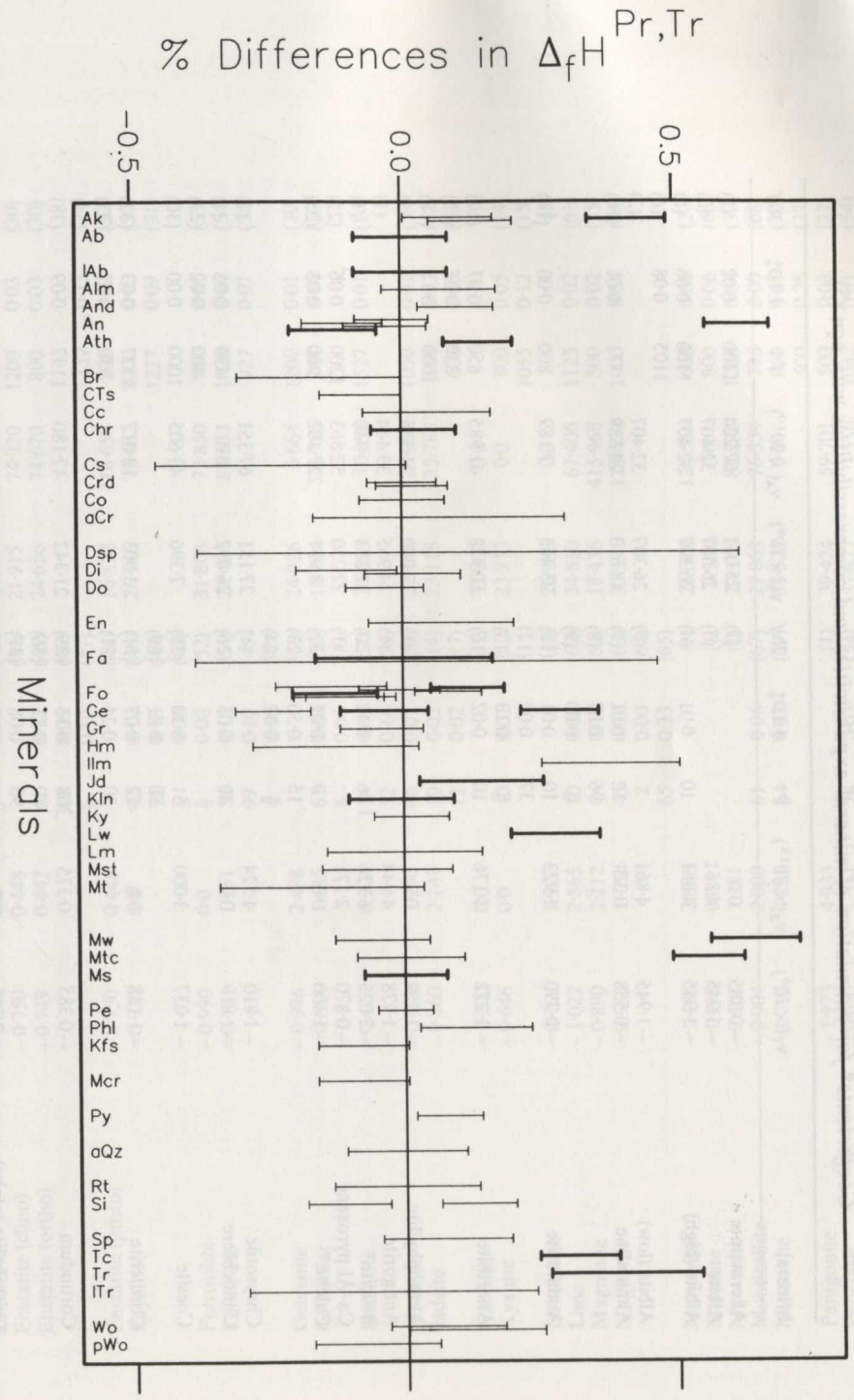

FIG. 3. Comparison of refined enthalpies of formation (represented by zero base line) with calorimetric measurements. Thick brackets represent data obtained by HF calorimetry; other brackets were obtained from high temperature heat of solution measurements. Calorimetric data are compiled in the Appendix.

TABLE 4

Coefficients for calculation of mineral expansivities and compressibilities with eqn (5)*

Mineral	$v_1(\times 10^6)$	$v_2(\times 10^{12})$	P†	*AAD*‡	*Ref*	$v_3(\times 10^6)$	$v_4(\times 10^{10})$	T†	*AAD*‡	*Ref*
Akermanite	−0·785	0·0			(1)	25·011	67·224	1100	0·02	(2)
Albite	−1·945	4·861			(3)	26·307	32·407			(3)
Albite (high)	−1·945	4·861	10	0·01	(4)	26·307	32·407	1100	0·06	(5)
								1105	0·08	(6)
Albite (low)	−1·945	4·861			(3)	26·307	32·407			(3)
Almandine	−0·558	0·321	12	0·01	(7)	18·613	74·539	771	0·01	(10)
			96	0·07	(8)					
			§	0·00	(9)					
Andalusite	−0·770	1·923	10	0·01	(11)	23·443	7·189	800	0·00	(14)
			37	0·07	(12)					
			§	0·13	(13)					
Anorthite	−1·272	3·176	10	0·02	(16)	10·918	41·985	850	0·07	(17)
								830	0·05	(18)
								1000	0·15	(19)
Anthophyllite	−1·259	0·0			(1)	27·060	31·325			(1)
Antigorite	−1·978	4·944			(1)	24·965	39·444			(1)
Brucite	−2·023	6·726	66	0·42	(20)	32·854	10·940			(1)
Ca–Al pyroxene	−0·870	2·171			(1)	22·250	52·863	1200	0·06	(21)
Calcite	−1·400	0·0	9	0·02	(22)	8·907	227·402	900	0·03	(25)
			15	0·50	(23)					
			§	0·02	(24)					
Chrysotile	−1·810	4·524			(1)	27·151	67·351			(1)
Clinochlore	−1·819	0·0	40	0·05	(26)	26·452	0·0	450	0·03	(1)
								400	0·02	(27)
Coesite	−1·037	3·000	51	0·10	(28)	7·396	43·605	1000	0·00	(30)
			80	0·81	(29)					
Cordierite	−1·158	0·0	12	0·07	(31)	3·003	18·017	1127	0·03	(32)
			30	0·24	(31)			950	0·05	(33)
								775	0·12	(34)
Corundum	−0·385	0·375	308	0·15	(35)	21·342	47·180	1197	0·09	(38)
			80	0·11	(36)					
			90	0·08	(37)					
Cristobalite (alpha)	−2·515	0·0			(1)	20·824	0·0	200	0·46	(30)
Cristobalite (beta)	−1·100	5·535			(1)	3·189	0·0	1200	0·07	(30)
Diaspore	−0·599	0·0			(1)	29·718	0·0			(1)

Diopside	−0·872	1·707	53	0·02	(39)	27·795	83·082	800	0·03	(41)
			§	0·03	(40)			1000	0·15	(42)
Dolomite	−1·070	0·0	§	0·02	(40)	14·230	363·778	700	0·10	(43)
Enstatite (clino)	−0·750	0·448			(44)	21·915	74·920	1200	0·03	(30)
Enstatite (ortho)	−0·749	0·447	61	0·12	(45)	24·656	74·670	800	0·03	(30)
			40	0·06	(46)					
			§	0·19	(47)					
Enstatite (proto)	−0·750	0·448			(44)	16·832	116·650	800	0·02	(30)
Fayalite	−0·730	0·0	42	0·19	(48)	26·546	79·482	1000	0·02	(50)
			73	0·18	(49)			1227	0·09	(51)
			§	0·00	(40)					
Ferrosilite	−0·990	0·0	§	0·00	(52)	31·808	75·850	980	0·01	(53)
Forsterite	−0·791	1·351	50	0·13	(54)	29·464	88·633	1020	0·04	(54)
			99	0·10	(45)			927	0·07	(55)
			§	0·00	(40)					
Gehlenite	−0·996	2·488			(1)	24·926	5·664	1200	0·01	(30)
Grossular	−0·654	1·635	61	0·08	(56)	18·994	79·756	707	0·04	(10)
			§	0·06	(9)					
Hematite	−0·479	0·304	114	0·09	(57)	38·310	1·650	1527	0·01	(16)
			52	0·14	(58)					
Ilmenite	−0·584	1·230	46	0·01	(59)	27·248	29·968	1050	0·01	(59)
Jadeite	−0·860	2·149	10	0·02	(4)	23·118	25·785	800	0·03	(42)
			12	0·02	(7)			600	0·03	(30)
Kaolinite	−1·200	0·0			(1)	32·000	0·0			(1)
Kyanite	−0·646	0·0	10	0·01	(11)	23·973	0·0	800	0·05	(14)
								1055	0·12	(15)
Lawsonite	−0·769	1·922			(1)	26·283	0·0			(1)
Lime	−1·022	2·565	10	0·02	(60)	34·610	67·406	1125	0·02	(61)
Magnesite	−0·890	2·212	§	0·02	(62)	18·436	415·968	500	0·02	(25)
Magnetite	−0·582	1·751	45	0·02	(63)	30·291	138·470	1000	0·04	(30)
			2	0·00	(64)					
			65	0·33	(65)					
Margarite	−1·155	2·886			(1)	21·019	124·556	600	0·01	(27)
Meionite	−1·110	0·0			(1)	9·340	0·0	800	0·06	(66)
Merwinite	−0·551	1·381			(1)	29·376	87·235	1200	0·04	(30)
Monticellite	−0·904	2·000	61	0·06	(67)	27·863	76·339	795	0·00	(68)
Muscovite	−1·717	4·295	§	0·03	(69)	33·527	0·0	650	0·05	(70)
								500	0.26	(27)
Paragonite	−1·973	4·933			(1)	39·424	59·701	500	0·08	(27)
Periclase	−0·622	1·511	24	0·03	(54)	37·477	3·556	1042	0·01	(54)
			§	0·01	(71)					
Phlogopite	−1·697	0·0	47	0·15	(26)	34·447	0·0	550	0·09	(27)
								802	0·05	(72)

TABLE 4 (*continued*)

Mineral	$v_1(\times 10^6)$	$v_2(\times 10^{12})$	P†	*AAD*‡	*Ref*	$v_3(\times 10^6)$	$v_4(\times 10^{10})$	T†	*AAD*‡	*Ref*
Potassium feldspar	−1·805	5·112	39	0·00	(22)	15·145	54·850	1000	0·02	(30)
								1000	0·04	(30)
Sanidine	−1·805	5·112			(73)	15·145	54·850			(73)
Microcline	−1·805	5·112			(73)	15·145	54·850			(73)
Prehnite	−1·427	0·0			(1)	1·468	1128·353			(1)
Pyrope	−0·576	0·442	100	0·03	(8)	22·519	37·044	758	0·01	(10)
			49	0·06	(74)			720	0·14	(76)
			56	0·24	(56)					
			§	0·00	(75)					
Pyrophyllite	−1·354	0·0			(1)	12·637	381·661	450	0·03	(27)
								402	0·27	(77)
Quartz (alpha)	−2·434	10·137	40	0·14	(23)	23·895	0·0	527	0·22	(80)
			73	0·25	(78)					
			61	0·23	(79)					
Quartz (beta)	−1·238	7·087	§	0·15	(81)	0·0	0·0	647	0·06	(80)
Rutile	−0·454	0·584	48	0·02	(82)	25·716	15·409	1110	0·01	(61)
Sillimanite	−0·753	0·0	10	0·01	(11)	13·431	0·0	1000	0·04	(14)
			§	0·19	(13)			1055	0·20	(15)
Sphene	−0·590	0·0			(1)	25·200	0·0			(1)
Spinel	−0·489	0·0	40	0·05	(63)	21·691	50·528	1200	0·01	(30)
Talc	−1·699	5·665	45	0·40	(23)	29·447	0·0			(1)
Tremolite	−1·392	3·481			(1)	24·374	98·338	700	0·01	(83)
Tridymite (low)	−2·508	0·0			(1)	19·339	0·0	100	0·24	(30)
Tridymite (high)	−0·740	3·735			(1)	4·829	0·0	1200	0·08	(30)
Wollastonite	−1·245	3·113	45	0·20	(23)	28·180	0·0			(84)
Pseudowollastonite	−1·245	3·113			(85)	28·180	0·0	1200	0·21	(30)
Zoisite (ortho)	−0·515	1·288			(1)	34·670	0·0			(1)
Zoisite (clino)	−0·515	1·288			(86)	34·670	0·0			(86)

* Tabulated $v_1 - v_4$ coefficients (units: b^{-1}, b^{-2}, K^{-1}, K^{-2}) are to be divided by 10^6, 10^{12}, 10^6, and 10^{10}, respectively.

† Maximum pressure (kb) and temperature (°C) of data.

‡ Average absolute per cent deviation between experimentally determined volumes and tabulated function.

§ Experimentally determined isothermal bulk modulus calculated from 1 b elastic constants.

References: (1) Estimate optimized by MAP analysis (see text); (2) Hemingway *et al.* (1986); (3) (same as high albite); (4) Yoder & Weir (1951); (5) Winter *et al.* (1979); (6) Prewitt *et al.* (1976); (7) Adams & Gibson (1929); (8) Sato *et al.* (1978); (9) Isaak & Graham (1976); (10) Skinner (1956); (11) Brace *et al.* (1969); (12) Ralph *et al.* (1984); (13) Vaughan & Weidner (1978); (14) Winter & Ghose (1979); (15) Skinner *et al.* (1961); (16) Robinson *et al.* (1982); (17) Grundy & Brown (1972); (18) Foit & Peacor (1973); (19) Czank & Schulz (1971); (20) Karpinskaya & Ostrovsky (1982); (21) Haselton *et al.* (1984); (22) Bridgman (1948); (23) Vaidya *et al.* (1973); (24) Thanh & Lacam (1984); (25) Markgraf & Reeder (1985); (26) Hazen & Finger (1978*a*); (27) Symmes (1986); (28) Levien & Prewitt (1981); (29) Bassett & Barnett (1970); (30) Skinner (1966); (31) Mirwald *et al.* (1984); (32) Schlenker *et al.* (1977); (33) Mirwald (1981); (34) Hochella *et al.* (1979); (35) Lewis & Drickamer (1966); (36) Finger & Hazen (1978); (37) d'Amour *et al.* (1978); (38) Schauer (1965); (39) Levien *et al.* (1979*b*); (40) Sumino & Anderson (1984); (41) Finger & Ohashi (1976); (42) Cameron *et al.* (1973); (43) Reeder & Markgraf (1986); (44) (same as orthoenstatite); (45) Olinger (1977); (46) Ralph *et al.* (1981); (47) Watt & Ahrens (1986); (48) Hazen (1977); (49) Yagi *et al.* (1975); (50) Suzuki *et al.* (1981); (51) Sumino (1979); (52) Bass & Weidner (1984); (53) Sueno *et al.* (1976); (54) Hazen (1976): (55) Matsui & Manghnani (1985); (56) Hazen & Finger (1978*b*); (57) Wilburn *et al.* (1978); (58) Finger & Hazen (1980); (59) Wechsler & Prewitt (1984); (60) Weir (1956); (61) Grain & Campbell (1962); (62) Christensen (1972); (63) Finger *et al.* (1986); (64) Bridgman (1925); (65) Wilburn & Bassett (1977); (66) Graziani & Lucchesi (1982); (67) Sharp *et al.* (1987); (68) Lager & Meagher (1978); (69) Vaughan & Guggenheim (1986); (70) Guggenheim *et al.* (1987); (71) Jackson & Niesler (1982); (72) Takeda & Morosin (1975); (73) (same as potassium feldspar); (74) Levien *et al.* (1979*a*); (75) Leitner *et al.* (1980); (76) Suzuki & Anderson (1983); (77) Taylor & Bell (1970); (78) d'Amour *et al.* (1979); (79) Levien *et al.* (1980); (80) Raz (1983); (81) Kammer *et al.* (1948); (82) Hazen & Finger (1981); (83) Sueno *et al.* (1973); (84) (same as pseudowollastonite); (85) (same as wollastonite); (86) (same as orthozoisite).

determined by Richardson *et al.* (1969) and by Holdaway (1971). Nor is either set of experiments inconsistent when considered with all other phase equilibrium constraints involving aluminosilicates in higher component systems. Nevertheless, recent experiments on the effects of grain size on the andalusite–sillimanite equilibrium (Kerrick & Heninger, 1984) and on the relative stability of sillimanite and fibrolite (Salje, 1986) support both the position of the triple point as determined by Holdaway (1971), as well as his conclusion that the presence of fibrolite in the starting materials of Richardson *et al.* (1969) was responsible for the higher temperature they observed for this reaction. The calculated position of the triple point is 3730 b and 506 °C.

Initial refinement of the thermodynamic properties of aluminosilicate phases led to a wedge-shaped stability field for the assemblage corundum and β-quartz, extending from 20 kb–1500 °C to higher pressures and temperatures. The extremely small $\Delta_r S$ of the equilibrium corundum + quartz = sillimanite makes its position highly uncertain, however, because of its extreme sensitivity to small perturbations in the free energy function of any of these minerals. For example, small changes (well within all experimental uncertainties) in the volume or *Cp* functions can move the location of this equilibrium down to about 800 °C or can make the assemblage corundum + quartz metastable at all pressures and temperatures. The few occurrences of corundum + quartz at lower temperatures in natural assemblages (e.g., Bohlen, 1986) and in many phase equilibrium experiments (e.g., Richardson *et al.*, 1968; Bird & Fawcett, 1973) offer little guidance because of the complications introduced by kinetic factors and mineral impurities. In this study, the *Cp* function of sillimanite was adjusted slightly during the MAP analysis in order to render corundum + quartz metastable at all pressures and temperatures.

Grossular, wollastonite, anorthite, gehlenite

Recent low temperature heat capacity measurements constrain the entropies of anorthite (Robie *et al.*, 1978), gehlenite (Hemingway & Robie, 1984), and wollastonite (Krupka *et al.*, 1985*a*). There is considerable disagreement, however, among different sets of measurements of the heat capacity and third law entropy of grossular. The entropy ($S^{P_r, T_r} = 260{\cdot}12$ J mol^{-1} K^{-1}) determined by Haselton & Westrum (1980) on a synthetic sample is approximately 2% greater than the values (256·48 and 254·72 J mol^{-1} K^{-1}) measured by Kolesnik *et al.* (1979) and Westrum *et al.* (1979) on natural samples (about 90% grossular) after correction for deviations from end-member composition. Similarly, the combined *Cp* data of Westrum *et al.* (1979) and Perkins *et al.* (1977) for a natural sample corrected to end-member composition are approximately 1% lower than the data for synthetic grossular reported by Krupka *et al.* (1979). The calorimetric data for synthetic grossular are difficult to reconcile with phase equilibrium data among CAS phases (Figs. 6–13), most notably the data for the equilibrium grossular = anorthite + wollastonite + gehlenite (Fig. 6b). With the exception of one reversal by Boettcher (1970), the various sets of experimental data bracketing this equilibrium are in good agreement, but could only be fitted using the calorimetric data for natural grossular, leading to $S^{P_r, T_r} = 255{\cdot}15$ J mol^{-1} K^{-1}. Use of the higher entropy value results in a shift in the position of this equilibrium to much higher temperature (about 100 °C higher in the database of Holland & Powell, 1985).

The overall agreement with the phase equilibrium data obtained in this study was achieved using a temperature-dependent disordering model for gehlenite. The function which results from optimizing agreement with the phase equilibrium data in Figs. 6(b), (c) and 10, produces an entropy increment of 11·47 J mol^{-1} K^{-1} between 425 and 1327 °C, compared to the maximum configurational disorder of 11·5 J mol^{-1} K^{-1}.

All experimental data in the system CaO–Al_2O_3–SiO_2 are consistent with the measured third law entropy of anorthite, with only a slight contribution (0·88 J mol^{-1} K^{-1}) for disorder on tetrahedral sites. The higher entropy (205·4 J mol^{-1} K^{-1}) derived by Helgeson *et al.* (1978) appears at least in part to be the result of their overestimation of the high temperature *Cp* of grossular using the Maier–Kelley function (see Berman & Brown, 1985). Although natural and heat treated plagioclases do show different heats of solution (Carpenter *et al.*, 1985), the absolute magnitude of these differences is not well defined. These data also do not indicate the nature of the temperature dependence of the disordering process, which is of critical importance in deriving the entropy of anorthite from phase equilibrium data that extend over the temperature range 400–1400 °C. Attempts to derive a temperature dependent disordering function, however, all led to marked degradation of the overall representation of these data. Until calorimetric data provide more stringent constraints, the present analysis indicates that some caution should be used in applying entropy corrections calibrated soley from high

TABLE 5

Thermodynamic parameters describing temperature dependent disordering (J/mol) with equations 15–20

Mineral	$T_D(K)$	$t(K)$	d_0	$d_1(\times 10^{-3})$	$d_2(\times 10^{-5})$	$d_3(\times 10^{2})$	$d_4(\times 10^{6})$	$d_5(\times 10^{-4})$
Dolomite	1423	298	−9·42	0·0	3·85	1·732	5·020	0·0
Gehlenite	1600	698	−221·74	0·0	172·91	36·950	−146·900	0·0
Potassium feldspar	1436	298	282·98	−4·83	36·21	−15·733	34·770	41·063

temperature phase equilibrium data (e.g., Gasparik, 1984; Wood & Holloway, 1984) to equilibria at lower temperature.

Calcium tschermak's pyroxene

Phase equilibrium data of Gasparik (1984) indicate breakdown of calcium tschermak's pyroxene (Fig. 7d) at significantly lower pressures than the data of Wood (1978), which may be attributed to the poisoning of Pt–PtRh thermocouples that is documented at high pressures, or to incorrect pressure calibration in the latter study. The data of Hays (1966) are in excellent accord if a friction correction of about 2 kb is used, as is suggested by comparison of his results with alternate data for the equilibria shown in Figs. 6a and 6b and by more recent calibrations of talc-soft glass piston cylinder assemblies (Gasparik & Newton, 1984). Gasparik's data (Fig. 7d), however, show pronounced curvature below 1300 °C, which he suggests may indicate problems with his pressure calibration below this temperature. Consequently, the position of the calculated curve was constrained by his brackets above 1300 °C, which show a similar slope to the data of Hays (1966). The derived entropy for calcium tschermak's pyroxene is 140·75 $Jmol^{-1}K^{-1}$, implying a zero point entropy contribution of 5·45 $Jmol^{-1}K^{-1}$ for cation disorder when compared to the measured entropy (135·3 $Jmol^{-1}K^{-1}$) of Haselton *et al.* (1984). If all brackets of Gasparik are fitted (including those below 1300 °C), the resulting entropy of 135·40 $Jmol^{-1}K^{-1}$ contradicts the results of cell refinements which indicate considerable disorder (Grove & Burnham, 1974; Okamura *et al.*, 1974), and also leads to an enthalpy of formation for Ca–Al pyroxene which is 8 $kJmol^{-1}$ higher than the value (−3296·28 $kJmol^{-1}$) measured by Charlu *et al.* (1978).

Calcite

The thermodynamic properties of calcite were retrieved from phase equilibrium data involving pure CO_2 and H_2O–CO_2 mixtures, using the equation of state derived by Kerrick & Jacobs (1981) for CO_2 fugacity coefficients and non-ideal mixing of H_2O and CO_2. These equations permit general agreement with most data involving CAS phases (other data are discussed below), although several inconsistencies point to specific *P–T* regions where their model may fail to predict accurate fugacity coefficients and activities.

The calculated position of the breakdown of calcite + quartz to wollastonite + CO_2 (Fig. 8a) is in accord with the low pressure reversals of Greenwood (1967*a*) and the 6 kb bracket of Jacobs & Kerrick (1981), even though the calcite I–IV transition at approximately 800 °C (Mirwald, 1979) has not been taken into account. The data of Ziegenbein & Johannes (1974) are displaced to slightly lower temperatures than the above data, but the source of these discrepancies cannot be explored further as details of their experimental method and results were not reported. Inconsistencies are also apparent between the various sets of reversals for the equilibrium wollastonite + calcite + anorthite = grossular + CO_2 summarized in Fig. 9a–c. The computed equilibrium curves agree with the data of Gordon & Greenwood (1971) at 2 kb, but not with most of the data reported by Hoschek (1974) and Shmulovich (1978). The most obvious difference between the different experimental techniques was the much larger fluid/mineral ratios used by Gordon & Greenwood (1971). The discordant results of Hoschek and Shmulovich might therefore be explained by small amounts of back-reaction during quench which, in consuming CO_2, would yield lower measured X_{CO_2} values than the equilibrium values at the conditions of the experimental runs.

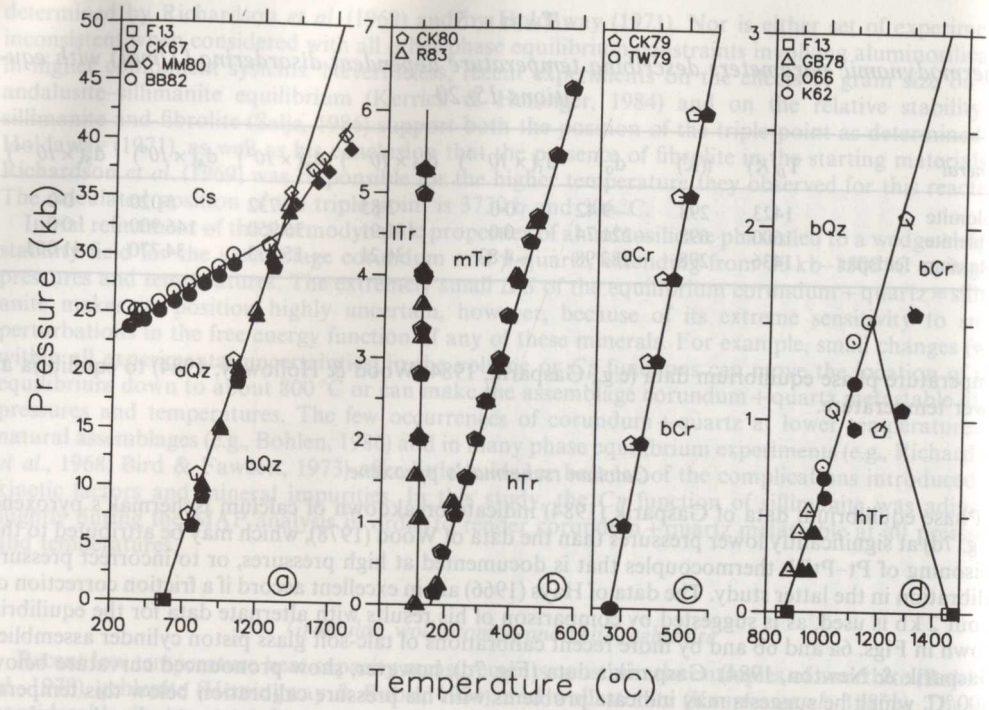

FIG. 4. Comparison of computed phase equilibria with experimental data in the system SiO_2: F13—Fenner (1913); CK67, CK79, CK80—Cohen & Klement (1967, 1979, 1980); MM80—Mirwald & Massonne (1980); BB82—Bohlen & Boettcher (1982); R83—Raz (1983); TW79—Thompson & Wennemer (1979); GB78—Grattan-Bellew (1978); O66—Ostrovsky (1966); K62—Kennedy *et al.* (1962). Symbols show the locations of experimental data after adjustment of nominal data (end of lines connected to symbol centers) for experimental uncertainties. Open and closed symbols depict half-brackets on opposite sides of each equilibrium.

The equilibrium calcite + andalusite + quartz = anorthite + CO_2 is computed (Fig. 8c) to lie about 30° lower at $X_{CO_2} = 0{\cdot}7$ than indicated by the data of Jacobs & Kerrick (1981), which were obtained monitoring reaction progress by weight changes in CO_2 consumed/produced. A smaller inconsistency is also apparent with the data of Kerrick & Ghent (1979), based on weight changes of quartz crystals. The general correspondence of these two studies, together with the good agreement with the experimental data for the same equilibrium with kyanite as the aluminosilicate polymorph (Fig. 8b) and the fact that the Gibbs free energy differences between andalusite and kyanite are tightly constrained by direct phase equilibrium data (Fig. 5c), suggests that these discrepancies result from inaccurate fugacities or activities of CO_2 calculated with the equation of state of Kerrick & Jacobs (1981) at low temperatures. This conclusion is supported by comparison of calculated activity coefficients of CO_2 at lower pressure (0·5 kb) with those based on the *P–V–T* data of Greenwood (1967*b*). The latter data indicate larger positive deviations from ideality for CO_2 than calculated, which would decrease the stability of the high temperature assemblage, and bring the computed equilibrium into better agreement with the phase equilibrium data.

Consistency with most of Hoschek's (1974) data defining the high temperature stability of gehlenite in H_2O–CO_2 fluids (Fig. 10) was accomplished by deriving the *Cp* of calcite from the low temperature data of Stavely & Linford (1969), the *Cp* data up to 600 K of Jacobs *et al.* (1981), and the heat content data up to 1200 K reported by Kelley (1960). This *Cp* function diverges from the *Cp* data of Jacobs *et al.* above 600 K, being approximately 2% lower at 1000 K. Calculated curves for the two highest temperature equilibria (Fig. 10a and e) are 10–20° higher than Hoschek's data. Although computed equilibria in the presence of pure CO_2 are compatible with experimental data (Figs. 11d and e), the overall comparison with both sets of phase equilibrium data suggests that the Kerrick & Jacobs (1981) model may slightly overestimate fugacity coefficients of CO_2 at temperatures above about 850°C.

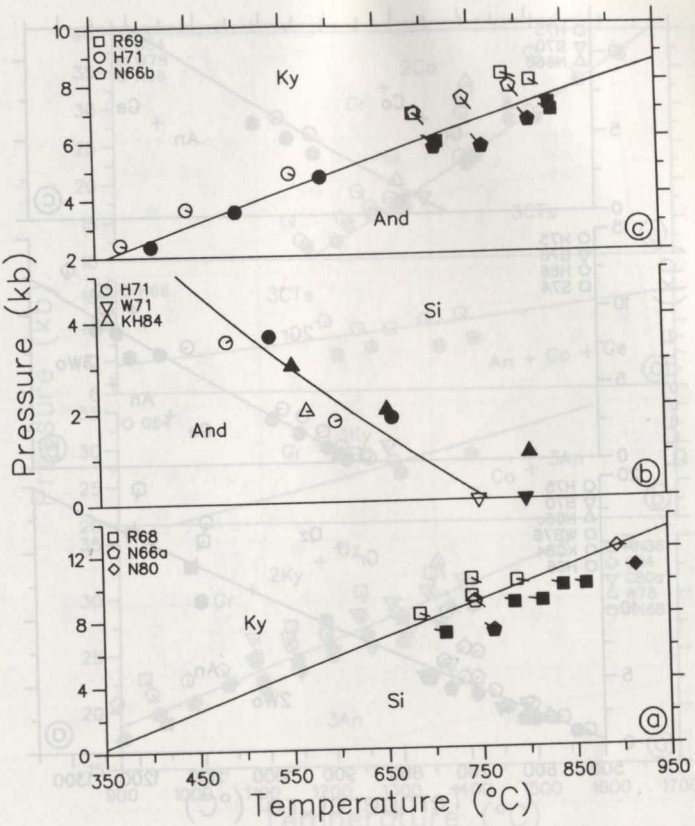

FIG. 5. Comparison of computed phase equilibria with experimental data in the system Al_2O_3–SiO_2: R68, R69—Richardson *et al.* (1968, 1969); H71—Holdaway (1971); N66a, N66b—Newton (1966*a*, *b*); W71—Weill (unpublished data reported by Holdaway, 1971); KH84—Kerrick & Heninger (1984); N80—Newton (unpublished data reported by Day & Kumin, 1980). Symbols as in Fig. 4.

Pseudowollastonite

Phase equilibrium data for the $CaSiO_3$ polymorphic transformation (Fig. 11a) lead to a somewhat smaller entropy for pseudowollastonite (85·28 $Jmol^{-1}K^{-1}$) than that reported (87·45 ± 0·84) by Kelley & King (1961). This small discrepancy may stem from the adopted volume functions of both polymorphs which are poorly constrained by existing data (Table 4).

Meionite

The thermodynamic properties of meionite were retrieved from the data for the breakdown reaction (Fig. 11b) which was studied by Goldsmith & Newton (1977). Oterdoom & Gunter (1983) proposed that the meionite in these experiments was metastably disordered on the basis of comparison of the meionite entropy (790·73 $Jmol^{-1}K^{-1}$) they derived from these data, using the Helgeson *et al.* (1978) entropy of anorthite (205·4 $Jmol^{-1}K^{-1}$)) with their estimated third law entropy (710·07 $Jmol^{-1}K^{-1}$). Recent low temperature calorimetry on an intermediate composition scapolite results in S^{P_r, T_r} = 701·11 $Jmol^{-1}K^{-1}$ for meionite (Moecher *et al.*, 1985). Computation of *P*–*T* slopes for scapolite equilibria led these authors to suggest that natural scapolites do not exhibit full Al–Si disorder, and they calculated a preferred entropy of 728·6 $Jmol^{-1}K^{-1}$. The third law entropy derived in this study, 730·00 $Jmol^{-1}K^{-1}$, is highly correlated with the estimated compressibility (Table 4), and must be considered provisional until compressibility data for meionite are collected.

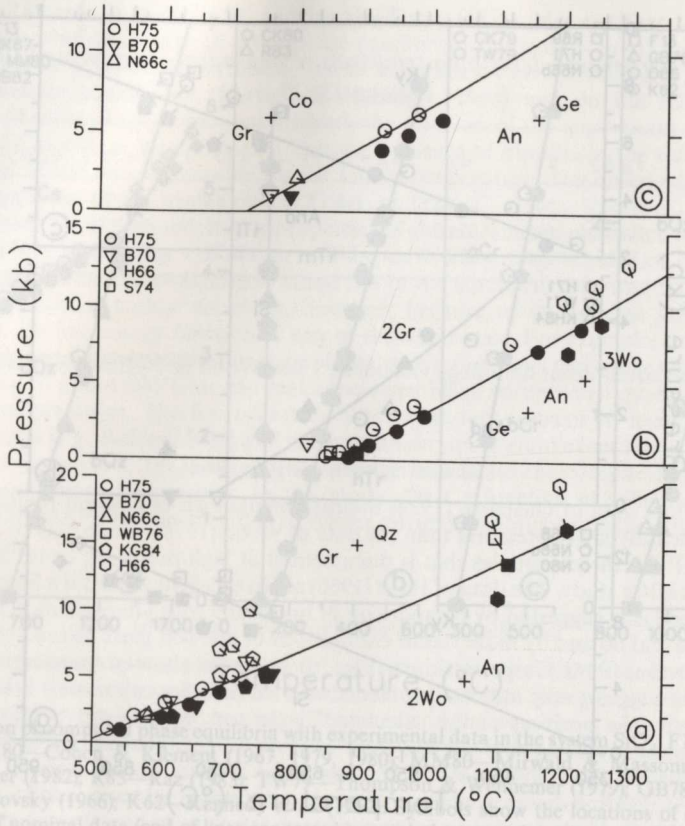

FIG. 6. Comparison of computed phase equilibria with experimental data in the system CaO–Al_2O_3–SiO_2: H75–Huckenholz *et al.* (1975); B70—Boettcher (1970, for clarity, one inconsistent high temperature half-bracket at 1 kb and 865°C is not shown in 6b); N66c—Newton (1966*c*); H66—Hays (1966); S74—Shmulovich (1974); WB76–Windom & Boettcher (1976); KG79—Kerrick & Ghent (1979). Symbols as in Fig. 4.

Lime

Various sets of experimental data for the breakdown of calcite to lime plus CO_2 are incompatible (Fig. 11f). With the thermodynamic properties of calcite constrained as above, only the experimental results of Smyth & Adams (1923) are reconcilable with the calorimetric data for lime.

Zoisite, margarite, clinozoisite

Thermophysical data for zoisite and margarite are in good agreement with phase equilibrium data involving these phases (Figs. 12 and 13) with two exceptions. First, the 4 kb bracket of Chatterjee *et al.* (1984) for the zoisite breakdown reaction shown in Fig. 12a is 5° lower than the computed equilibrium curve, and is difficult to reconcile with best estimates of the volumetric properties of zoisite. Second, the experiments of Storre & Nitsch (1974) on the equilibrium margarite + quartz = kyanite + zoisite + H_2O (Fig. 13e) are inconsistent with data for the other margarite equilibria shown in Fig. 13, and have not been corroborated by the more recent work of Jenkins (1984). As observed by Helgeson *et al.* (1978), the near-vertical distribution of their brackets for this equilibrium is compatible with the slope calculated with andalusite instead of kyanite. Nevertheless, the source of their experimental error remains uncertain, because all starting materials were reported to be kyanite, and all runs were made in the kyanite stability field.

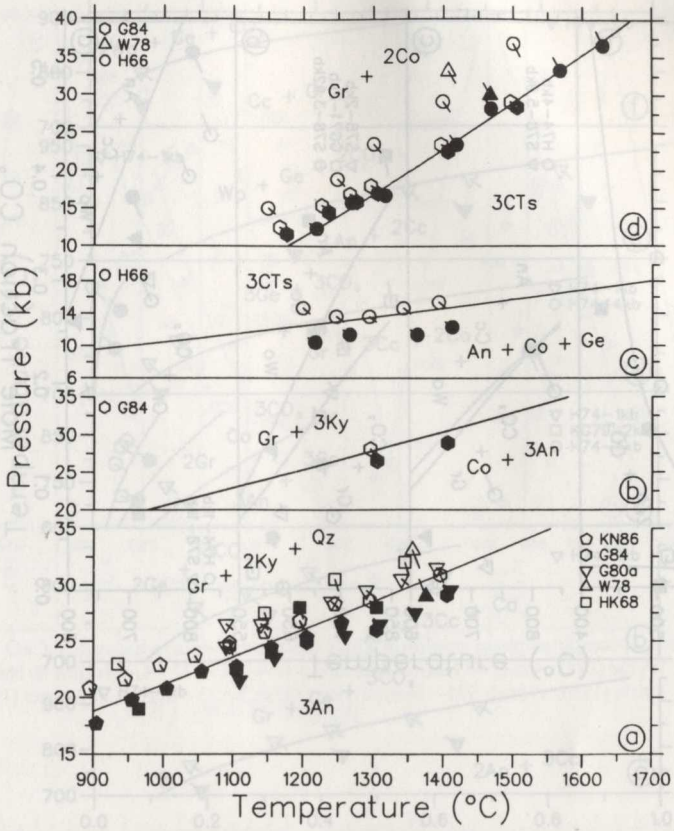

FIG. 7. Comparison of computed phase equilibria with experimental data in the system CaO–Al_2O_3–SiO_2: G84—Gasparik (1984); W78—Wood (1978); H66—Hays (1966); KN86—Koziol & Newton (1986); G80a—Goldsmith (1980*a*); HK68—Hariya & Kennedy (1968). Symbols as in Fig. 4.

Jenkins *et al.* (1985) determined the relative stability of zoisite and clinozoisite by reversing the breakdown reactions of anorthite + H_2O to zoisite/clinozoisite + kyanite + quartz (Fig. 12d and e). The volume difference between polymorphs is well constrained by X-ray powder diffraction measurements (Chatterjee *et al.*, 1984), and the entropy difference was taken from estimates of Jenkins *et al.* (1985) based on Fe^{3+}/Al distributions between these polymorphs in natural assemblages equilibrated over a range of temperatures. The combined data, which are also in agreement with constraints derived from a study of single crystal zoisite/clinozoisite overgrowths (Prunier & Hewitt, 1985), indicate a transition temperature of approximately 240 °C at 1 b, much lower than Helgeson *et al.* (1978) derived (630 °C) from the experiments of Holdaway (1972) involving epidote. Additional data of Jenkins *et al.* (1985) on the ortho-clinozoisite transition at 15 kb confirm the stability of orthozoisite at temperatures above 300 °C. It should be noted, however, that the strong fractionation of Fe^{3+} into clinozoisite accounts for the common occurrence of this phase is metamorphic assemblages estimated to have equilibrated at higher temperatures.

Lawsonite, pyrophyllite, diaspore

Phase equilibrium data constraining the stability of lawsonite are internally consistent (Figs. 14b and 15c–e), and agree with the entropy of lawsonite determined by Perkins *et al.* (1980). Impurities in the natural sample probably account for the higher value (237·65 compared to 230·04 $Jmol^{-1}K^{-1}$)

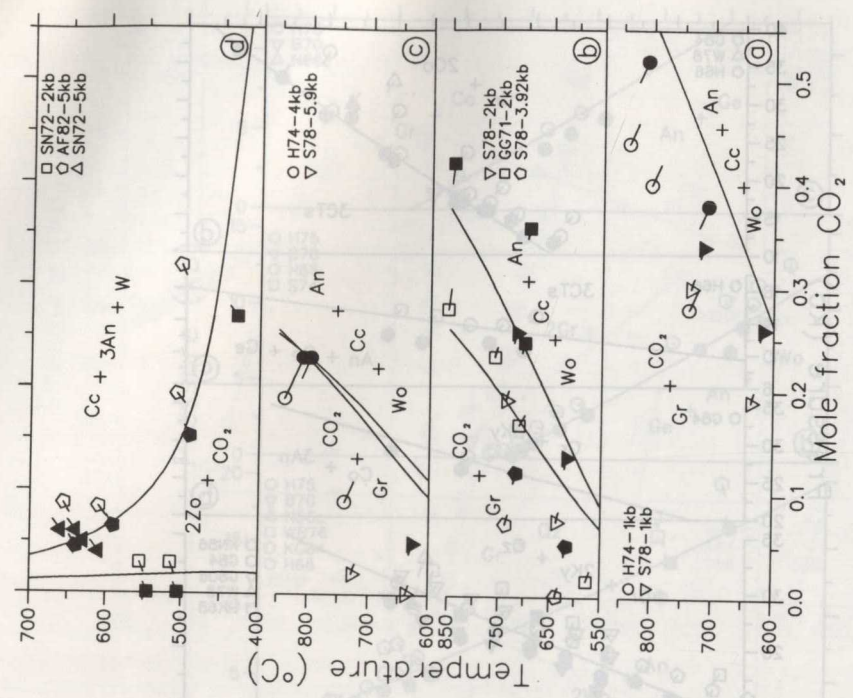

FIG. 9. Comparison of computed phase equilibria with experimental data in the system $CaO–Al_2O_3–SiO_2–H_2O–CO_2$: SN72—Storre & Nitsch (1972); AF82—Allen & Fawcett (1982); H74—Hoschek (1974); S78—Shmulovich (1978); GG71—Gordon & Greenwood (1971). Symbols as in Fig. 4.

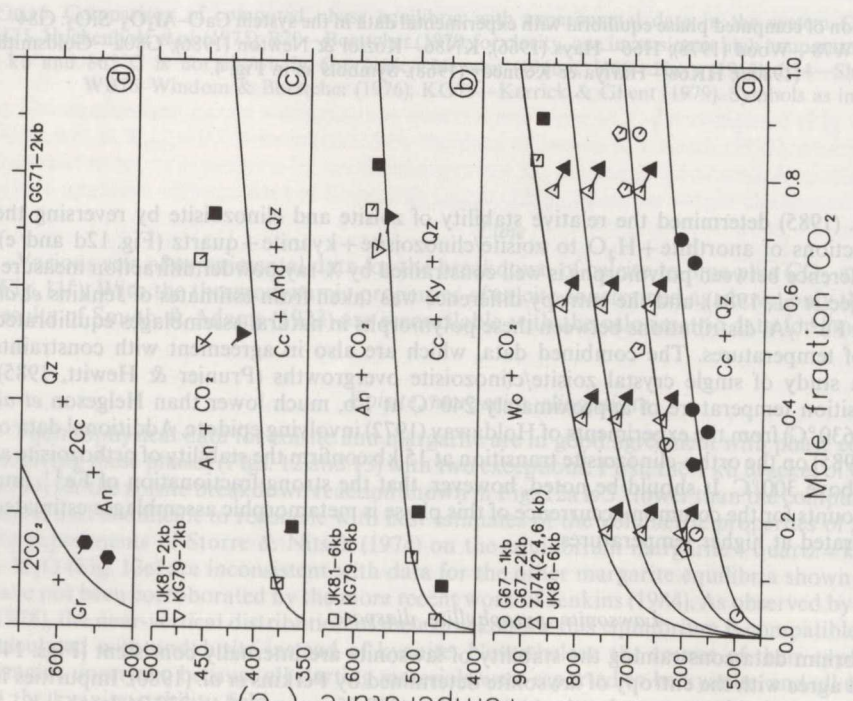

FIG. 8. Comparison of computed phase equilibria with experimental data in the system $CaO–Al_2O_3–SiO_2–CO_2$: GG71—Gordon & Greenwood (1971); JK81—Jacobs & Kerrick (1981); KG79—Kerrick & Ghent (1979); G67—Greenwood (1967*a*); ZJ74—Ziegenbein & Johannes (1974). Symbols as in Fig. 4.

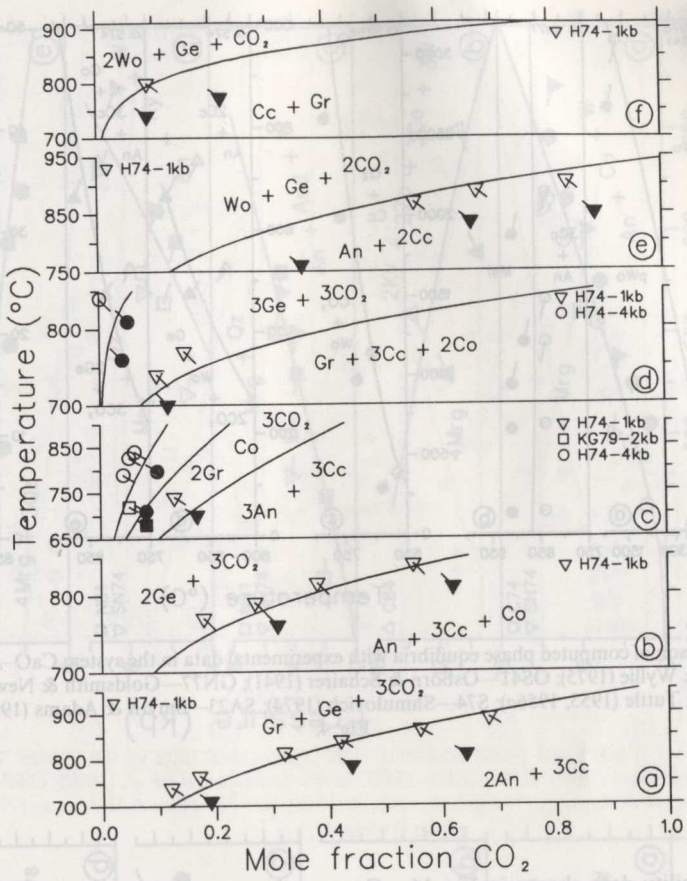

FIG. 10. Comparison of computed phase equilibria with experimental data in the system CaO–Al_2O_3–SiO_2–CO_2: H74—Hoscheck (1974); KG79—Kerrick & Ghent (1979). Symbols as in Fig. 4.

measured by King & Weller (1961*b*). The experimental data shown for the equilibrium lawsonite = anorthite + H_2O (Fig. 15c) were taken from Perkins *et al.* (1980), who report errors in the published results of Crawford & Fyfe (1965). The derived enthalpy of formation of lawsonite ($-4865{\cdot}7$ Jmol^{-1}) is approximately 13 kJmol^{-1} less stable than the value based on Barany's (1962) hydroflouric acid heat of solution data.

With the exception of the experimental results of Matsushima *et al.* (1967), most phase equilibrium data involving pyrophyllite and diaspore show internal consistency (Figs. 14 and 15), and are in agreement with thermophysical measurements. Minor inconsistencies are apparent between the data of Haas & Holdaway (1973) and Kerrick (1968) on the equilibrium: pyrophyllite = andalusite + quartz + H_2O (Fig. 15b), in which reaction progress was monitored by weight changes in quartz and/or andalusite crystals; the combined results suggest slightly greater uncertainties in the location of equilibrium temperatures using this experimental technique. The highly discordant data of Matsushima *et al.* (1967) shown in Fig. 14c and 14d most likely result from poor phase characterization; they do not report details of synthesis conditions, nor the amounts of phase proportion changes on which they inferred their reversals.

For comparisons with solubility data involving aqueous silica, the equation of state of Helgeson *et al.* (1981) was used, while the standard state properties of $SiO_{2(aq)}$ given in Table 2 were derived from

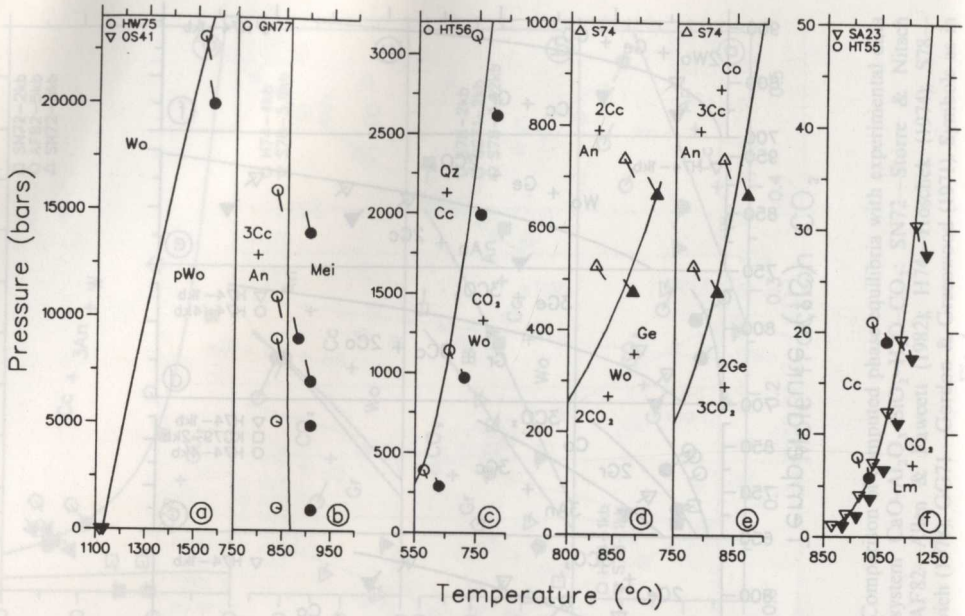

FIG. 11. Comparison of computed phase equilibria with experimental data in the system CaO–Al_2O_3–SiO_2–CO_2. HW75—Huang & Wyllie (1975); OS41—Osborn & Schairer (1941); GN77—Goldsmith & Newton (1977); HT55, HT56—Harker & Tuttle (1955, 1956*a*); S74—Shmulovich (1974); SA23—Smyth & Adams (1923). Symbols as in Fig. 4.

the quartz solubility data shown in Fig. 16a. Computed concentrations of aqueous silica in equilibrium with various mineral assemblages (Fig. 16) are in accord with those solubility data of Hemley *et al.* (1980) which show changes between initial and final solution compositions that are greater than analytical uncertainties (approximately 0·02 log units). Their data for equilibrium solubilities of andalusite–corundum suggest much higher values of silica than computed. The critical runs approached from supersaturation all show changes in silica concentrations that are close to limits of analytical precision, or which contradict results of runs approached from undersaturation. These discrepancies are not surprising in view of the very small $\Delta_r G$ of this equilibrium, which provides little driving force to overcome the dominant effect of kinetics.

Kaolinite

The standard state properties of kaolinite were derived from recent hydrothermal data for the equilibrium kaolinite + quartz = pyrophyllite + H_2O (D. C. McPhail, unpublished data obtained at The University of British Columbia). Although the amount of reaction observed in the most constraining experiments was small (15–30%), no conflicting results were observed, and the results indicate a reversal at 5 kb between 311 ± 5 and 328 ± 6 °C. These results (Fig. 15f) contradict the weight change experiments of Thompson (1970), but are in reasonable agreement with Hemley *et al.*'s (1980) solubility data (Fig. 16f–g).

Prehnite

Liou's (1971) data for the stable and metastable prehnite breakdown reactions (Fig. 17) are thermodynamically inconsistent with each other unless the third law entropy of prehnite (292·75 $Jmol^{-1}K^{-1}$) measured by Perkins *et al.* (1980) is too large by about 20 $Jmol^{-1}K^{-1}$. Recent data of Hammerstrom (unpublished data obtained at the University of British Columbia) and

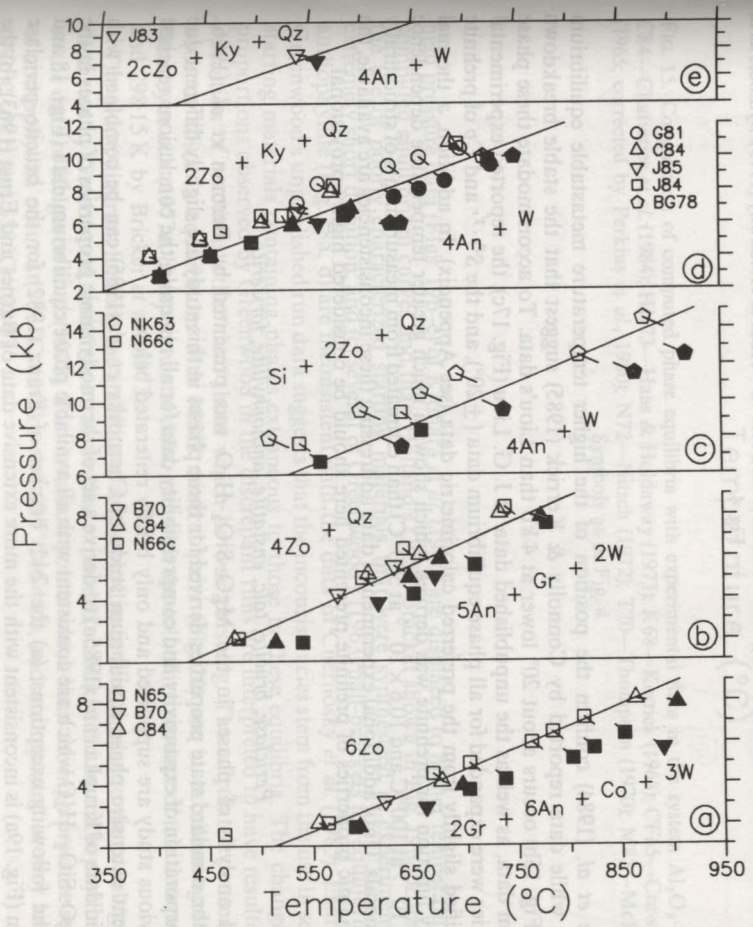

FIG. 12. Comparison of computed phase equilibria with experimental data in the system CaO–Al_2O_3–SiO_2–H_2O: J85—Jenkins *et al.* (1985); G81—Goldsmith (1981); C84—Chatterjee *et al.* (1984); J84—Johannes (1984); BG78—Best & Graham (1978); NK63—Newton & Kennedy (1963); N65, N66c—Newton (1965, 1966*c*); B70—Boettcher (1970). Symbols as in Fig. 4.

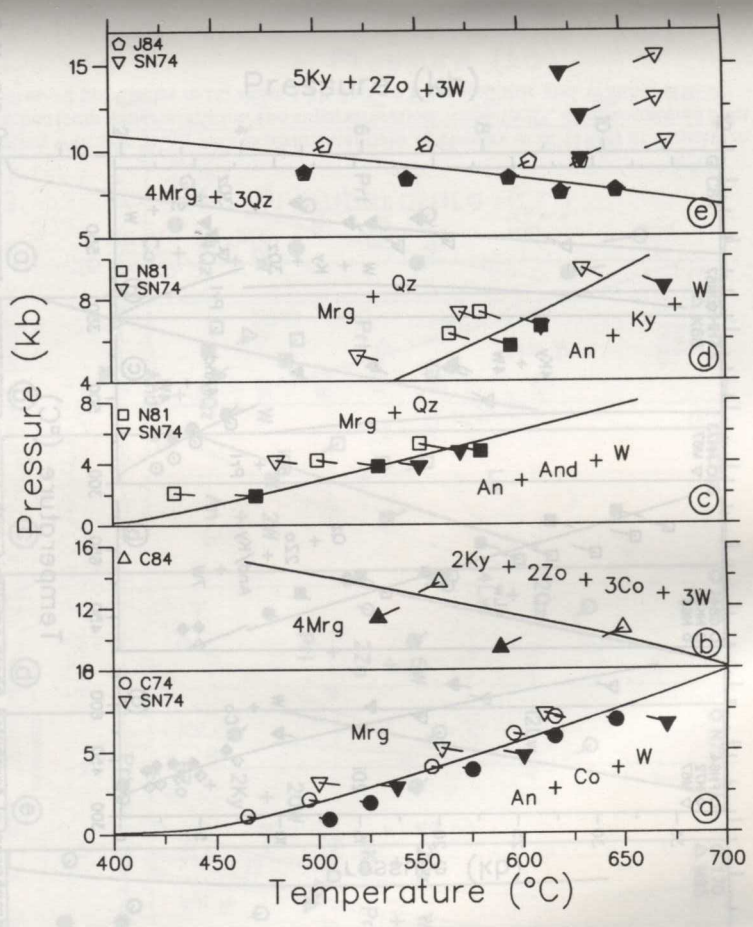

FIG. 13. Comparison of computed phase equilibria with experimental data in the system CaO–Al_2O_3–SiO_2–H_2O: J84—Jenkins (1984); SN74—Storre & Nitsch (1974); N81—Nitsch *et al.* (1981); C84—Chatterjee *et al.* (1984); C74—Chatterjee (1974). Symbols as in Fig. 4.

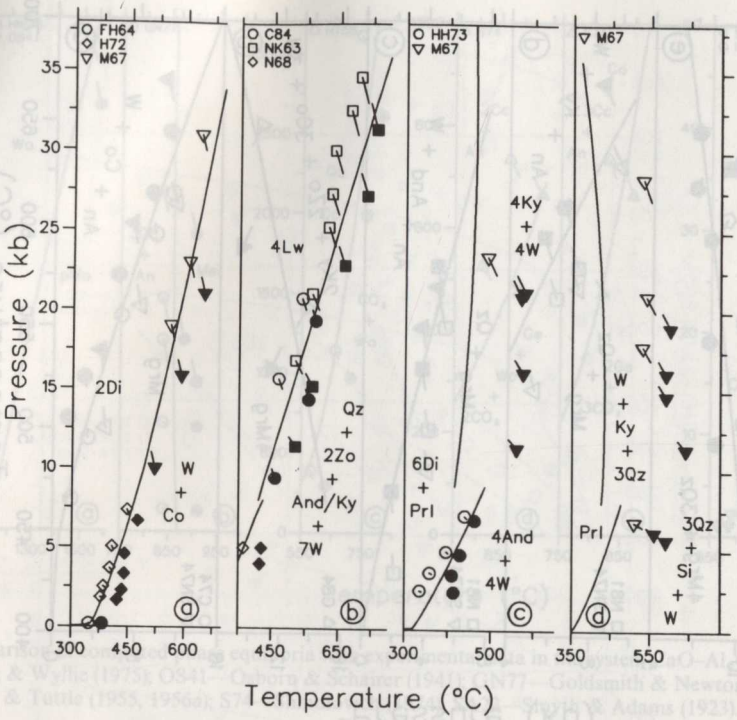

FIG. 14. Comparison of computed phase equilibria with experimental data in the system Al_2O_3–SiO_2–H_2O: FH64—Fyfe & Hollander (1964); H72—Haas (1972); M67—Matsushima *et al.* (1967); C84—Chatterjee *et al.* (1984); NK63—Newton & Kennedy (1963); N68—Nitsch (1968); HH 73—Haas & Holdaway (1973). Symbols as in Fig. 4.

Chatterjee *et al.* (1984) confirm the position of the higher temperature metastable equilibrium (Fig. 15a), while data reported by Connolly & Kerrick (1985) suggest that the stable breakdown reaction (Fig. 15b) occurs about 20° lower at 4 kb than Liou's data. To accommodate these phase equilibrium data, as well as the unpublished data of J. G. Liou (Fig. 17c), the reported experimental uncertainties were expanded for all phase equilibrium data (±20°), and the S^{P_r,T_r} and Cp of prehnite were modified slightly from the preferred calorimetric data (see Appendix). In addition, a thermal expansivity function for prehnite was derived which shows a much greater temperature dependence ($\alpha = 1{\cdot}85 \times 10^{-5}$ at 100 °C and 10.6×10^{-5} at 500 °C) than estimated from measurements of structurally similar minerals. Until additional experimental data addressing these inconsistencies are available, the thermodynamic properties of prehnite presented here should be considered highly provisional.

Periclase, brucite, talc, enstatite, anthophyllite, forsterite

Detailed analysis of phases in the MgO–SiO_2–H_2O was presented by Berman *et al.* (1986). Although the standard state properties derived for these phases in this study are slightly different due to the incorporation of expansivity and compressibility data for all minerals, the conclusions reached in the previous study are supported and only briefly reiterated below.

The recent extensive phase equilibrium study of Chernosky *et al.* (1985) can be combined with calorimetric data of Krupka *et al.* (1985*a*) to derive a set of thermodynamic properties of phases in the system MgO–SiO_2–H_2O which are consistent with all available phase equilibrium data (Figs. 18 and 19) with the following exceptions: (a) the 2 kb bracket of Franz (1982) for the brucite–periclase equilibrium (Fig. 19a) is inconsistent with the more extensive data of Barnes and Ernst (1963); (b) the

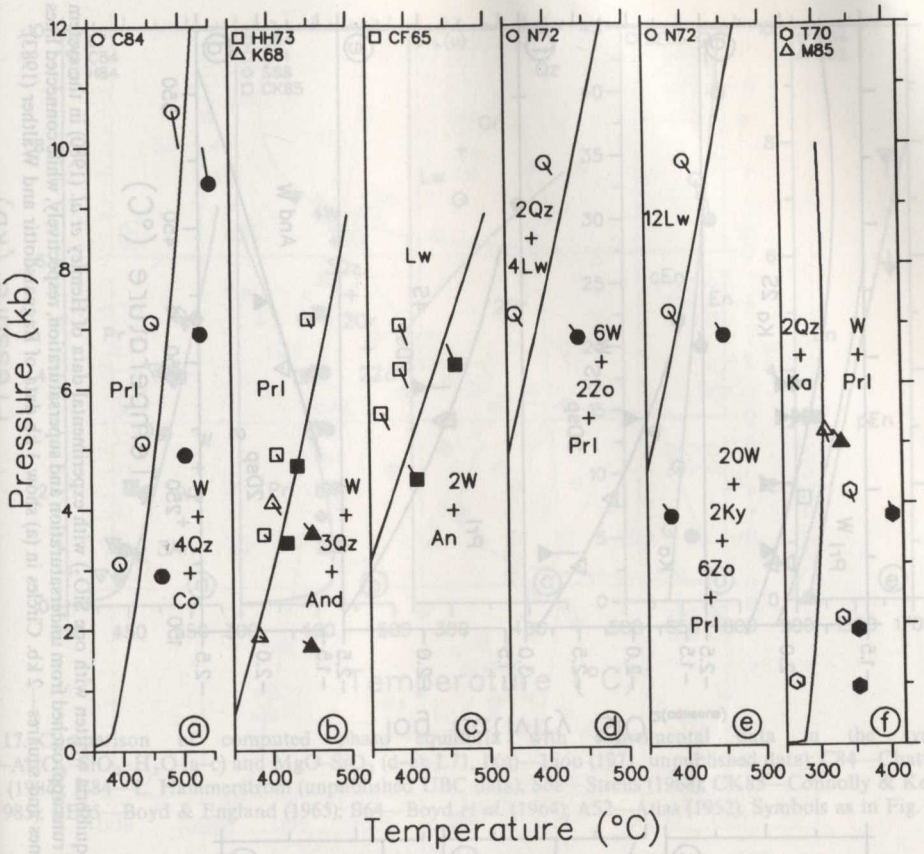

FIG. 15. Comparison of computed phase equilibria with experimental data in the system Al_2O_3–SiO_2–H_2O: C84—Chatterjee *et al.* (1984); HH73—Haas & Holdaway (1973); K68—Kerrick (1968); CF65—Crawford & Fyfe (1965; corrected by Perkins *et al.*, 1980); N72—Nitsch (1972); T70—Thompson (1970); M85—McPhail (1985). Symbols as in Fig. 4.

high pressure data (Figs. 19b–c) of Kitihara *et al.* (1966) are displaced to higher temperature than the computed equilibrium curves and than Holland's (1985) bracket shown in Fig. 19b, probably due to the use of poorly characterized starting materials that were synthesized in experimental runs of extremely short duration; and (c) several of Greenwood's (1963) half-brackets for equilibria involving anthophyllite (Fig. 18a, d) are inconsistent with the data of Chernosky *et al.* (1985). Examination of Greenwood's unpublished run data suggests that the inconsistencies stem from the use in some runs of starting materials containing phases extraneous to those in these equilibria. The changes in phase proportions observed by Greenwood in the discrepant runs are interpreted to have resulted from the operation of reactions other than those which he was persuing. The calculated concentrations of aqueous silica in equilibrium with MSH mineral pairs (Fig. 20) are in excellent agreement with Hemley *et al.*'s (1977*a*, *b*) experimental data, and with the solubility product of talc determined at 1 b and 298·15 K by Bricker *et al.* (1973).

The phase diagram limiting the stability of anthophyllite is very similar to the topology originally predicted by Greenwood, and shows a somewhat expanded stability field for anthophyllite compared to the data of Helgeson *et al.* (1978). Two invariant points which limit the high pressure stability field of anthophyllite occur at 793 °C–12·0 kb and 685 °C–6·4 kb, and are repeated at very low pressures (552 °C–62 b and 553 °C–128 b).

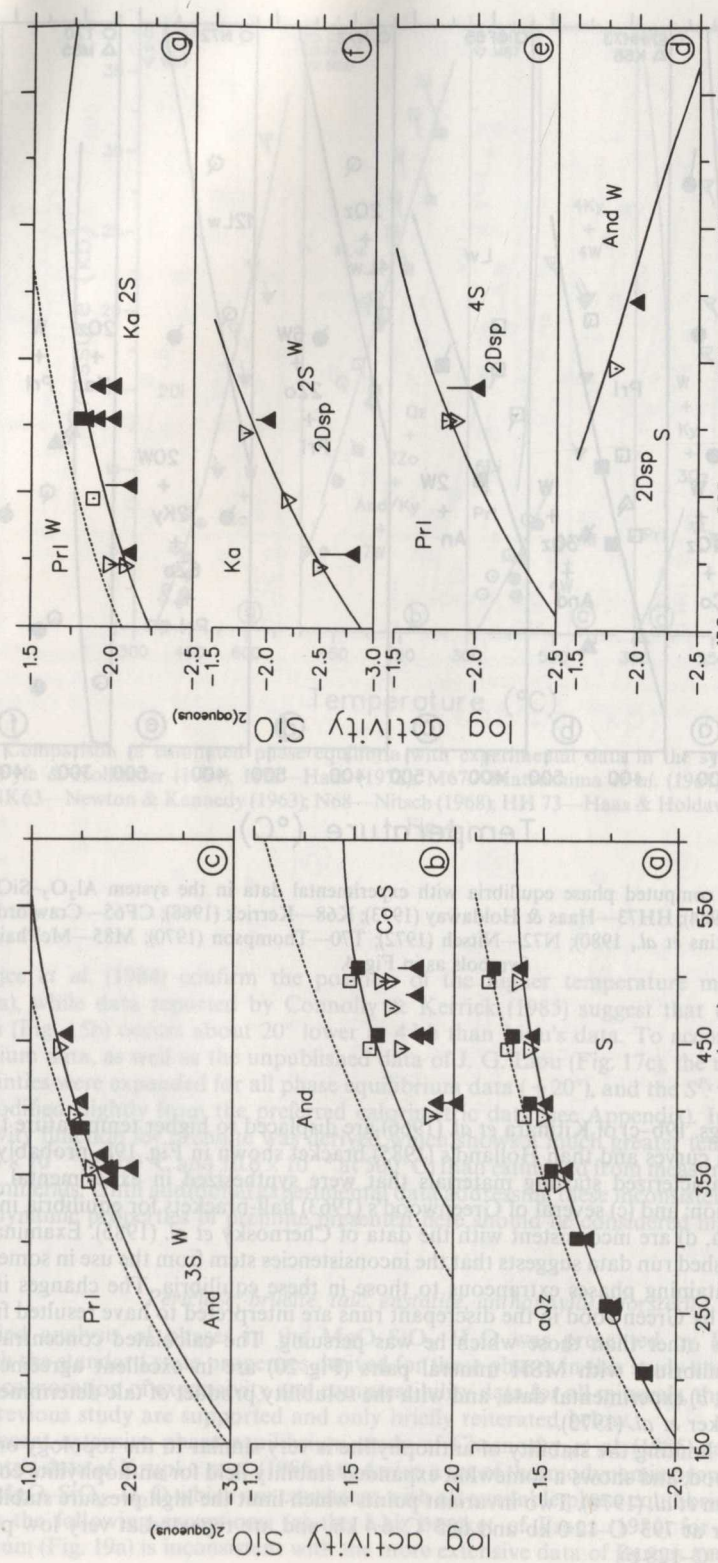

FIG. 16. Comparison of computed aqueous silica (S) activities (referenced to equilibria written with one SiO_2) with experimental data of Hemley *et al.* (1980) in the system Al_2O_3–SiO_2–H_2O. Filled and open symbols show initial silica concentrations of runs approached from undersaturation and supersaturation, respectively, while connected lines indicate final silica concentrations. Solid lines and triangles—1 kb; dotted lines and squares—2 kb. Circles in (a) show 1 kb data of Ragnarsdottir and Walther (1983).

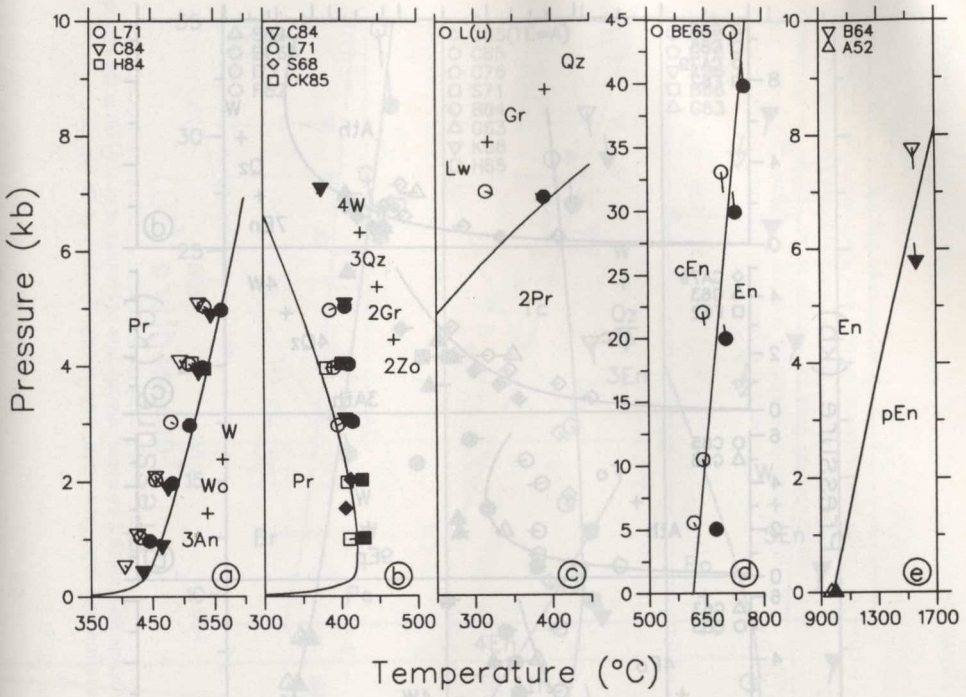

FIG. 17. Comparison of computed phase equilibria with experimental data in the systems $CaO–Al_2O_3–SiO_2–H_2O$ (a–c) and $MgO–SiO_2$ (d–e): L71, L(u)—Liou (1971, unpublished data); C84—Chatterjee *et al.* (1984); H84—L. Hammerstrom (unpublished UBC data); S68—Strens (1968); CK85—Connolly & Kerrick (1985); BE65—Boyd & England (1965); B64—Boyd *et al.* (1964); A52—Atlas (1952). Symbols as in Fig. 4.

Chernosky's (1982) data for the upper thermal stability of chrysotile are not completely compatible with calorimetric and volumetric data for chrysotile, talc, and forsterite. The tabulated thermodynamic properties of chrysotile are consistent with all thermophysical data and with all phase equilibrium brackets except for those at 0·5 kb (+10°) and 2 kb (+5°), in which the amount of reaction was reported to have been moderate and weak, respectively. Additional experimental data at 1 and 2 kb (Fig. 21a) support the position of the computed equilibrium curve.

The thermodynamic properties of chrysotile and antigorite are not consistent with the solubility data (Fig. 22) of Hemley *et al.* (1977*a*, *b*), who may have obtained spurious results due to grain size effects. Thermodynamic properties of these phases derived from Hemley *et al.*'s work (Helgeson *et al.*, 1978) render chrysotile metastable with respect to antigorite and brucite at all temperatures and pressures, in contrast to geologic evidence (Evans, 1977). The computed position for this equilibrium resulting from the present analysis is 250 °C at 2 kb.

Thermophysical data for all phases are compatible with the phase equilibrium data, with two exceptions: the enthalpies of formation of talc and anthophyllite are about 19 and 17 $kJmol^{-1}$ less negative, respectively, than determined by Weeks (1955).

Akermanite, monticellite, merwinite, diopside

Recent calorimetric determinations of the heats of solution of akermanite, monticellite, and merwinite (Brousse *et al.*, 1984) are 10–30 $kJmol^{-1}$ less negative than the earlier measurements of Neuvonen (1952*a*, *b*). In addition, Brousse *et al.* (1984) confirmed the data of Moore & Araki (1972) which show that the molar volume of merwinite is about 0·6 Jb^{-1} smaller than that tabulated by Robie *et al.* (1967), and utilized in the analysis of Helgeson *et al.* (1978). These significant refinements

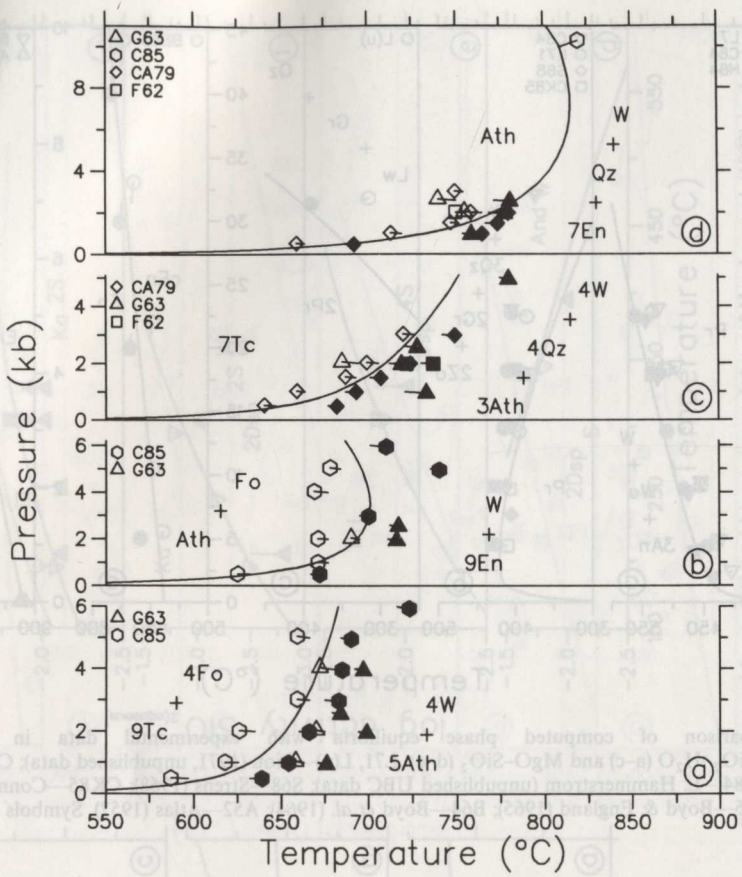

FIG. 18. Comparison of computed phase equilibria with experimental data in the system MgO–SiO_2–H_2O: G63—Greenwood (1963); C85—Chernosky *et al.* (1985); CA79—Chernosky & Autio (1979); F62—Fyfe (1962). Symbols as in Fig. 4.

in calorimetric/volumetric data are in excellent agreement with volatile-absent phase equilibria (Fig. 23a, b), with mixed volatile equilibria (Fig. 24) studied by Zharikov *et al.* (1977), and with the P_{CO_2}–T data (Walter, 1963*a*, *b*) shown in Figs. 25b–d. The latter agreement is somewhat surprising in that the locations of Walter's experimental data for the four equilibria shown in Figs. 25a–d are virtually indistinguishable from one another. The calculated position for the breakdown of forsterite + calcite to monticellite + periclase + CO_2 (Fig. 25a), however, is approximately 100° above Walter's (1963*b*) data, a discrepancy which is likely due to Walter's failure to recognize periclase in any run products. The small amount of monticellite reported by Walter in these run products could have formed via the reaction: forsterite + calcite + diopside = monticellite + CO_2 (Fig. 25b) if starting mixes contained a slight excess of SiO_2.

Tremolite

The data of Yin & Greenwood (1983) on the upper stability of tremolite (Fig. 25e) tightly constrain the thermodynamic properties of tremolite, when taken in conjunction with redeterminations of the entropies of diopside and orthoenstatite (Krupka *et al.*, 1985*a*). The derived properties of tremolite are also in excellent agreement with the phase equilibrim data of Jenkins (1983) on the breakdown of

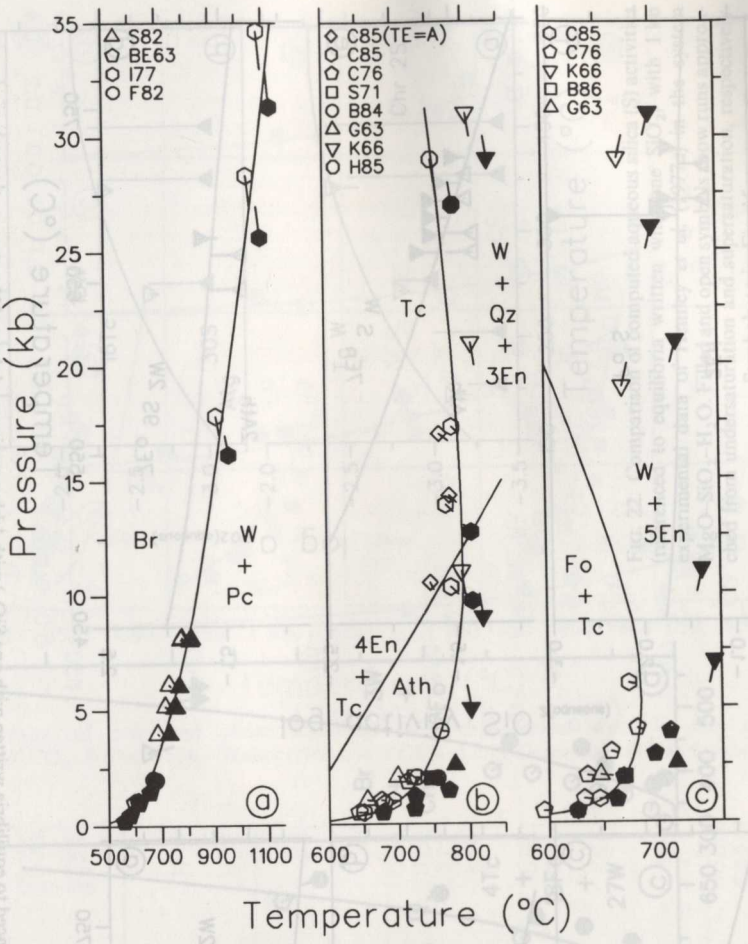

FIG. 19. Comparison of computed phase equilibria with experimental data in the system MgO–SiO_2–H_2O: S82—Schramke *et al.* (1982); BE63—Barnes & Ernst (1963); 177—Iriving *et al.* (1977); F82—Franz (1982); C85—Chernosky *et al.* (1985); C76—Chernosky (1976); S71—Skippen (1971); B84—P. Bartholomew (unpublished UBC data); G63—Greenwood (1963); K66—Kitihara *et al.* (1966); H85—T. J. B. Holland (unpublished data reported by Chernosky *et al.*, 1985); B86—Berman *et al.* (1986). Symbols as in Fig. 4.

tremolite + forsterite at high pressure (Fig. 23c), and with numerous equilibria studied in mixed volatile fluids (Figs. 26b, c and 27). The data of Metz (1970) for the equilibrium tremolite + calcite + quartz = diopside + CO_2 + H_2O (Fig. 27b) indicate higher temperatures than determined by Slaughter *et al.* (1975) and computed with the thermodynamic properties derived in this study. This inconsistency is larger than can be reasonably ascribed to differences in the tremolite compositions in these two studies, and would seem to require further experimental work to resolve.

The calculated enthalpy of formation of tremolite is approximately 50 $kJmol^{-1}$ less negative than the value derived from the HF measurements of Weeks (1955); some of this discrepancy may be related to grain size effects that markedly affect the heats of solution of tremolite (Nitkiewicz *et al.*, 1984).

Dolomite

Disordering of Ca and Mg atoms in dolomite has been incorporated using the model of Navrotsky & Loucks (1977), and 1423 K as the temperature at which dolomite is completely disordered (Reeder

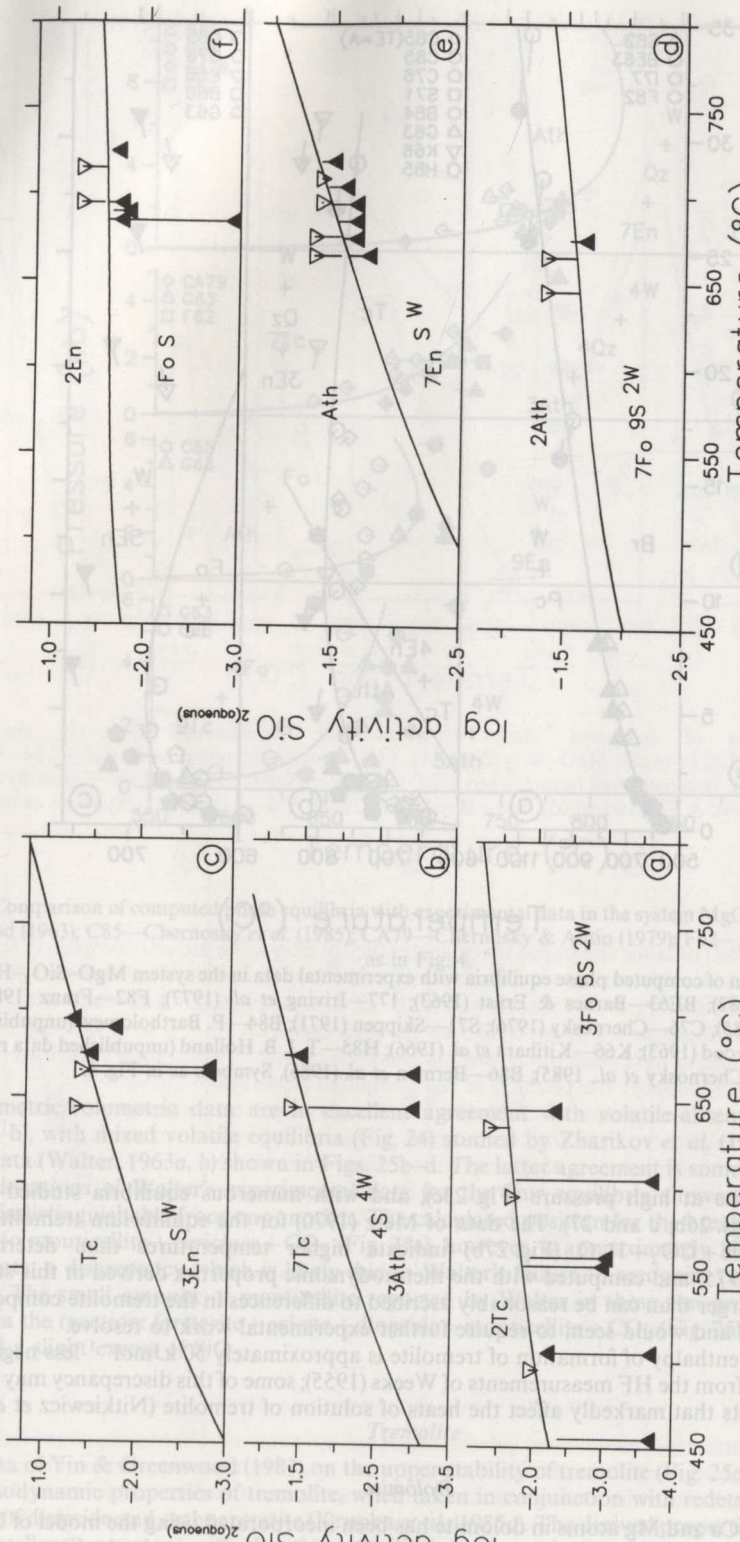

FIG. 20. Comparison of computed aqueous silica (S) activities (referenced to equilibria written with one SiO_2) with 1 kb experimental data of Hemley *et al.* (1977*b*) in the system $MgO–SiO_2–H_2O$. Filled and open symbols show runs approached from undersaturation and supersaturation, respectively. Symbols as in Fig. 16.

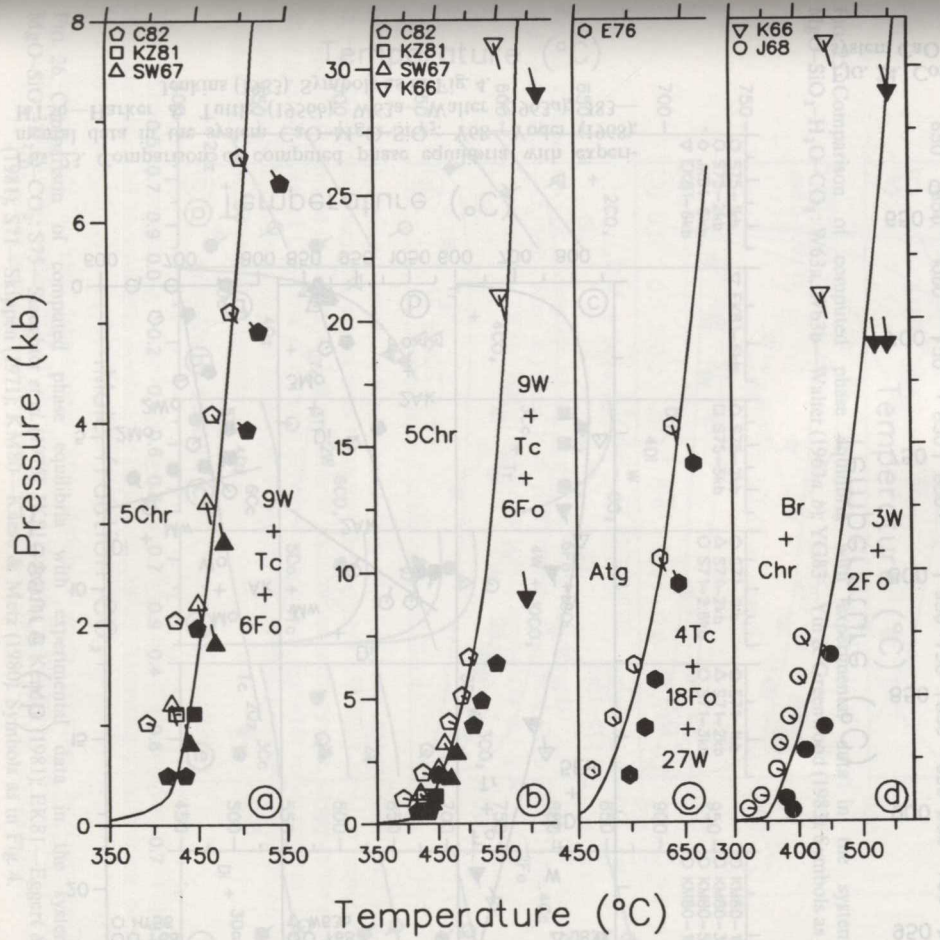

FIG. 21. Comparison of computed phase equilibria with experimental data in the system MgO–SiO_2–H_2O: C82—Chernosky (1982); KZ81—Kalinin & Zubkov (1981); SW67—Scarfe & Wyllie (1967); K66—Kitihara *et al.* (1966); E76—Evans *et al.* (1976); J68—Johannes (1968). Symbols as in Fig. 4.

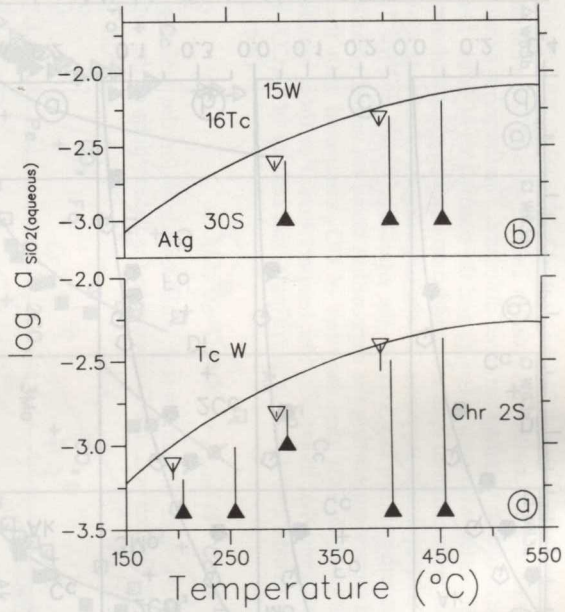

FIG. 22. Comparison of computed aqueous silica (S) activities (referenced to equilibria written with one SiO_2) with 1 kb experimental data of Hemley *et al.* (1977*a*) in the system MgO–SiO_2–H_2O. Filled and open symbols show runs approached from undersaturation and supersaturation, respectively. Symbols as in Fig. 16.

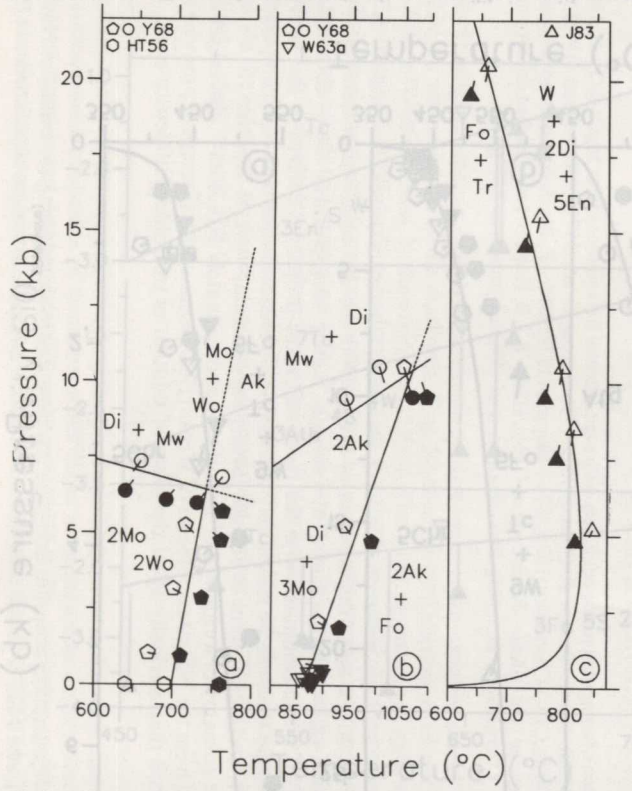

FIG. 23. Comparison of computed phase equilibria with experimental data in the system CaO–MgO–SiO_2: Y68—Yoder (1968); HT56—Harker & Tuttle (1956*b*); W63a—Walter (1963*a*); J83—Jenkins (1983). Symbols as in Fig. 4.

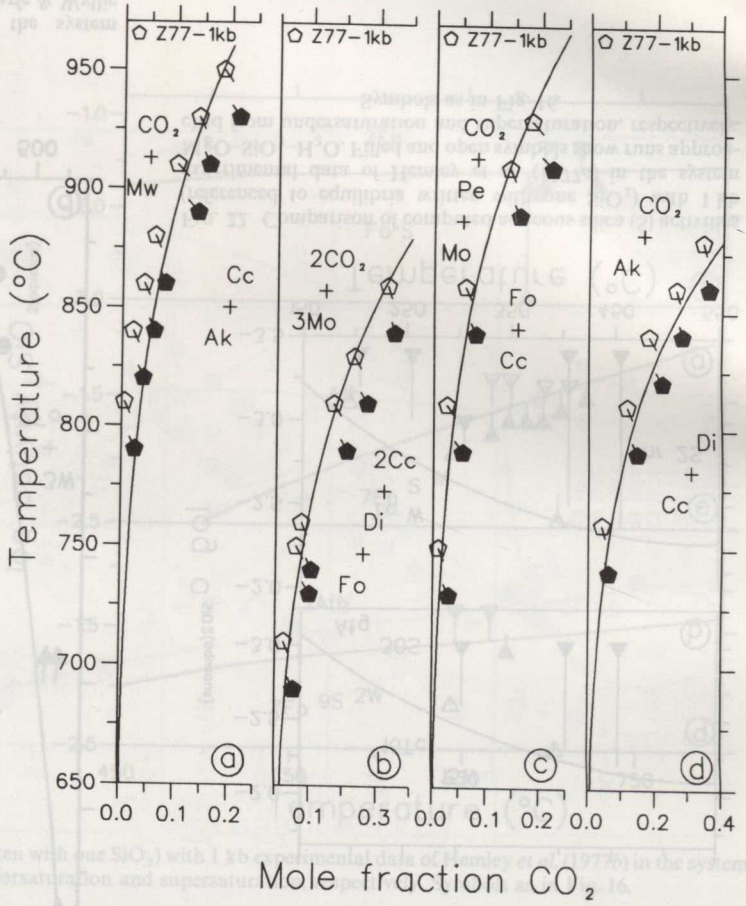

FIG. 24. Comparison of computed phase equilibria with experimental data in the system CaO–MgO–SiO_2–CO_2: Z77—Zharikov *et al.* (1977). Symbols as in Fig. 4.

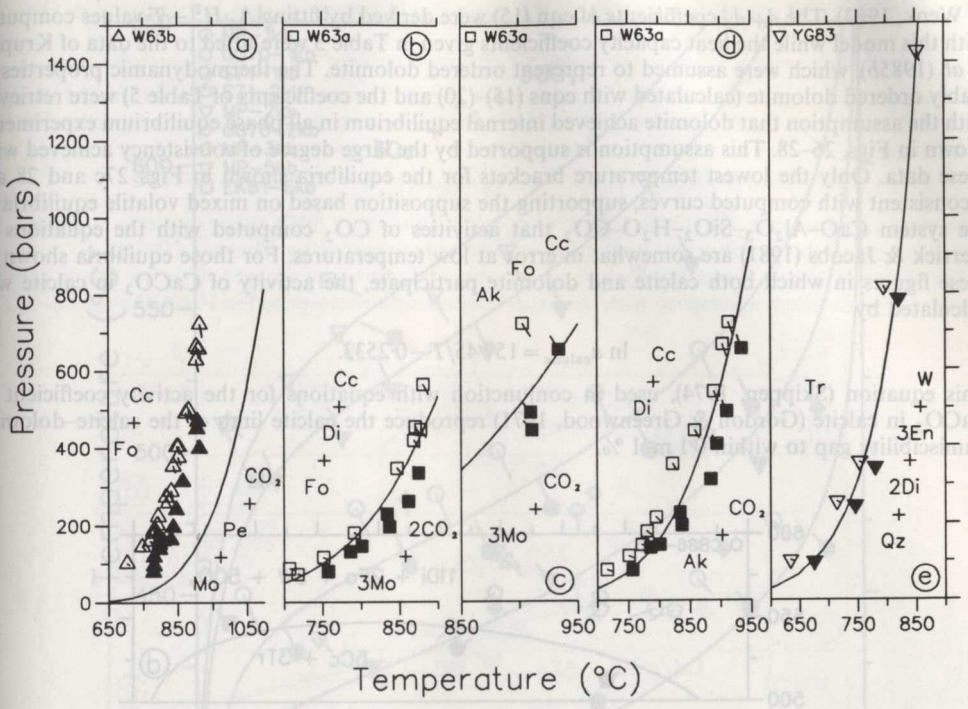

FIG. 25. Comparison of computed phase equilibria with experimental data in the system CaO–MgO–SiO_2–H_2O–CO_2: W63a, W63b—Walter (1963*a*, *b*); YG83—Yin & Greenwood (1983). Symbols as in Fig. 4.

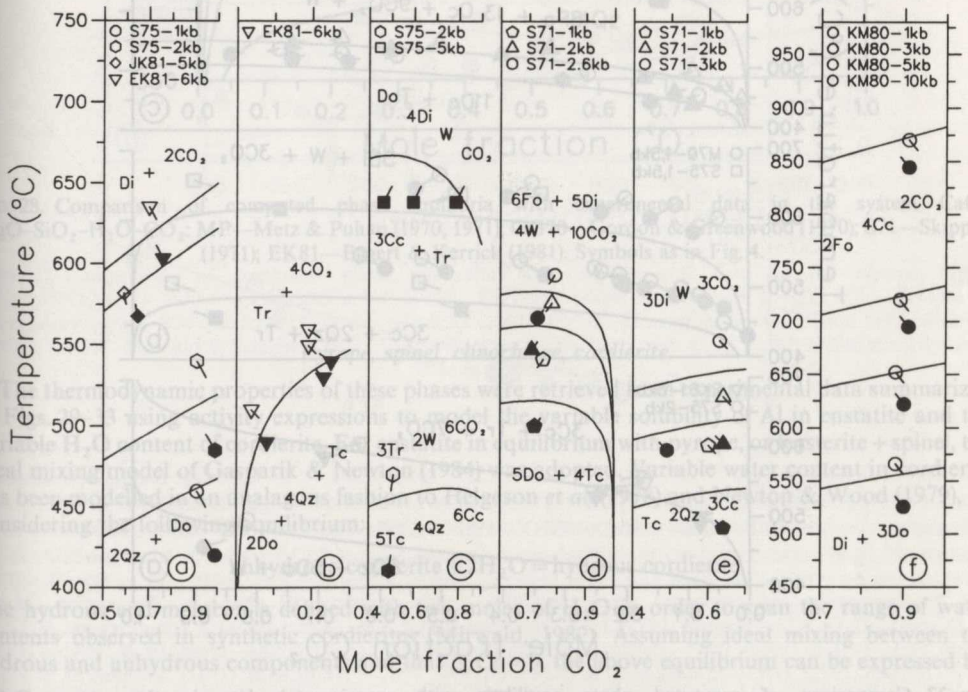

FIG. 26. Comparison of computed phase equilibria with experimental data in the system CaO–MgO–SiO_2–H_2O–CO_2: S75—Slaughter *et al.* (1975); JK81—Jacobs & Kerrick (1981); EK81—Eggert & Kerrick (1981); S71—Skippen (1971); KM80—Kaese & Metz (1980). Symbols as in Fig. 4.

& Wenk, 1983). The d_0–d_5 coefficients of eqn (15) were derived by fitting $\Delta_{ds}H^T - T$ values computed with this model while the heat capacity coefficients given in Table 3 were fitted to the data of Krupka *et al.* (1985*b*), which were assumed to represent ordered dolomite. The thermodynamic properties of stably ordered dolomite (calculated with eqns (15)–(20) and the coefficients of Table 5) were retrieved with the assumption that dolomite achieved internal equilibrium in all phase equilibrium experiments shown in Figs. 26–28. This assumption is supported by the large degree of consistency achieved with these data. Only the lowest temperature brackets for the equilibria shown in Figs. 27c and 28 are inconsistent with computed curves, supporting the supposition based on mixed volatile equilibria in the system CaO–Al_2O_3–SiO_2–H_2O–CO_2 that activities of CO_2 computed with the equations of Kerrick & Jacobs (1981) are somewhat in error at low temperatures. For those equilibria shown in these figures in which both calcite and dolomite participate, the activity of $CaCO_3$ in calcite was calculated by

$$\ln a_{\text{calcite}} = 157{\cdot}45/T - 0{\cdot}2533.$$

This equation (Skippen, 1974), used in conjunction with equations for the activity coefficient of $CaCO_3$ in calcite (Gordon & Greenwood, 1971) reproduce the calcite limb of the calcite–dolomite immiscibility gap to within 0·1 mol %.

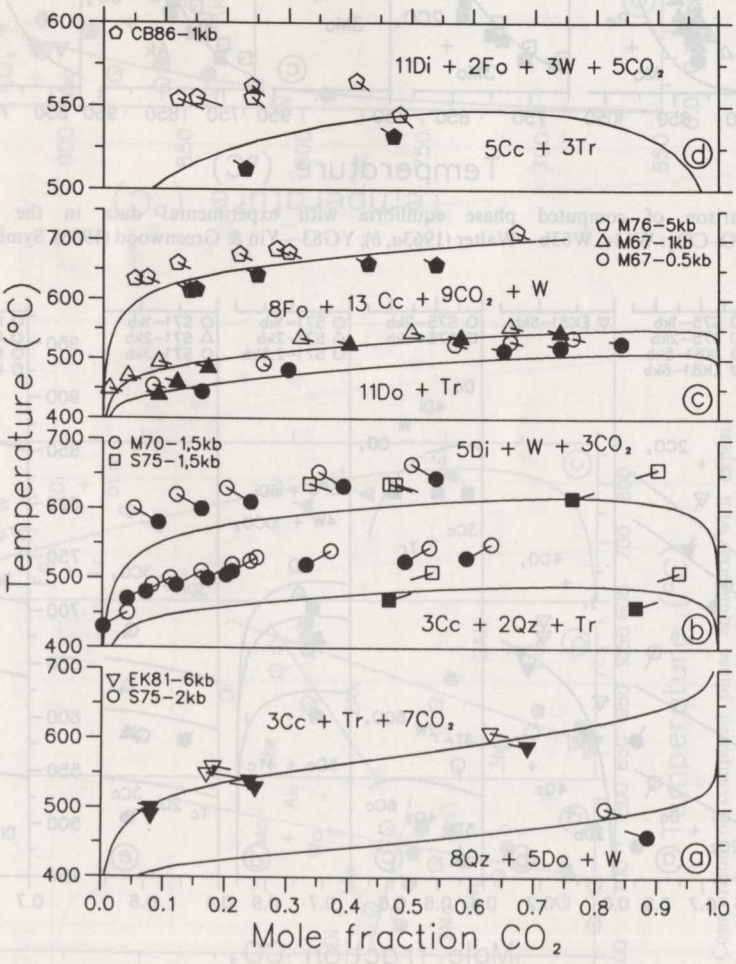

FIG. 27. Comparison of computed phase equilibria with experimental data in the system CaO–MgO–SiO_2–H_2O–CO_2: CB86—Chernosky & Berman (1986*a*); M67, M70, M76—Metz (1967, 1970, 1976); S75—Slaughter *et al.* (1975); EK81—Eggert & Kerrick (1981). Symbols as in Fig. 4.

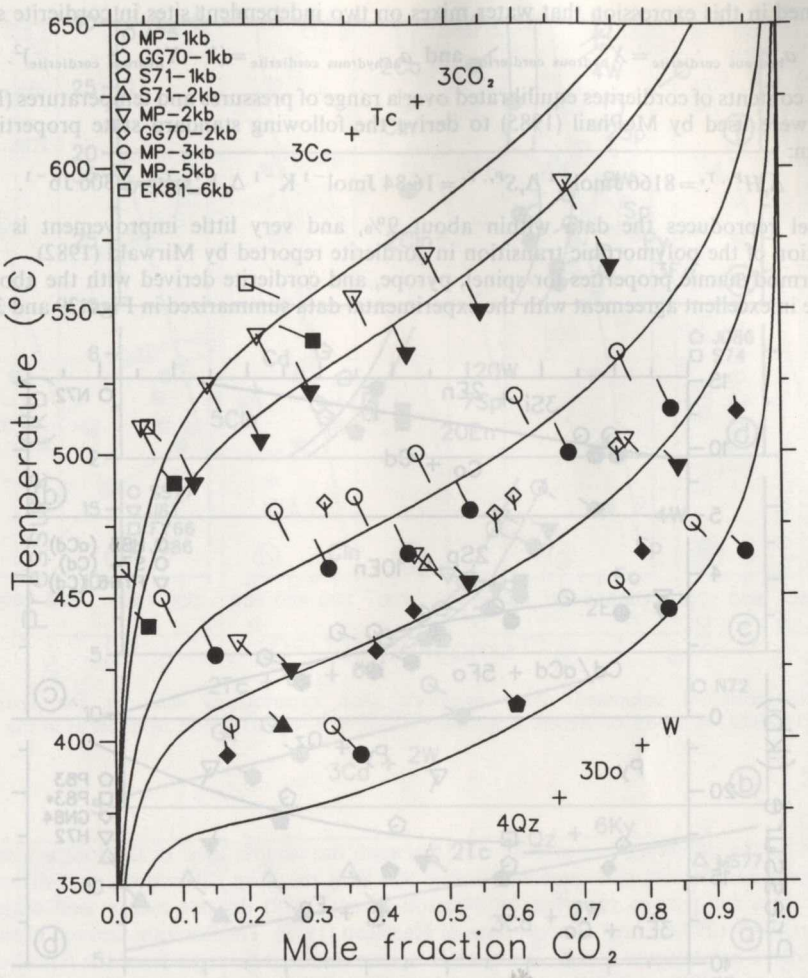

FIG. 28. Comparison of computed phase equilibria with experimental data in the system CaO–MgO–SiO_2–H_2O–CO_2: MP—Metz & Puhan (1970, 1971); GG70—Gordon & Greenwood (1970); S71—Skippen (1971); EK81—Eggert & Kerrick (1981). Symbols as in Fig. 4.

Pyrope, spinel, clinochlore, cordierite

The thermodynamic properties of these phases were retrieved from experimental data summarized in Figs. 29–33 using activity expressions to model the variable solubility of Al in enstatite and the variable H_2O content of cordierite. For enstatite in equilibrium with pyrope, or forsterite + spinel, the ideal mixing model of Gasparik & Newton (1984) was adopted. Variable water content in cordierite has been modelled in an analagous fashion to Helgeson *et al.* (1978) and Newton & Wood (1979), by considering the following equilibrium:

$$\text{anhydrous cordierite} + 2H_2O = \text{hydrous cordierite}$$

The hydrous end-member is defined with two moles of H_2O in order to span the range of water contents observed in synthetic cordierites (Mirwald, 1982). Assuming ideal mixing between the hydrous and anhydrous components and that $\Delta_r Cp = 0$, the above equilibrium can be expressed by:

$$-\Delta_r H^{P_r,T_r} + T\Delta_r S - (P-P_r)\Delta_r V_{\text{solid}} + 2\int_{P_r}^{P} V_{H_2O}\,dp = 2RT \ln\left(\frac{X_{\text{hydrous cordierite}}}{X_{\text{anhydrous cordierite}}}\right).$$

It is assumed in this expression that water mixes on two independent sites in cordierite so that

$$a_{\text{hydrous cordierite}} = X^2_{\text{hydrous cordierite}} \text{ and } a_{\text{anhydrous cordierite}} = (1 - X_{\text{hydrous cordierite}})^2.$$

The water contents of cordierites equilibrated over a range of pressures and temperatures (Mirwald *et al.*, 1979) were used by McPhail (1985) to derive the following standard state properties for this equilibrium:

$$\Delta_r H^{P_r, T_r} = 8166 \text{ Jmol}^{-1} \quad \Delta_r S^{P_r, T_r} = 16{\cdot}84 \text{ Jmol}^{-1} \text{ K}^{-1} \quad \Delta_r V^{P_r, T_r}_{\text{solid}} = 2{\cdot}306 \text{ Jb}^{-1}.$$

This model reproduces the data within about 9%, and very little improvement is gained by consideration of the polymorphic transition in cordierite reported by Mirwald (1982).

The thermodynamic properties for spinel, pyrope, and cordierite derived with the above activity models are in excellent agreement with the experimental data summarized in Figs. 29 and 30a–b. The

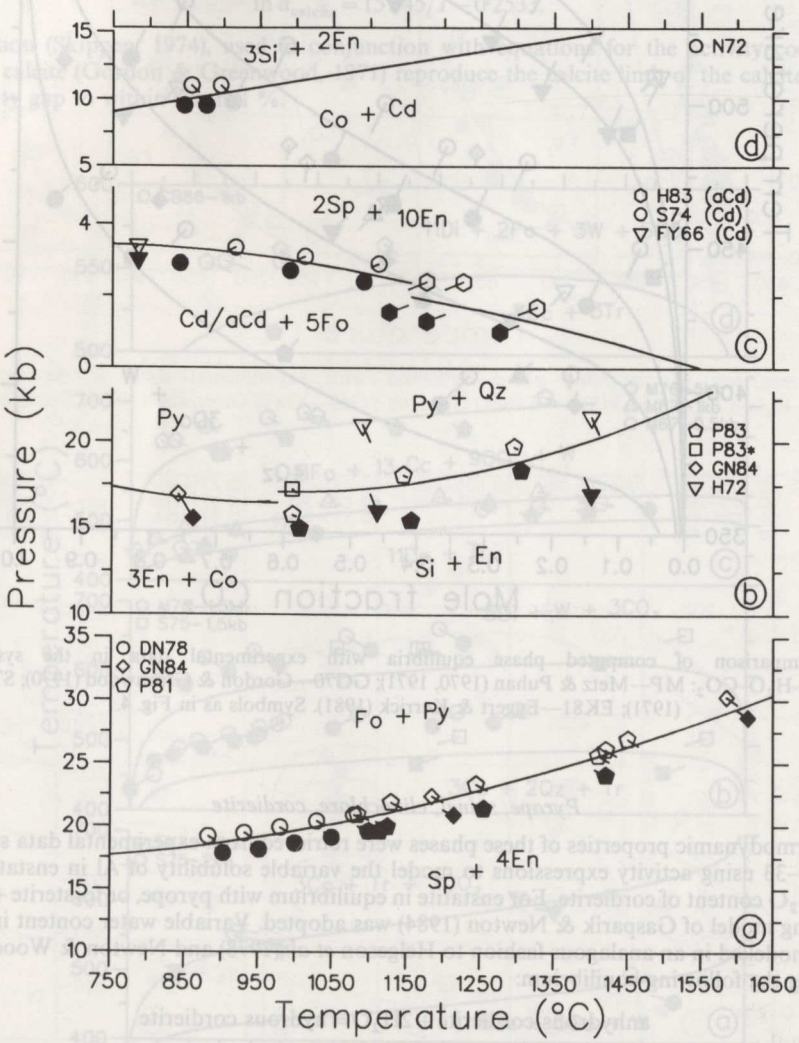

FIG. 29. Comparison of computed phase equilibria with experimental data in the system MgO–Al_2O_3–SiO_2–H_2O: N72—Newton (1972); H83—Herzberg (1983); S74—Seifert (1974); FY66—Fawcett & Yoder (1966); P83—Perkins (1983); P83*—Perkins (1983; uncorrected for friction); GN84—Gasparik & Newton (1984); H72—Hensen (1972); DN78—Danckwerth & Newton (1978); P81—Perkins *et al.* (1981). Symbols as in Fig. 4. Note that the lower temperature curve in (c) with hydrous cordierite reproduces the $P_{H_2O} = P_{\text{total}}$ data of Seifert (1974) and Fawcett & Yoder (1966), while the higher temperature curve with anhydrous cordierite (aCd) reproduces the $P_{H_2O} = 0$ data of Herzberg (1983).

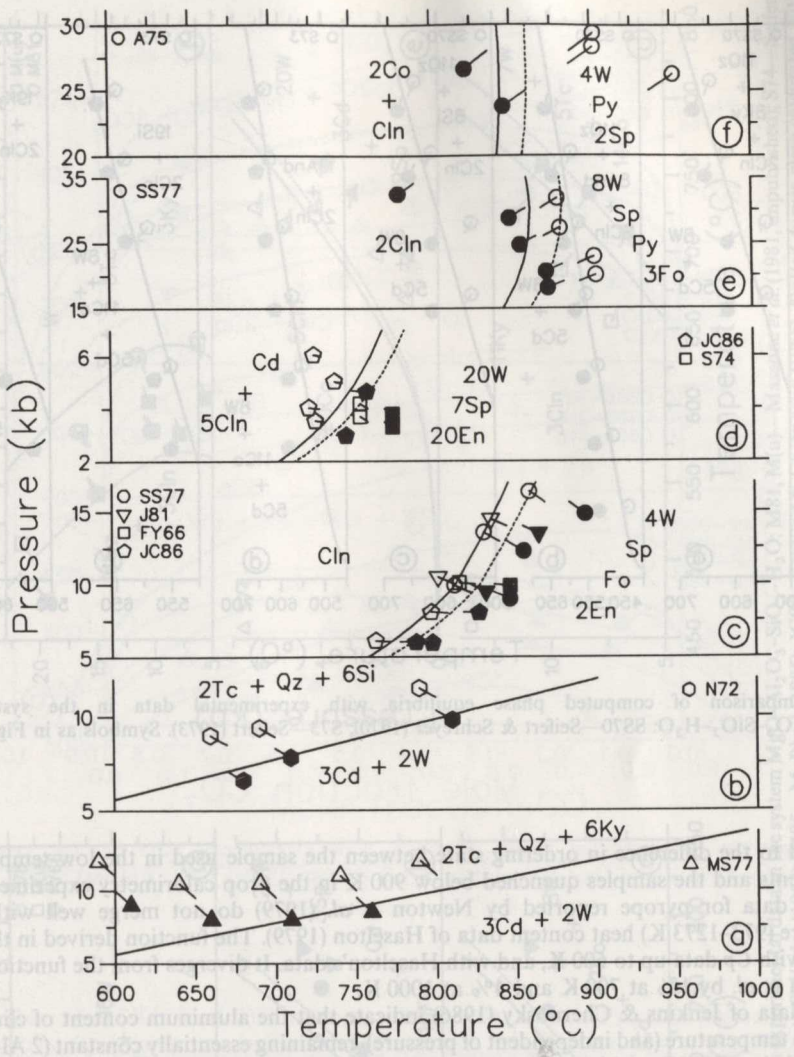

FIG. 30. Comparison of computed phase equilibria with experimental data in the system MgO–Al_2O_3–SiO_2–H_2O: A75—Ackermand *et al.* (1975); SS77—Staudigel & Schreyer (1977); JC86—Jenkins & Chernosky (1986); S74—Seifert (1974); J81—Jenkins (1981); FY66—Fawcett & Yoder (1966); N72—Newton (1972); MS77—Mirwald & Schreyer (1977). Dotted lines were calculated with $a_{\text{clinochlore}} = 0{\cdot}70$ (see text). Symbols as in Fig. 4.

refined entropy of spinel ($S^{P_r, T_r} = 84{\cdot}54$ Jmol^{-1} K^{-1}) is 3·96 Jmol^{-1} K^{-1} higher than that resulting from the low temperature *Cp* measurements of King (1955). This difference can be attributed to a zero point contribution for partial disordering of Mg and Al atoms between tetrahedral and octahedral sites. Although the disordering process is undoubtably dependent on temperature (e.g., Navrotsky, 1986; Wood *et al.*, 1986), the energetics of this process have not been sufficiently constrained by calorimetric data to provide the necessary data to derive temperature-dependent disordering parameters. In addition, more data regarding the kinetics of this process are needed to allow estimation of the degree of disorder in the spinel samples used to obtain the high temperature heat content data, from which the *Cp* function for spinel given in Table 3 was obtained. The data summarized by Navrotsky (1986) imply that samples equilibrated above about 900 K probably have reached internal equilibrium in the drop calorimetry experiments, and therefore that the entropy correction should

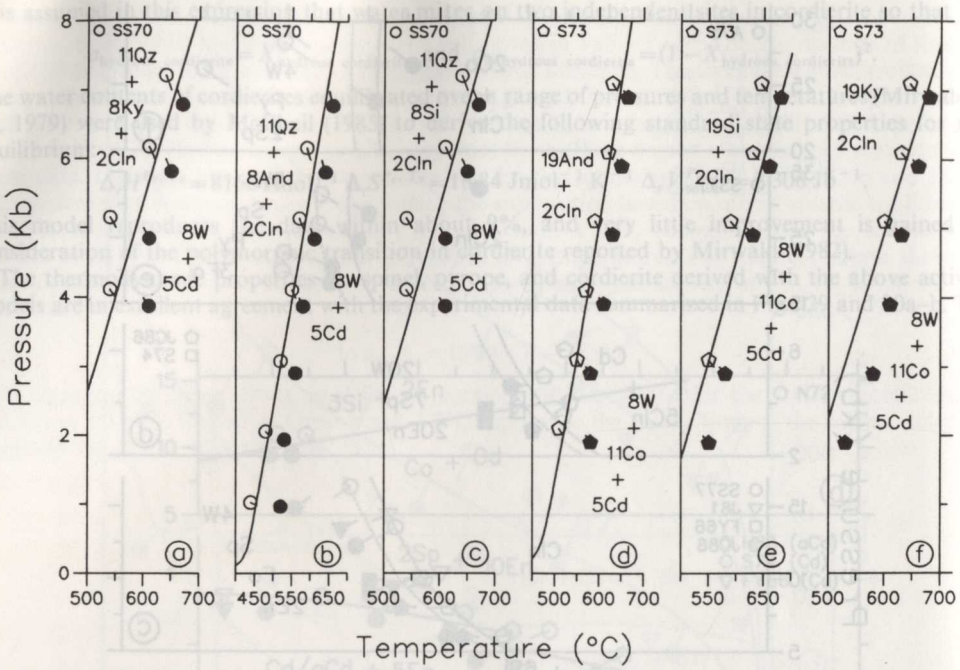

FIG. 31. Comparison of computed phase equilibria with experimental data in the system MgO–Al_2O_3–SiO_2–H_2O: SS70—Seifert & Schreyer (1970); S73—Seifert (1973). Symbols as in Fig. 4.

correspond to the difference in ordering state between the sample used in the low temperature *Cp* measurements and the samples quenched below 900 K in the drop calorimetry experiments.

The *Cp* data for pyrope reported by Newton *et al.* (1979) do not merge well with the high temperature (973–1273 K) heat content data of Haselton (1979). The function derived in this study is in accord with *Cp* data up to 600 K, and with Haselton's data. It diverges from the function reported by Newton *et al.* by 1% at 700 K and 4% at 1000 K.

Recent data of Jenkins & Chernosky (1986) indicate that the aluminum content of clinochlore is sensitive to temperature (and independent of pressure), remaining essentially constant (2 Al atoms/formula unit) below 700 °C, and increasing to 2·4 Al atoms/formula unit by its breakdown temperature. Various assumptions regarding the nature of this solid solution result in activities of clinochlore ranging from 0·6 to 0·8 in this aluminous chlorite. As a first approximation, the dependence of this tschermak's substitution on bulk composition has been ignored. It can be seen from Figs. 30c–f and 32a–b that accounting for this nonstoichiometry (dotted lines in these figures show the displaced equilibria computed with a clinochlore activity of 0·7) leads to very reasonable agreement with the phase equilibrium data.

The refined thermodynamic properties of 14 A° clinochlore are in excellent agreement with all experimental data shown in Figs. 30–33, with the exception of: (a) the equilibria shown in Fig. 32f (discussed below); (b) the 3 kb half-bracket of Chernosky (1978) for the equilibrium shown in Fig. 32c which is inconsistent with the unpublished results of Massone and with the other experimental constraints on the thermodynamic properties of clinochlore; (c) Seifert's (1974) data shown in Figs. 30d and 32e, which may be related to a greater abundance of 7 A° clinochlore in his starting materials that were produced in relatively short synthesis runs; and (d) Widmark's (1980) data (Fig. 33b) which lie at slightly higher temperatures than the computed equilibrium curves and at least in part reflect the more aluminous chlorites produced in his experiments. The analysis of the combined data yield $S^{P_r,T_r}_{\text{clinochlore}} = 435{\cdot}15$ Jmol^{-1} K^{-1}, which indicates substantial disorder (the maximum configurational entropy due to Mg, Al disorder between octahedral and tetrahedral sites is 41·4 Jmol^{-1} K^{-1}) in this phase when compared to the measured $S^{P_r,T_r}_{\text{clinochlore}}$ (397·6 Jmol^{-1} K^{-1}) reported by Henderson *et al.*

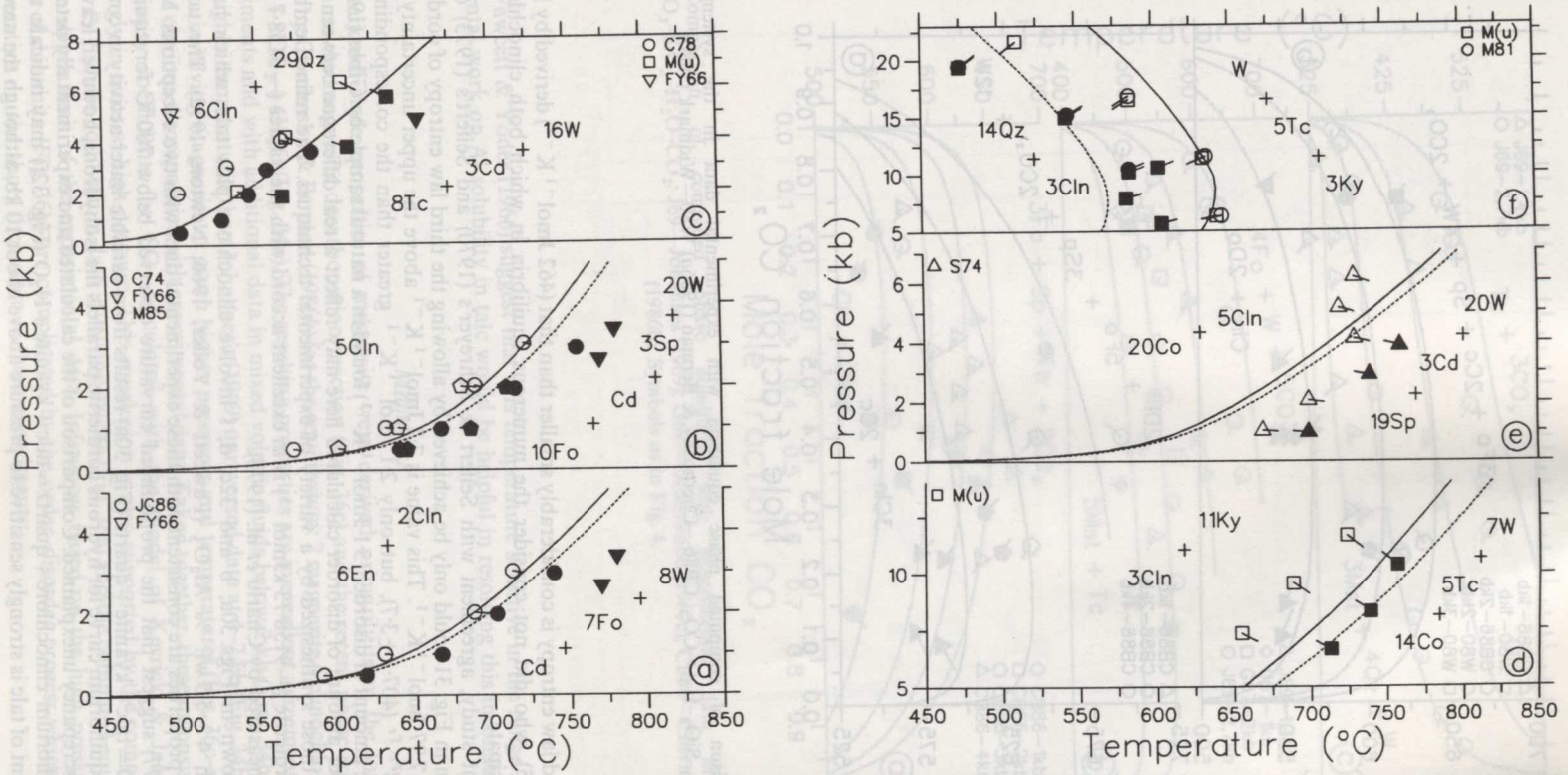

FIG. 32. Comparison of computed phase equilibria with experimental data in the system $MgO–Al_2O_3–SiO_2–H_2O$: M81, M(u)—Massone *et al.* (1981, unpublished); S74—Seifert (1974); C74, C78—Chernosky (1974, 1978); FY66—Fawcett & Yoder (1966); M85—McPhail (1985); JC86—Jenkins & Chernosky (1986). Dotted curves were calculated with $a_{clinochlore} = 0{\cdot}70$ in (a–e), and with $a_{talc} = 0{\cdot}60$ in (f) (see text). Symbols as in Fig. 4.

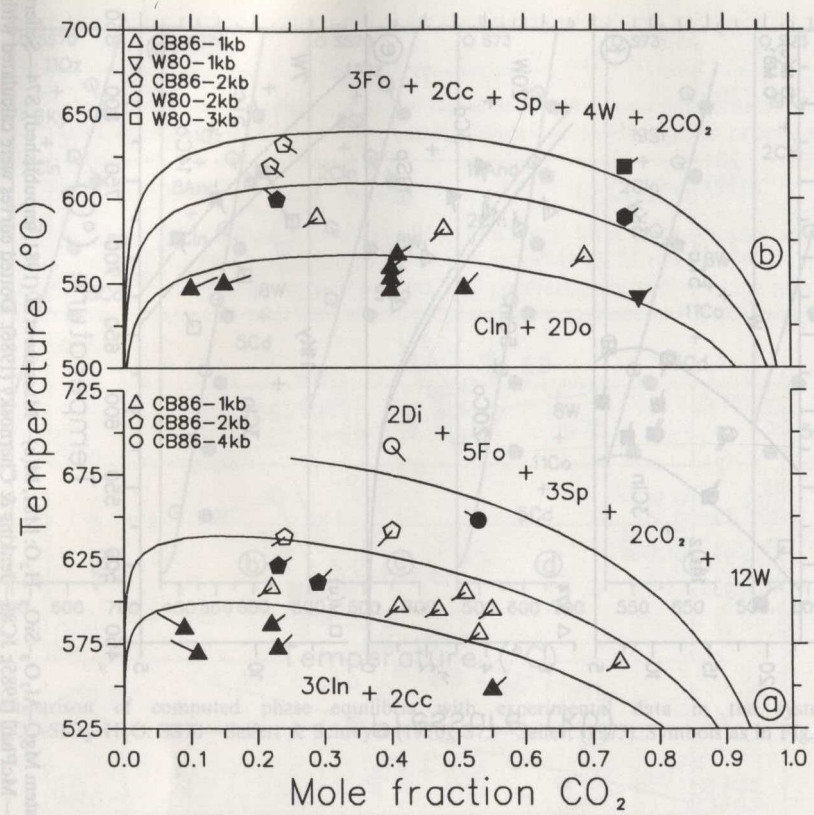

FIG. 33. Comparison of computed phase equilibria with experimental data in the system MgO–Al_2O_3–SiO_2–H_2O–CO_2: CB86—Chernosky & Berman (1986*a*) W80—Widmark (1980).

(1983). This third law entropy is considerably smaller than that (462 $Jmol^{-1}K^{-1}$) derived by Holland & Powell (1985), who did not consider the numerous equilibria in which both clinochlore and cordierite participate.

In the present study, agreement with Seifert & Schreyer's (1970) and Seifert's (1973) data for equilibria shown in Fig. 31 could only be achieved by allowing the third law entropy of cordierite to be as high as 417·97 $Jmol^{-1}K^{-1}$. This value is 7·2 $Jmol^{-1}K^{-1}$ above the upper uncertainty limit of the measured S^{P_r, T_r} (407·1 ± 3·7), but only 2·1 $Jmol^{-1}K^{-1}$ greater than the corresponding value corrected for the amount of disorder (5·1 $Jmol^{-1}K^{-1}$) found in a natural sample by Gibbs (1966). The somewhat greater amount of disorder calculated here may reflect a real difference between natural cordierites and those synthesized by a variety of experimental techniques. The refined enthalpy of formation of cordierite (−9158·73 $kJmol^{-1}$) is in excellent accord with the values (−9158·7 ± 6 and −9160·43 ± 6) measured by Charlu *et al.* (1975).

Equilibria shown in Figs. 30a, b and 32c, d, f involve clinochlore plus talc, which has been synthesized with 4·3–5·5 wt. % Al_2O_3 (Fawcett & Yoder, 1966; Newton, 1972). The tabulated thermodynamic properties are consistent with these experimental data with two exceptions. Mirwald & Schreyer (1977) suggest that the pronounced curvature observed below 700 °C for equilibrium cordierite + H_2O = talc + kyanite + quartz (Fig. 30a) results from variable water activity in cordierite. The calculated equilibrium curve for hydrous cordierite parallels the isohydrons, however, leaving the source of this discrepancy unexplained. Comparison of the calculated and experimentally determined position of equilibrium clinochlore + quartz = talc + kyanite + H_2O (Fig. 32f) may indicate that the aluminum content of talc is strongly sensitive to pressure above about 10 kb, although the unreversed

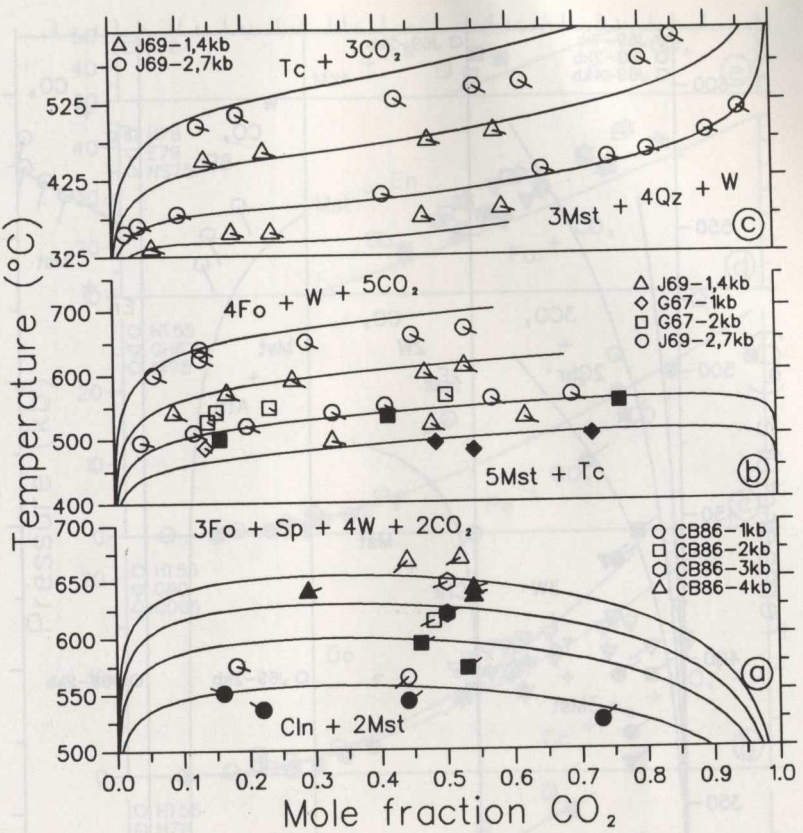

FIG. 34. Comparison of computed phase equilibria with experimental data in the system $MgO–Al_2O_3–SiO_2–H_2O–CO_2$: J69—Johannes (1969); G67—Greenwood (1967c); CB86—Chernosky & Berman (1986b). Symbols as in Fig. 4.

data of Fawcett & Yoder (1966) suggest that it is temperature sensitive in the range 2–10 kb. More experimental work on Al solubility in talc would be helpful in resolving this inconsistency.

Magnesite

The standard state properties of magnesite were derived primarily from the low temperature reversals on the magnesite decarbonation reaction (Fig. 36c) and the recent phase equilibrium data reported by Chernosky & Berman (1986*b*) for the equilibrium: 2 magnesite + clinochlore = 3 forsterite + spinel + $2CO_2$ + $4H_2O$ (Fig. 34a). The resulting properties are in excellent agreement with both sets of experiments and with additional data in mixed volatile fluids below 2 kb (Figs. 34b, c and 35), but lead to higher temperatures than Johannes's (1969) unreversed data at 4–7 kb (Fig. 34b, c). Calculated equilibria involving magnesite at much higher pressures and temperatures (Fig. 36c–e) show similar, but more obvious discrepancies with experimental data. Taken together, these inconsistencies suggest that fugacity coefficients for CO_2 calculated with the model of Kerrick & Jacobs (1981) are increasingly in error at high pressure. This conclusion is also supported by the comparison between the high P–T phase equilibrium data involving calcite (Fig. 36a) and the computed equilibrium which is at the upper limit of the experimental data. Inferences based on the high pressure breakdown reaction of dolomite (Fig. 36b) are complicated by the order–disorder process which seems to have been operative on the short time scale of these experiments.

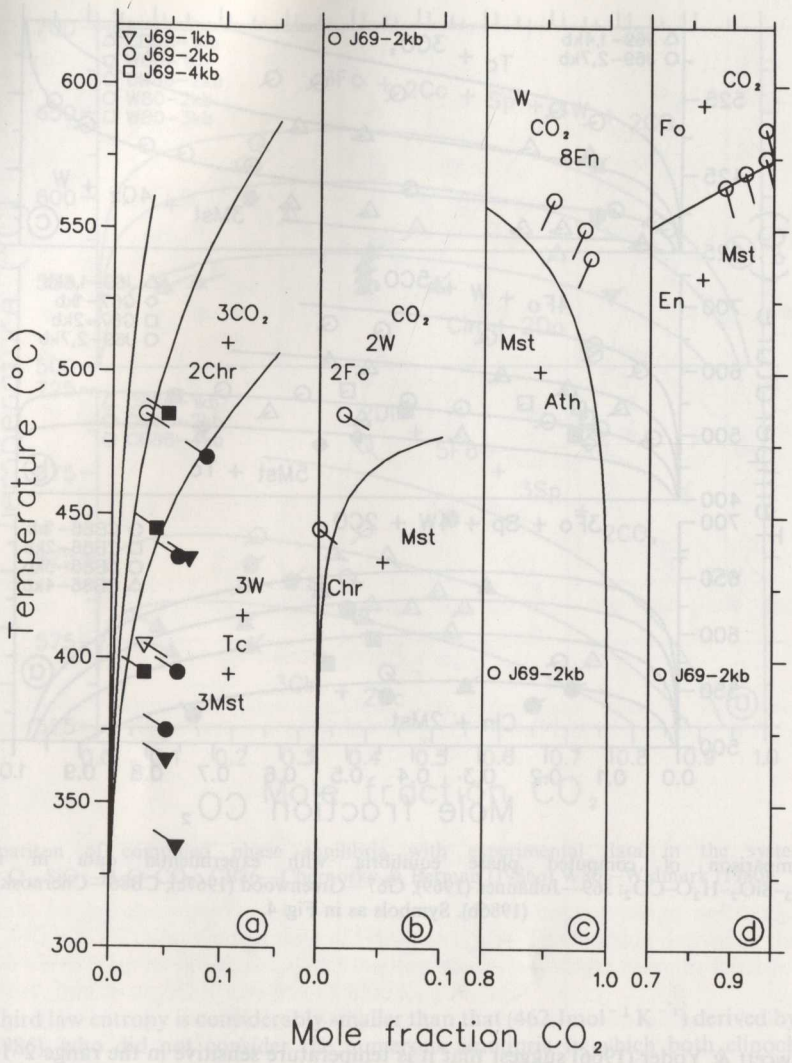

FIG. 35. Comparison of computed phase equilibria with experimental data in the system $MgO–SiO_2–H_2O–CO_2$: J69—Johannes (1969). Symbols as in Fig. 4.

Paragonite, albite, jadeite

Provision for the triclinic-monoclinic transition and for Al–Si disorder in albite was made using Salje's (1985) recent theoretical advancement which describes each of these processes with a separate, but not independent, order parameter. Salje *et al.* (1985) present equations that quantitatively account for both phenomena and are in excellent agreement with calorimetric measurements of the enthalpy differences between low and high albite (Holm & Kleppa, 1968; Waldbaum, 1968) as well as the temperature dependence of Al–Si disordering experimentally reversed by Goldsmith & Jenkins (1985).

Iterative solution of eqns (4) and (5), combined with eqns. (20)–(22) of Salje *et al.* (1985) give the temperature dependence of both order parameters as well as the thermodynamic properties of albite (relative to monalbite) in internal equilibrium. The Gibbs free energy, enthalpy, and entropy differences at 298·15 K between stable albite (low albite) and fully disordered monalbite are 8422 $Jmol^{-1}$, 13482 $Jmol^{-1}$, and 16·97 $Jmol^{-1}K^{-1}$, respectively. These values correspond to the

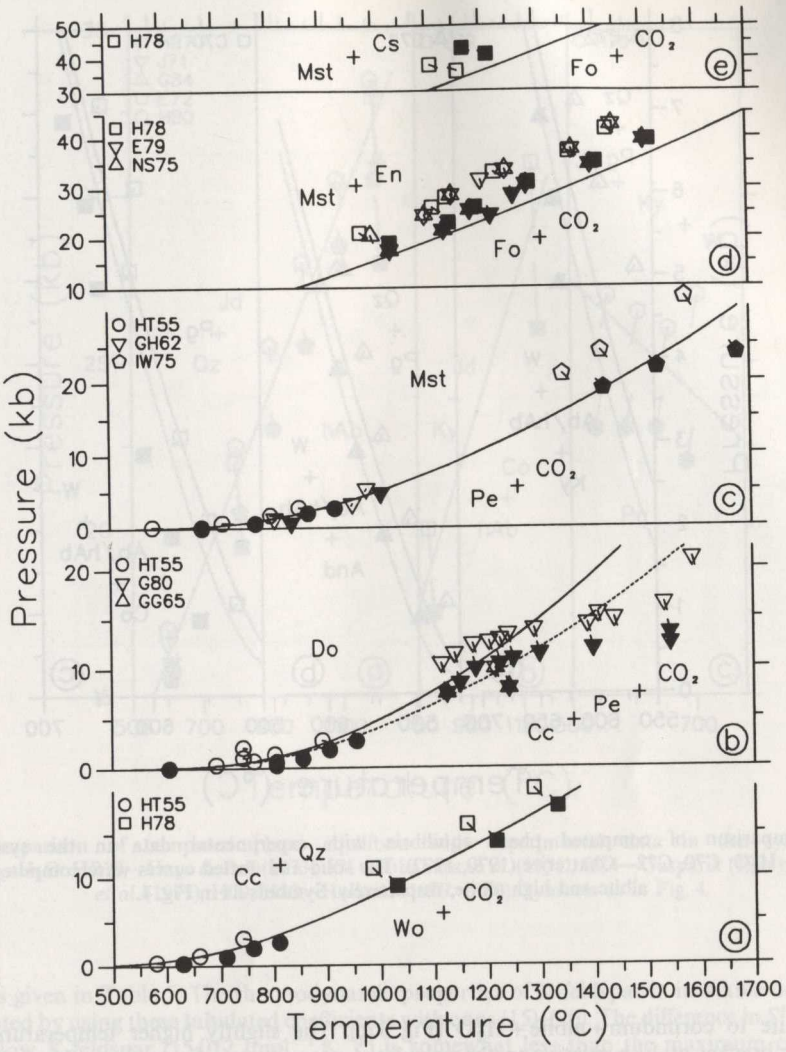

FIG. 36. Comparison of computed phase equilibria with experimental data in the system $CaO–MgO–SiO_2–H_2O–CO_2$: H78—Haselton *et al.* (1978); E79—Eggler *et al.* (1979); NS75—Newton & Sharp (1975); HT55—Harker & Tuttle (1955); GH62—Goldsmith & Heard (1962); IW75—Irving & Wyllie (1975); G80—Goldsmith (1980*b*); GG55—Graf & Goldsmith (1955). Solid and dotted curves in (b) represent equilibria computed with fully ordered and stably disordered dolomite, respectively. Symbols as in Fig. 4.

differences in standard state properties of low and high albite given in Table 2. The thermodynamic properties of stable albite are given by addition of the excess enthalpies and entropies computed with eqns (20)–(22) of Salje *et al.* (1985) to the corresponding properties for high albite. The volume change of stable albite due to ordering is approximated by dividing the computed excess enthalpies (eqn (21) of Salje *et al.*, 1985) with a scaling factor (335282·925 b^{-1}) that reproduces the measured difference in standard state volumes between low and high albite 0·04 Jb^{-1}).

Cell parameters of feldspars produced in Chatterjee's (1970) experimental run products indicate that albites attained internal equilibrium in runs up to 150 days in duration. Consequently, thermodynamic properties for albite were derived by assuming that albites reached stable internal equilibrium in all experimental runs at high temperature. All experimental data (Fig. 37) are successfully accounted for with this assumption, except for the lowest P/T brackets for the breakdown

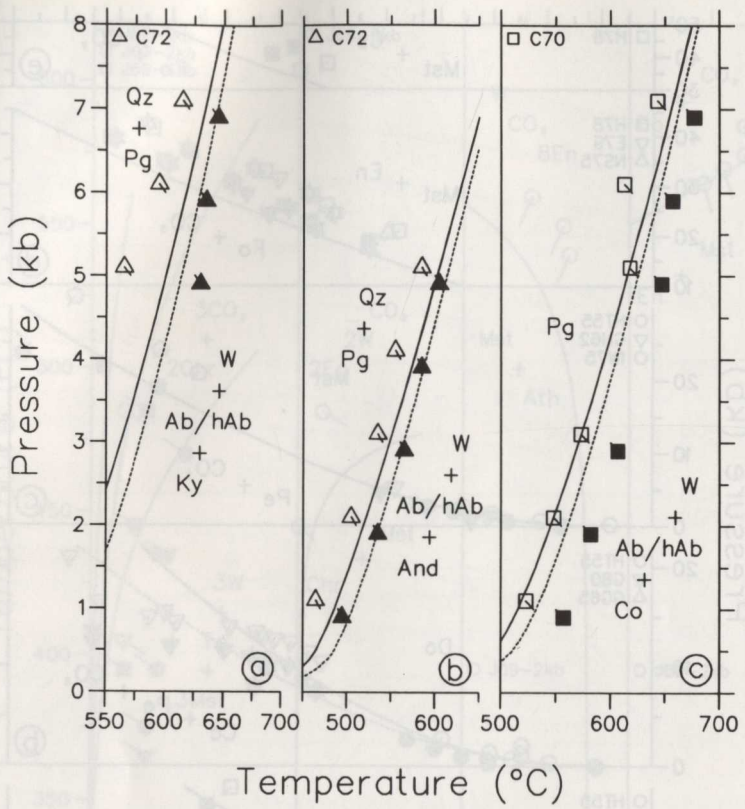

FIG. 37. Comparison of computed phase equilibria with experimental data in the system Na_2O–Al_2O_3–SiO_2–H_2O: C70, C72—Chatterjee (1970, 1972). The solid and dotted curves were computed with stable albite and high albite, respectively. Symbols as in Fig. 4.

of paragonite to corundum + albite + H_2O (Fig. 37c). The slightly higher temperature (< 5°) of Chatterjee's bracket at 1 kb relative to the calculated curve may indicate that albites did not fully equilibrate in the lowest P/T experimental runs. This conclusion is in qualitative agreement with observations that the Al–Si disordering process is greatly enhanced by elevated pressures (Goldsmith & Jenkins, 1985).

Consistency of the above data with the measured entropy of paragonite (Robie & Hemingway, 1984*b*) implies that disordering of this phase in these experiments is negligible. Because of very short run times with high albite as a starting material, high albite was assumed to be present in all experimental runs at high pressure. This assumption leads to excellent agreement with all phase equilibrium data shown in Fig. 38.

Muscovite, potassium feldspar

Disordering of Al and Si atoms in K-feldspar was accounted for using the equations of Thompson *et al.* (1974) which give the Z ordering parameter as a function of temperature. Solution calorimetric measurements by Hovis (1974) constrain the enthalpy difference (11088 $Jmol^{-1}$) between microcline and sanidine. The dependence of the disordering enthalpy on Z is given by:

$$\Delta_{ds}H^T = 11088\,(1-Z)\,\text{Jmol}^{-1}.$$

$\Delta_{ds}H^T$ values calculated with this equation were fitted as a function of temperature with the

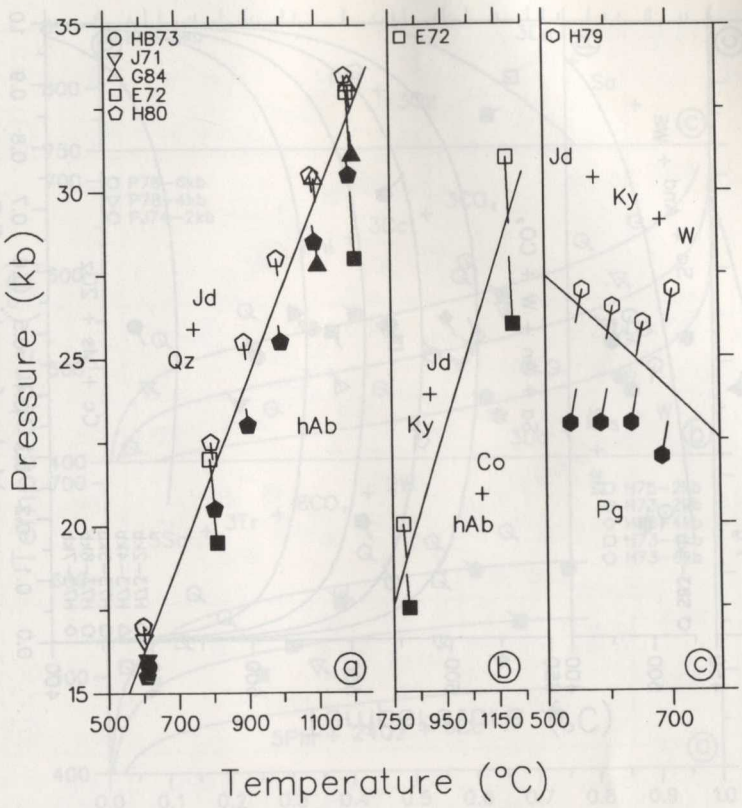

FIG. 38. Comparison of computed phase equilibria with experimental data in the system Na_2O–Al_2O_3–SiO_2–H_2O: HB73—Hays & Bell (1973); J71—Johannes *et al.* (1971); G84—Gasparik (1984); E72—Essene *et al.* (1972); H79, H80—Holland (1979, 1980). Symbols as in Fig. 4.

coefficients given in Table 5. The thermodynamic properties of K-feldspar in its stable ordering state are computed by using these tabulated coefficients with eqns (15)–(20). The difference in S^{P_r, T_r} between high and low K-feldspar (15·012 $Jmol^{-1}K^{-1}$) is somewhat less than the maximum configuration entropy of disorder on tetrahedral sites (18·7 $Jmol^{-1}K^{-1}$).

Chatterjee & Johannes (1974) used sanidine ($Z=0{\cdot}11$) in their starting materials, and their experiments of more than 100 days produced feldspars which ordered only slightly ($Z=0{\cdot}14$–$0{\cdot}17$, with higher P/T runs producing the more ordered feldspars). All phase equilibrium data of Chatterjee & Johannes (1974) and Hoschek (1973) can be reproduced with sanidine (Figs. 39 and 40a). The distribution of experimental brackets relative to computed equilibria involving both sanidine and stable K-feldspar (Fig. 39) is consistent with K-feldspars ordering more in the higher P/T experimental runs. In contrast, the brackets of Johannes (1980) for the equilibrium shown in Fig. 39d could only be reproduced with stable K-feldspar. Details of the structural state of the feldspars produced in these experiments were not reported.

The refined third law entropy of muscovite (293·16 $Jmol^{-1}K^{-1}$) is somewhat higher than that derived from low temperature Cp measurements (287·7 $Jmol^{-1}K^{-1}$), indicating partial disorder in muscovite. This conclusion, which differs from that reached by Helgeson *et al.* (1978), Krupka *et al.* (1979), and Berman *et al.* (1985), results from the consideration here of the much larger thermal expansivity of muscovite compared to K-feldspar and corundum, and is more in accord with structural refinements of natural muscovites that indicate substantial Al–Si disorder (Guven, 1971; Guggenheim & Bailey, 1975).

The data of Day (1973) for the equilibrium muscovite + quartz = sanidine + sillimanite + H_2O (Fig. 39b) are displaced approximately 20 degrees higher than the data of Chatterjee & Johannes

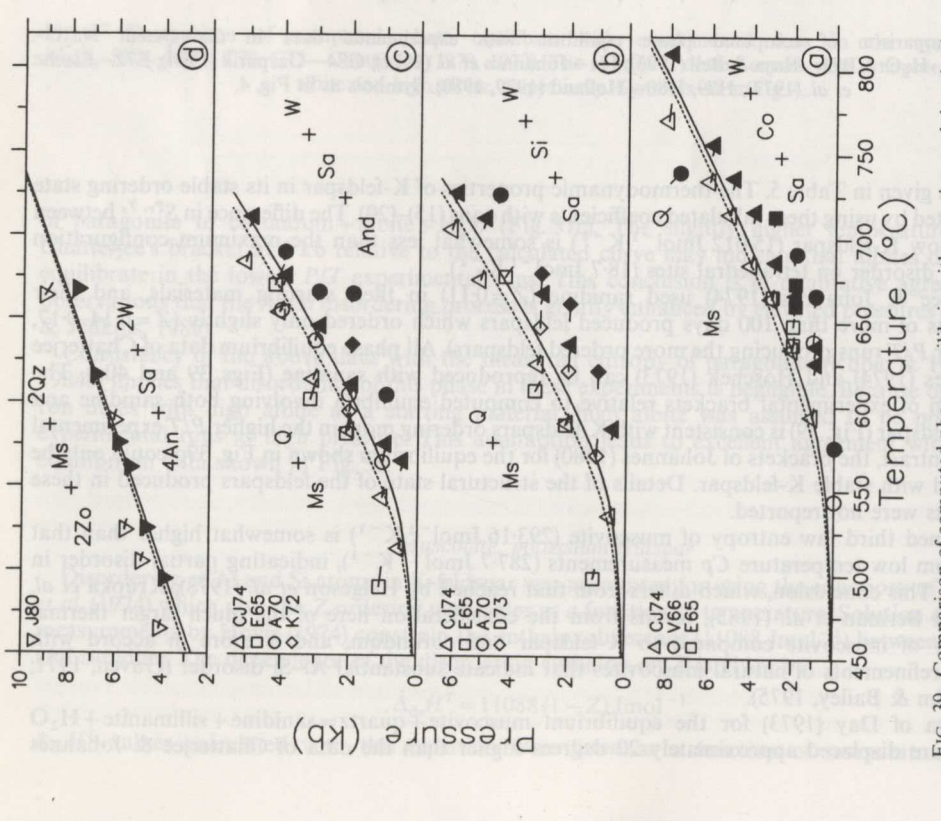

FIG. 39. Comparison of computed phase equilibria with experimental data in the system K_2O–CaO–Al_2O_3–SiO_2–H_2O: J80—Johannes (1980); CJ74—Chatterjee & Johannes (1974); E65—Evans (1965); A70—Althaus *et al.* (1970); K72—Kerrick (1972); D73—Day (1973); V66—Velde (1966). The solid and dotted curves were computed with sanadine and stable K-feldspar, respectively. Symbols as in Fig. 4.

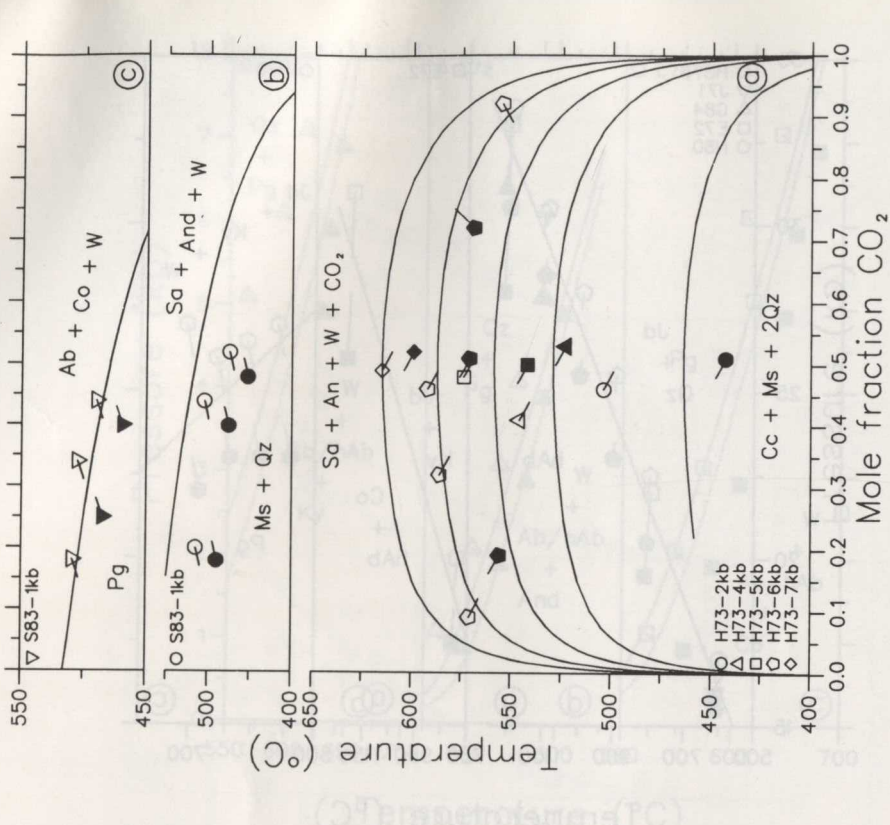

FIG. 40. Comparison of computed phase equilibria with experimental data in the system K_2O–Na_2O–CaO–Al_2O_3–SiO_2–H_2O–CO_2: S83—Shvedenkov *et al.* (1983); H73—Hewitt (1973). Symbols as in Fig. 4.

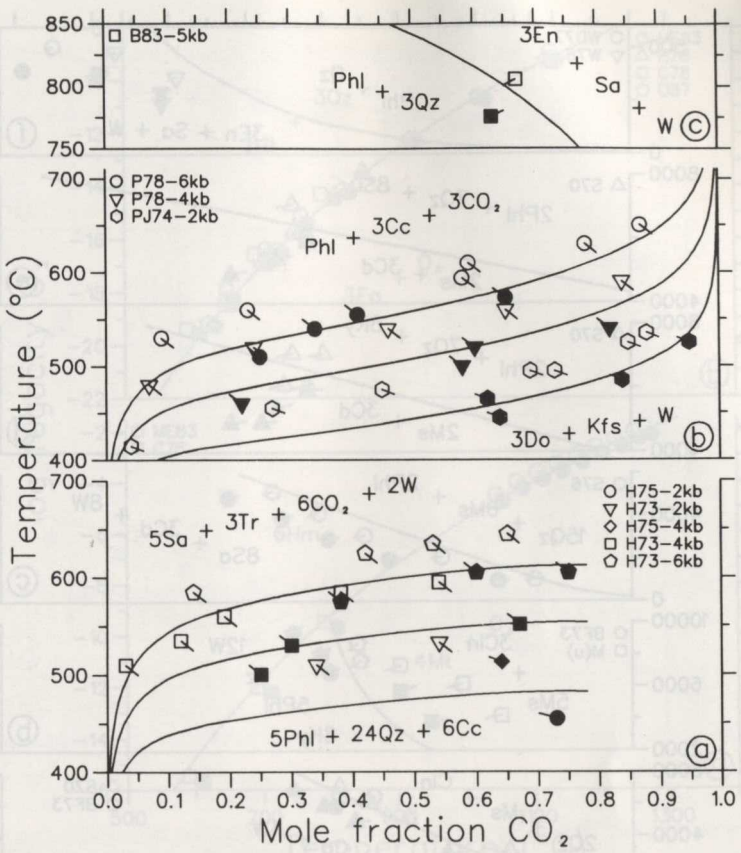

FIG. 41. Comparison of computed phase equilibria with experimental data in the system K_2O–CaO–MgO–Al_2O_3–SiO_2–H_2O–CO_2: B83—Bohlen *et al.* (1983*a*); P78—Puhan (1978); PJ74—Puhan & Johannes (1974); H75—Hewitt (1975); H73—Hoschek (1973).

(1974), although both studies utilized synthetic starting materials. The latter set of experiments were favored in this analysis because Day had to rely on textural evidence to infer reaction directions in runs which showed very little change in the proportions of starting materials. The data of Shvedenkov *et al.* (1983) for this equilibrium in mixed volatile fluids (Fig. 40b) are displaced to low temperatures, but reported experimental details are too few to infer the cause of this discrepancy. Other experimental data shown in Fig. 39 were obtained with natural starting materials containing appreciable Na in muscovite and K-feldspar. Most of these data show a somewhat expanded stability field for muscovite, although Velde's (1966) data indicate a much steeper slope for the breakdown of muscovite to corundum + K-feldspar (Fig. 39a) than do any of the other data sets.

Phlogopite

The thermodynamic properties for phlogopite were derived primarily from the phase equilibrium data involving mixed volatiles (Fig. 41), because of inconsistencies among other sets of experimental data that could not be resolved on the basis of reported experimental methods or results. Calculated equilibria are in accord with all data summarized in Fig. 41, and with most of the data shown in Fig. 42a, b. The experimental data obtained for the equilibrium phlogopite + quartz = enstatite + sanidine + H_2O with $P_{H_2O} = P_{total}$ (Fig. 42f) are incompatible with results obtained in mixed volatile fluids (Fig. 41c). Discrepancies between computed equilibria and experimental data shown in

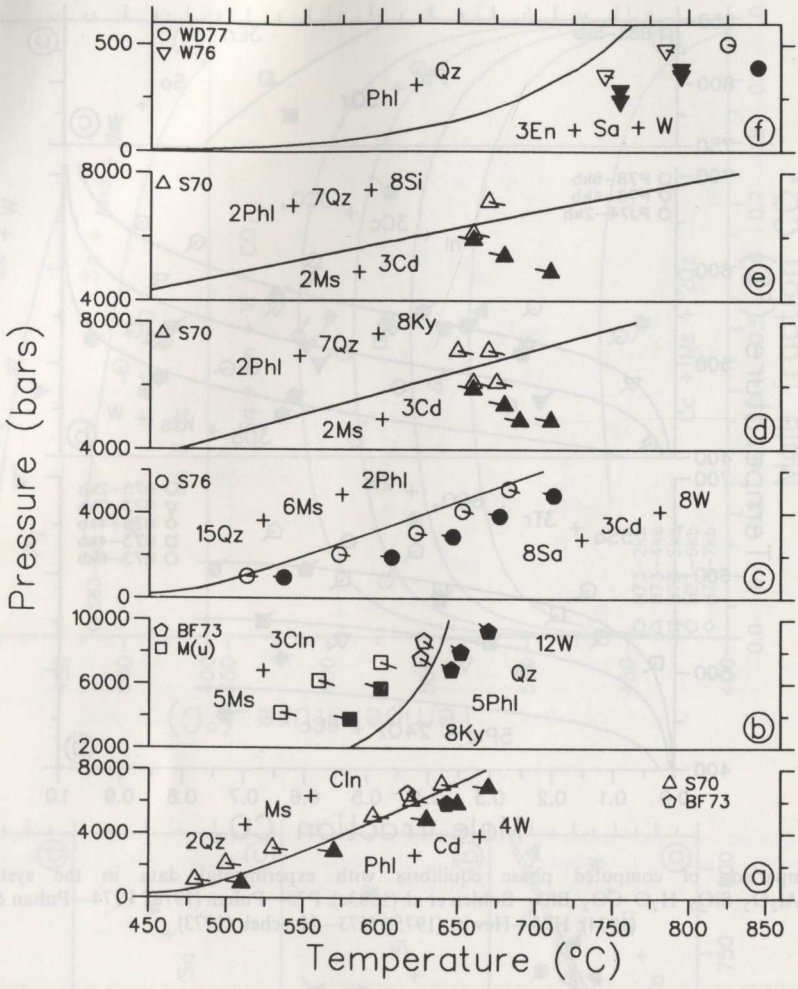

FIG. 42. Comparison of computed phase equilibria with experimental data in the system K_2O–MgO–Al_2O_3–SiO_2–H_2O: WD77—Wones & Dodge (1977); W76—Wood (1976); S70, S76—Seifert (1970, 1976); BF73—Bird & Fawcett (1973); M(u)—H.-J. Massone (unpublished data); Symbols as in Fig. 4.

Fig. 42c–e could all be accounted for by nonstoichiometry in phlogopite which has been observed by Bird & Fawcett (1973). More experimental work on the nature of this nonstoichiometry would be useful in resolving these inconsistencies.

Comparison of the derived entropy of phlogopite (334·16 $Jmol^{-1}K^{-1}$) with the measured value (315·9) is indicative of almost complete disorder on tetrahedral sites (maximum disorder $= 18{\cdot}7\ Jmol^{-1}K^{-1}$).

Magnetite, hematite, fayalite, ferrosilite

Thermodynamic properties for these phases are consistent with experimental data summarized in Figs. 43 and 44a, as well as available calorimetric data for all phases. The data of O'Neill (1987) and Myers & Eugster (1983) for the oxygen buffer equilibria (Fig. 43) were preferred over other data sets due to the precision and presumed accuracy of their experimental techniques. The derived third law entropy of ferrosilite (95·9 $Jmol^{-1}K^{-1}$) is slightly higher than that (94·6 $Jmol^{-1}K^{-1}$) reported by Bohlen *et al.* (1983*b*) without estimates of uncertainty.

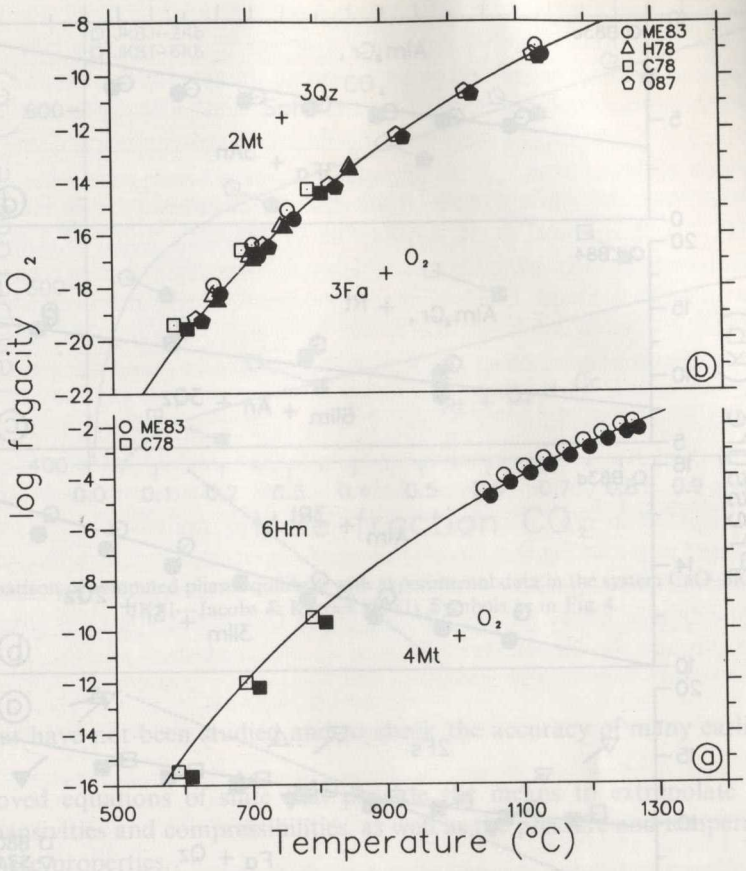

FIG. 43. Comparison of computed phase equilibria at 1 b pressure with experimental data in the system FeO–Fe_2O_3–SiO_2: ME83—Myers & Eugster (1983); H78—Hewitt (1978); C78—Chou (1978) O87—O'Neill (1987). Symbols as in Fig. 4.

Almandine, rutile, ilmenite

The thermodynamic properties of these phases were refined through consideration of the extremely tight phase equilibrium constraints (Fig. 44b) determined by Bohlen *et al.* (1983*d*). The refined $\Delta_f H^{P_r,T_r}$ for almandine ($-5265{\cdot}5$ kJmol^{-1}) is in accord with the calorimetrically determined value ($-5269{\cdot}2 \pm 5{\cdot}5$) measured by Chatillon-Colinet *et al.* 1983), while the derived $\Delta_f G^{P_r,T_r}$ for ilmenite ($-1155{\cdot}32$ kJmol^{-1}) is very close to the value ($-1153{\cdot}9$ kJmol^{-1}) derived by Anovitz *et al.* (1985) from consideration of redox equilibria. Additional experimental data (Fig. 44c, d) reported by Bohlen *et al.* (1983c) and Liotta & Bohlen (1984) involve grossular–almandine solid solutions. The calculated equilibria assuming ideal site mixing are in reasonable agreement with these phase equilibrium data.

Sphene

The 2 and 6 kb data of Jacobs & Kerrick (1981) for the breakdown of sphene to rutile in mixed volatile fluids (Fig. 45) are incompatible with one another. The discrepancies with the low pressure brackets, which mimic those observed in Fig. 8c, may reflect inaccurate CO_2 fugacities or activities computed with the Kerrick & Jacobs (1981) equation of state.

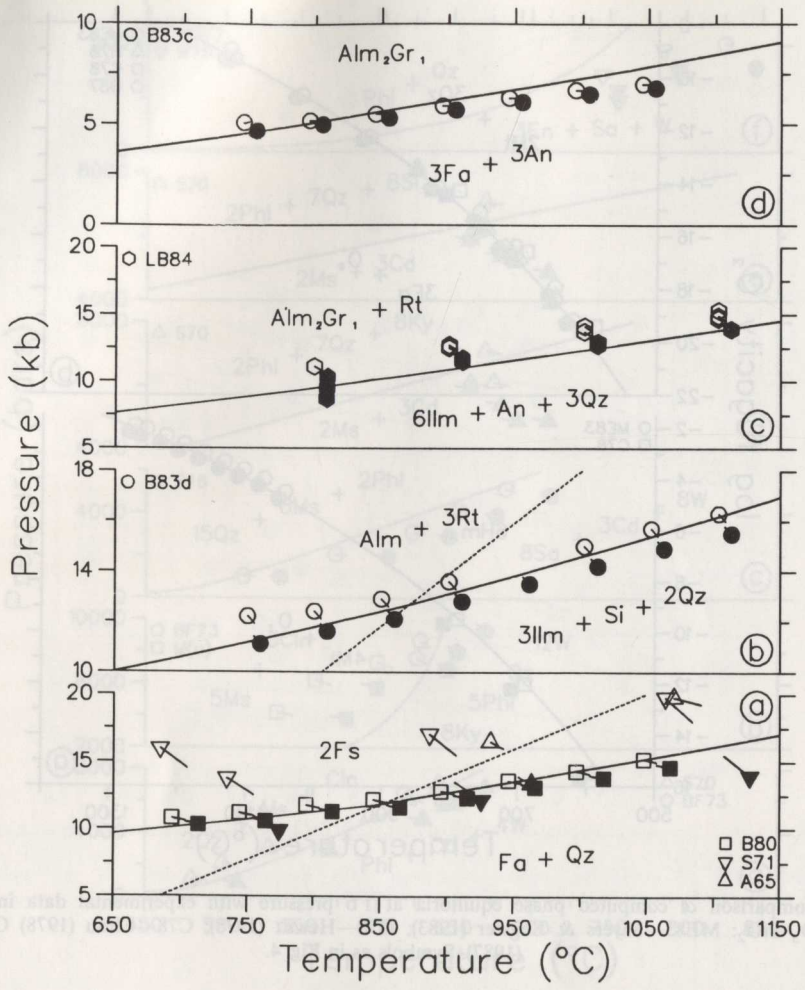

FIG. 44. Comparison of computed phase equilibria with experimental data in the system $FeO–CaO–Al_2O_3–SiO_2–TiO_2$: B80, B83c, B83d—Bohlen *et al.* (1980, 1983*c*, *d*); LB84—Liotta & Bohlen (1984); S71—Smith (1971); A65—Akimoto *et al.* (1965). Dotted curves in (a) and (b) represent the α–β quartz transition. Note that the curves in (c) and (d) were computed assuming ideal mixing between almandine and grossular. Symbols as in Fig. 4.

CONCLUSIONS

The results detailed above demonstrate the high degree of consistency achieved with thermophysical measurements and with phase equilibrium data obtained from solubility measurements, weight change studies, and conventional hydrothermal techniques involving both single and mixed volatile species (Figs. 4–45). While this overall agreement emphasizes the praise that is deserving for the techniques pioneered, and the care taken by experimentalists, it also shows the power of the mathematical programming method for successful analysis of this large body of diverse experimental data.

The most critical factors needed to improve the data set presented in this study are:

(1) Accurate expansivity and compressibility data to constrain these properties for those

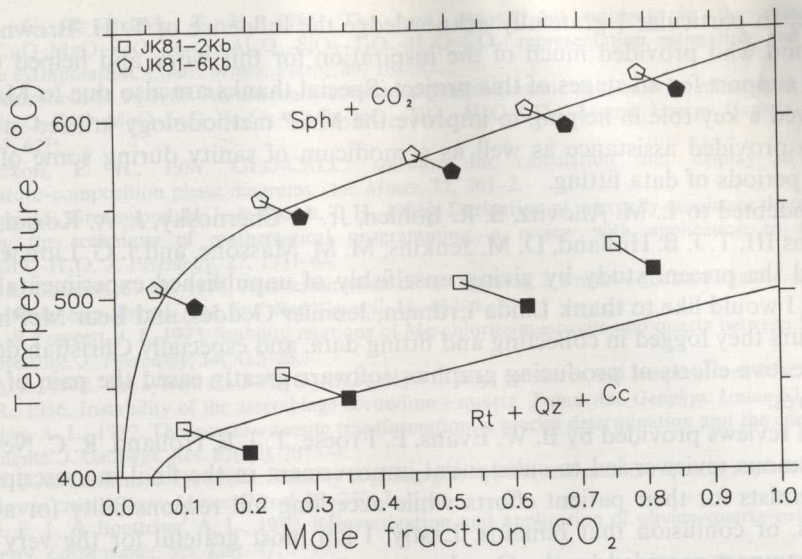

FIG. 45. Comparison of computed phase equilibria with experimental data in the system $CaO–SiO_2–TiO_2–CO_2$: JK81—Jacobs & Kerrick (1981). Symbols as in Fig. 4.

minerals that have not been studied and to check the accuracy of many earlier measurements.

(2) Improved equations of state that provide the means to extrapolate and predict mineral expansivities and compressibilities, as well as the pressure and temperature dependences of these properties.

(3) Improved equations of state for CO_2 and $H_2O–CO_2$ mixtures that allow accurate representation of fugacities and activities over a wider range of pressure and temperature.

(4) Additional calorimetric and spectroscopic data aimed at determining the amount, and the temperature dependence of disordering in minerals.

(5) Additional phase equilibrium experiments aimed at resolving the inconsistencies noted in the discussion of results above.

To the extent that the thermodynamic properties derived in this study successfully account for most experimental observations, confidence can be derived that they will allow accurate prediction of complex phase relationships among stoichiometric minerals. Further work is needed to develop suitable activity models for rigorous application to geologic problems in which end-member minerals are rare. In order to facilitate calculations with this data set, software has been developed that quickly computes stable phase diagrams in entirety, and versions are available for use on mainframe computers (Perkins *et al.*, 1986) or microcomputers (Berman *et al.*, 1987). The latter program, as well as the thermodynamic database and FORTRAN 77 software for tabulating thermodynamic parameters of specific minerals or selected equilibria can be obtained from the author of this paper.

ACKNOWLEDGEMENTS

The work presented in this paper could not have been accomplished without the influence, assistance, and support of many people to whom I would like to extend my

gratitude. In particular I gratefully acknowledge the influence of T. H. Brown and H. J. Greenwood who provided much of the inspiration for this work and helped to arrange financial support for all stages of this project. Special thanks are also due to Martin Engi, who played a key role in helping to improve the MAP methodology utilized in this study and who provided assistance as well as a modicum of sanity during some of the more arduous periods of data fitting.

I am indebted to L. M. Anovitz, S. R. Bohlen, Jr. V. Chernosky, J., A. Koziol, Z. Sharp, D. Perkins III, T. J. B. Holland, D. M. Jenkins, M. M. Massone, and J. G. Liou who greatly facilitated the present study by giving unselfishly of unpublished experimental work. In addition, I would like to thank Linda Erdman, Jennifer Geddes, and Bear McPhail for the many hours they logged in collecting and fitting data, and especially Christian de Capitani whose creative efforts at producing graphics software greatly eased the pain of preparing final figures.

Careful reviews provided by B. W. Evans, E. Froese, T. J. B. Holland, R. C. Newton, and an anonymous reviewer led to substantial improvement in the final manuscript. I thank these scientists for their patient efforts while accepting full responsibility for any errors, omissions, or confusion that remains. Lastly, I am most grateful for the very generous financial support provided by the Geochemistry & Applied Chemistry Branch of Atomic Energy of Canada, Ltd. (contract A-7436/R1) and by the Lithosphere and Canadian Shield Development Division of the Geological Survey of Canada (EMR-DSS contract 1ST85-00380 set up through the industrious efforts of T. M. Gordon).

REFERENCES

Ackermand, D., Seifert, F., & Schreyer, W., 1975. Instability of sapphirine at high pressures. *Contr. Miner. Petrol.* **50,** 79–92.

Adams, L. H., & Gibson, R. E., 1929. The elastic properties of certain basic rocks and of their constituent minerals. *Natl. Acad. Sci. Proc.* **15,** 713–24.

Akimoto, S.-I., Katsura, T., Syono, Y., Fujisawa, H., & Komada, E., 1965. Polymorphic transition of pyroxenes $FeSiO_3$ and $CoSiO_3$ at high pressures and temperatures. *J. Geophys. Res.* **70,** 5269–78.

Allen, J. M., & Fawcett, J. J., 1982. Zoisite–anorthite–calcite stability relations in H_2O–CO_2 fluids at 5000 bars: an experimental and SEM study. *J. Petrology*, **23,** 215–39.

Althaus, E., Karotke, E., Nitsch, K. H., & Winkler, H. G. F., 1970. An experimental re-examination of the upper stability limit of muscovite plus quartz. *N Jh. Miner. Monatshefte* **1970,** 325–36.

Anderson, C. T., 1936. The heat capacities of quartz, cristobalite and tridymite at low temperatures. *J. Am. Chem. Soc.* **58,** 568–70.

Anderson, P. A. M., & Kleppa, O. J., 1969. The thermochemistry of the kyanite-sillimanite equilibrium. *Am. J. Sci.* **267,** 285–90.

——Newton, R. C., & Kleppa, O. J., 1977. The enthalpy change of the andalusite-sillimanite reaction and the Al_2SiO_5 diagram. Amer. J. Sci. **277,** 585–593.

Anovitz, L. M., Treiman, A. H., Essene, E. J., Hemingway, B. S., Westrum, E. F. Jr., Wall, V. J., Burriel, R., & Bohlen, S. R., 1985. The heat capacity of ilmenite and phase equilibrium in the system Fe–Ti–O. *Geochim. Cosmochim. Acta*, **49,** 2027–40.

Atlas, L., 1952. The polymorphism of $MgSiO_3$ and solid state equilibria in the system $MgSiO_3$–$CaMgSi_2O_6$. *J. Geol.* **60,** 125–47.

Austin, J. B., 1954. The coefficient of linear thermal expansion of tridymite. *Am. Chem. Soc. J.* **76,** 6019–20.

Barany, R., 1962. Heats and free energies of formation of some hydrated and hydrous sodium- and calcium–aluminum silicates. U.S. Bur. Mines Rep. Invest. 5900, 17pp.

——1963. Heats of formation of gehlenite and talc. U.S. Bur. Mines Rep. Invest. 6251, 9p.

Barnes, H. L., & Ernst, W. G., 1963. Ideality and ionization in hydrothermal fluids: the system MgO–H_2O–NaOH. *Am. J. Sci.* **261,** 129–50.

Barron, T. H. K., Berg, W. T., & Morrison, J. A., 1959. On the heat capacity of crystalline magnesium oxide. *Proc. R. Soc. Lond.* **A250,** 70–83.

Bass, J. D., & Weidner, J., 1984. Elasticity of single-crystal orthoferrosilite. *J. Geophys. Res.* **89,** 4359–71.

Bassett, W. A., & Barnett, J. D., 1970. Isothermal compression of stishovite and coesite up to 85 kilobars at room temperature by X-ray diffraction. *Phys. Earth Planet. Int.* **3,** 54–60.

Benson, S. W., 1968. *Thermochemical Kinetics.* New York: Wiley, 223 pp.

Berman, R. G., & Brown, T. H., 1985. The heat capacity of minerals in the system K_2O–Na_2O–CaO–MgO–FeO–Fe_2O_3–Al_2O_3–SiO_2–TiO_2–H_2O–CO_2: representation, estimation, and high temperature extrapolation. *Contr. Miner. Petrol.* **89,** 168–83.

——Greenwood, H. J., 1985. An internally-consistent thermodynamic data base for minerals in the system Na_2O–K_2O–CaO–MgO–FeO–Fe_2O_3–Al_2O_3–SiO_2–TiO_2–H_2O–CO_2. Atomic Energy Canada Ltd. Tech. Rep. 377, 62P.

——Perkins, E. H., 1987. GEO-CALC: software for calculation and display of pressure–temperature–composition phase diagrams. *Am. Miner.* **72,** 861–2.

——Engi, M., Greenwood, H. J., & Brown, T. H., 1986*b*. Derivation of internally-consistent thermodynamic data by the technique of mathematical programming, a review with application to the system MgO–SiO_2–H_2O. *J. Petrology*, **27,** 1331–64.

Best, N. F., & Graham, C. M., 1978. Redetermination of the reaction 2 zoisite + quartz + kyanite = 4 anorthite + H_2O. *Prog. Exp. Petrol. Nat. Env. Res. Council*, **11,** 153–4.

Bird, G. W., & Fawcett, J. J., 1973. Stability relations of Mg-chlorite-muscovite and quartz between 5 and 10 kb water pressure. *J. Petrology*, **14,** 415–28.

Boettcher, A. L., 1970. The system CaO–Al_2O_3–SiO_2–H_2O at high pressures and temperatures. *Ibid.* **11,** 337–79.

Bohlen, S. R., 1986. Instability of the assemblage corundum + quartz. *Trans. Am. Geophys. Union* **67,** 1280.

—— Boettcher, A. L., 1982. The quartz = coesite transformation: a precise determination and the effects of other components. *J. Geophys. Res.* **87**(B8), 7073–8.

—— Wall, V. J., & Clemens, J. D., 1983*a*. Stability of phlogopite–quartz and sanidine–quartz: a model for melting in the lower crust. *Contr. Miner. Petrol.* **83,** 270–7.

—— Essene, E. J., & Boettcher, A. L., 1980. Reinvestigation and application of olivine–quartz–orthopyroxene barometry. *Earth planet. Sci. Lett.* **47,** 1–10.

—— Metz, G. W., Essene, E. J., Anovitz, L. M., Westrum, E. F. Jr., & Wall, V. J., 1983*b*. Thermodynamics and phase equilibrium of ferrosilite as a potential oxygen barometer in mantle rocks. *Trans. Am. Geophys. Union* **64,** 350.

—— Wall, V. J., & Boettcher, A. L., 1983*c*. Experimental investigation and application of garnet granulite equilibria. *Contr. Miner. Petrol.* **83,** 52–61.

———— 1983*d*. Experimental investigations and geological applications of equilibria in the system FeO–TiO_2–Al_2O_3–SiO_2–H_2O. *Am. Miner.* **68,** 1049–58.

Bonnickson, K. R., 1955. High temperature heat contents of aluminates of calcium and magnesium. *J. Phys. Chem.* **59,** 220–1.

Boyd, F. R., & England, J. L., 1965. The rhombic enstatite-clinoenstatite inversion. *Yb. Carn. Inst.*, Wash. **64,** 117–20.

———— Davis, B. T. C., 1964. Effects of pressure on the melting and polymorphism of enstatite, $MgSiO_3$. *J. Geophys. Res.* **69,** 2101–9.

Brace, W. F., Scholz, C. H., & La Mori, P. N., 1969. Isothermal compressibility of kyanite, andalusite, and sillimanite from synthetic aggregates. *Ibid.* **74,** 2089–98.

Bricker, O. P., Nesbitt, H. W., & Gunter, W. D., 1973. The stability of talc. *Am. Miner.* **58,** 64–72.

Bridgman, P. W., 1925. Linear compressibility of fourteen natural crystals. *Am. J. Sci.* **10,** 485–98.

—— 1948. Rough compressions of 177 substances to 40 000 kg/cm^2. *Am. Acad. Arts Sci. Soc.* **76,** 71–87.

Brousse, C., Newton, R. C., & Kleppa, O. J., 1984. Enthalpy of formation of forsterite, enstatite, akermanite, montecellite and merwinite at 1073 K determined by alkali borate solution calorimetry. *Geochim. Cosmochim. Acta*, **48,** 1081–8.

Cameron, M., Sueno, S., Prewitt, C. T., & Papike, J. J., 1973. High-temperature crystal chemistry of acmite, diopside, hedenbergite, jadeite, spodumene, and ureyite. *Am. Miner.* **58,** 594–618.

Carpenter, M. A., McConnell, J. D. C., & Navrotsky, A., 1985. Enthalpies of ordering in the plagioclase feldspar solid solution. *Geochim. Cosmochim. Acta*, **49,** 947–66.

Charlu, T. V., Newton, R. C., & Kleppa, O. J., 1975. Enthalpies of formation at 970 K of compounds in the system MgO–Al_2O_3–SiO_2 from high temperature solution calorimetry. *Ibid.* **39,** 487–97.

———— 1978. Enthalpy of formation of some lime silicates by high-temperature solution calorimetry, with discussion of high pressure phase equilibria. *Ibid.* **42,** 367–75.

———— 1981. Thermochemistry of synthetic $Ca_2Al_2SiO_7$ (gehlenite)—$Ca_2MgSi_2O_7$ (akermanite) melities. *Ibid.* **45,** 1609–17.

Chatillon-Colinet, C., Kleppa, O. J., Newton, R. C., & Perkins III, D., 1983. Enthalpy of formation of $Fe_3Al_2Si_3O_{12}$ (almandine) by high temperature alkali borate solution calorimetry. *Ibid.* **47,** 439–44.

Chatterjee, N. D., 1970. Synthesis and upper stability of paragonite. *Contr. Miner. Petrol.* **27,** 244–57.

—— 1972. The upper stability limit of the assemblage paragonite + quartz and its natural occurrences. *Ibid.* **34,** 288–303.

—— 1974. Synthesis and upper stability limit of 2M-margarite, $CaAl_2[Al_2Si_2O_{10}(OH)_2]$. *Schweizer. Miner. Petrograph. Mitt.* **54,** 753–67.

—— Johannes, W., 1974. Thermal stability and standard thermodynamic properties of synthetic 2M-muscovite, $KAl_2[AlSi_3O_{10}(OH)_2]$. *Contr. Miner. Petrol.* **48,** 88–114.

———— Leistner, H., 1984. The system CaO–Al_2O_3–SiO_2–H_2O: new phase equilibria data, some calculated phase relations, and their petrological applications. *Contr. Miner. Petrol.* **88,** 1–13.

Cheng, V. M., Allen, P. C., & Lazarus, D., 1975. Pressure coefficient of thermoelectric power of platinum/platinum-10% rhodium and chromel/alumel thermocouples. *Appl. Phys. Lett.* **26,** 6–7.

Chernosky, J. V., Jr., 1974. The upper stability of clinochlore at low pressure and the free energy of formation of Mg-cordierite. *Am. Miner.* **59,** 496–507.

——1976. The stability of anthophyllite—a reevaluation based on new experimental data. *Ibid.* **61,** 1145–55.

——1978. The stability of clinochlore + quartz at low pressure. *Ibid.* **63,** 73–82.

——1982. The stability of clinochrysotile. *Can. Miner.* **20,** 19–27.

—— Autio, L. K., 1979. The stability of anthophyllite in the presence of quartz. *Am. Miner.* **64,** 294–303.

—— Berman, R. G., 1986*a*. The stability of clinochlore in mixed volatile, H_2O–CO_2 fluids. *Trans. Am. Geophys. Union* **67,** 407.

———— 1986*b*. Experimental reversal of the equilibrium: clinochlore + 2 magnesite = 3 forsterite + spinel + $2CO_2$ + $4H_2O$. *Ibid.* **67,** 1279.

—— Day, H. W., & Caruso, L. J., 1985. Equilibria in the system MgO–SiO_2–H_2O: I. Experimental determination of the stability of Mg-anthophyllite. *Am. Miner.* **70,** 223–36.

Chou, I.-M., 1978. Calibration of oxygen buffers at elevated P and T using the hydrogen fugacity sensor. *Am. Miner.* **63,** 690–703.

Christensen, N. I., 1972. Elastic properties of polycrystalline magnesium, iron, and manganese carbonates to 10 kbars. *J. Geophys. Res.* **77,** 369–72.

Clemens, J. D., Navrotsky, A., Mcmillan, P., Smyth, B. K., & Wall, V. J., 1987. Phlogopite thermochemistry. *Trans. Am. Geophys. Union* **68,** 460.

Codata Task Group on Key Values for Thermodynamics (1978) CODATA recommended key values for thermodynamics 1977. *CODATA Bull.* **28,** 1–17. *Am. Miner.* **59,** 1099–104.

Cohen, L. H., & Klement, W. Jr., 1967. High-low quartz inversion: determination to 35 kilobars. *J. Geophys. Res.* **72,** 4245–51.

———— 1979. High-low cristobalite transitions in SiO_2, $AlPO_4$ and $GaPO_4$. Investigations by differential thermal analysis under hydrostatic pressure < 6 kbar. *Phil. Mag.* **39A,** 399–404.

———— 1980. Tridymite: Effect of hydrostatic pressure to 6 kbars on temperatures of two rapidly reversible transitions. *Contr. Miner. Petrol.* **71,** 401–5.

Connolly, J. A. D., & Kerrick, D. M., 1985. Experimental and thermodynamic analysis of prehnite stability. *Trans. Am. Geophys. Union* **66,** 388.

Coughlin, J. P., King, E. G., & Bonnickson, K. R., 1951. High-temperature heat contents of ferrous oxide, magnetite and ferric oxide. *J. Am. Chem. Soc.* **73,** 3891–3.

Cox, J. D., 1979. Manual of symbols and terminology for physicochemical quantities and units. Appendix IV: Notation for states and processes, significance of the word 'standard' in chemical thermodynamics, and remarks on functions used in tables of thermodynamics. *Pure Appl. Chem.* **51,** 393–403.

Crawford, W. A., & Fyfe, W. S., 1965. Lawsonite equilibria. *Am. J. Sci.* **263,** 262–70.

Czank, M., & Schulz, H., 1971. Thermal expansion of anorthite. *Naturwissenschaften* **58,** 94.

D'amour, H., Denner, W., & Schulz, H., 1979. Structure determination of alpha-quartz up to 68×10^8 Pa. *Acta Crysal.* **B35,** 550–5.

—— Schiferl, D., Denner, W., Schulz, H., & Holzapfel, W. B., 1978. High-pressure single-crystal structure determinations for ruby up to 90 kbar using an automatic diffractometer. *J. Appl. Phys.* **49,** 4411–16.

Danckwerth, A., & Newton, R. C., 1978. Experimental determination of the spinel peridotite to garnet peridotite reaction in the system MgO–Al_2O_3–SiO_2 in the range 900°–1100 °C and Al_2O_3 isopleths of enstatite in the spinel field. *Contr. Miner. Petrol.* **66,** 189–201.

Day, H. W., 1973. The high temperature stability of muscovite plus quartz. *Am. Miner.* **58,** 255–62.

Day, H. W., & Kumin, H. J., 1980. Thermodynamic analysis of the aluminium silicate triple point. *Am. J. Sci.* **280,** 265–87.

Delany, J. M., & Helgeson, H. C., 1978. Calculation of the thermodynamic consequences of dehydration in subducting oceanic crust to 100 kb and 800 °C. *Ibid.* **278,** 638–86.

Ditmars, D. A., & Douglas, T. B., 1971. Measurement of the relative enthalpy of pure Al_2O_3 (NBS heat capacity and enthalpy standard reference material no. 720) from 273 to 1173 K. *J. Res. National Bur. Standards* **75A,** 401–20.

Eggert, R. G., & Kerrick, D. M., 1981. Metamorphic equilibria in the silicious dolomite system: 6 kbar experimental data and geologic implications. *Geochim. Cosmochim. Acta.* **45,** 1039–49.

Eggler, D. H., Kushiro, I., & Holloway, J. R., 1979. Free energies of decarbonation reactions at mantle pressures: I. Stability of the assemblage forsterite-enstatite-magnesite in the system MgO–SiO_2–CO_2–H_2O to 60 kbar. *Am. Miner.* **64,** 288–93.

Elsner Von Gronow, H., & Schwiete, H. E., 1933. Die spezifischen Wärmen von CaO, Al_2O_3, $CaO{\cdot}Al_2O_3$, $3CaO{\cdot}Al_2O_3$, $2CaO{\cdot}SiO_2$, $3CaO{\cdot}SiO_2$, $2CaO{\cdot}Al_2O_3{\cdot}SiO_2$ von 20° bis 1500 °C. Z. anorgan. allgemeine Chem. **216,** 185–95.

Essene, E. J., Boettcher, A. L., & Furst, G. A., 1972. Indirect measurements for ΔG for quartz + corundum = kyanite. *Trans. Amer. Geophys. Union* **53,** 554.

Evans, B. W., 1965. Application of a reaction-rate method to the breakdown equilibria of muscovite and muscovite plus quartz. *Am. J. Sci.* **263,** 647–67.

—— 1977. Metamorphism of alpine peridotite and serpentinite. Ann. *Rev. Earth planet. Sci.* **5,** 397–447.

——Johannes, W., Oterdoom, W. H., & Trommsdorff, V., 1976. Stability of chrysotile and antigorite in the serpentine multisystem. *Schweizer. Miner. Petrograph. Mitt.* **56,** 79–93.
Fawcett, J. J., & Yoder, H. S., Jr., 1966. Phase relations of the chlorites in the system MgO–$Al_2O_3SiO_2$–H_2O. Am. Miner. **51,** 353–80.
Fenner, C. L., 1913. The stability relations of the silica minerals. *Am. J. Sci.* **36,** 331–84.
Finger, L. W., & Hazen, R. M., 1978. Crystal structure and compression of ruby to 46 kbar. *J. Appl. Phys.* **49,** 5823–6.
————1980. Crystal structure and isothermal compression of Fe_2O_3, Cr_2O_3, and V_2O_3 to 50 kbars. *Ibid.* **51,** 5362–7.
————Hofmeister, A., 1986. High pressure crystal chemistry of spinel ($MgAl_2O_4$) and magnetite (Fe_3O_4): comparisons with silicate spinels. *Phys. Chem. Miner.* **13,** 215–20.
——Ohashi, Y., 1976. The thermal expansion of diopside to 800 °C and a refinement of the crystal structure at 700 °C. *Am. Miner.* **61,** 303–10.
Foit, F. F., Jr., & Peacor, D. R., 1973. The anorthite crystal structure at 410 and 830 °C. *Ibid.* **58,** 665–75.
Franz, G., 1982. The brucite-periclase equilibrium at reduced H_2O activities: some information about the system H_2O–NaCl. *Am. J. Sci.* **282,** 1325–39.
Fyfe, W. S., 1962. On the relative stability of talc, anthophyllite, and enstatite. *Am. J. Sci.* **260,** 460–6.
——Hollander, M. A., 1964. Equilibrium dehydration of diaspore at low temperatures. *Ibid.* **262,** 709–12.
Gasparik, T., 1984. Experimental study of subsolidus phase relations and mixing properties of pyroxene in the system CaO–Al_2O_3–SiO_2. *Geochim. Cosmochim. Acta,* **48,** 2537–45.
——Newton, R. C., 1984. The reversed alumina contents orthopyroxene in equilibrium with spinel and forsterite in the system MgO–Al_2O_3–SiO_2. *Contr. Miner. Petrol.* **85,** 186–96.
Ghiorso, M. S., Carmichael, I. S. E., & Moret, L. K., 1979. Inverted high-temperature quartz. Unit cell parameters and properties of the alpha–beta inversion. *Contr. Miner. Petrol.* **68,** 307–23.
————Rivers, M. L., & Sack, R. O., 1983. The Gibbs free energy of mixing of natural silicate liquids: an expanded regular solution approximation for the calculation of magmatic intensive variables. *Ibid.* **87,** 107–45.
Giauque, W. F., & Archibald, R. C., 1937. The entropy of water from the third law of thermodynamics. The dissociation pressure and calorimetric heat of the reaction $Mg(OH)_2 = MgO + H_2O$. The heat capacities of $Mg(OH)_2$ and MgO from 20 to 300 K. *J. Am. chem. Soc.* **59,** 561–9.
Gibbs, G. V., 1966. The polymorphism of cordierite I: the crystal structure of low cordierite. *Am. Miner.* **51,** 1068–87.
Gmelin, E., 1969. Thermal properties of alkaline-earth-oxides. Z. *Naturforschung* **24A,** 1794–800.
Goldsmith, J. R., 1980*a*. The melting and breakdown reactions of anorthite at high pressures and temperatures. *Am. Miner.* **65,** 272–84.
——1980*b*. Thermal stability of dolomite at high temperatures and pressures. *J. Geophys. Res.* **85,** 6949–54.
——1981. The join $CaAl_2Si_2O_8$–H_2O (anorthite-water) at elevated pressures and temperatures. *Am. Miner.* **66,** 1183–8.
——Heard, H. C., 1962. Subsolidus phase relations in the system $CaCO_3$–$MgCO_3$. *J. Geol.* **69,** 45–74.
——Jenkins, D. M., 1985. The high-low albite relations revealed by reversal of degree of order at high pressures. *Am. Miner.* **70,** 911–23.
——Newton, R. C., 1977. Scapolite–plagioclase stability relations at high pressures and temperatures in the system $NaAlSi_3O_8$–$CaAl_2Si_2O_8$–$CaCO_3$–$CaSO_4$. *Am. Miner.* **62,** 1063–81.
Gordon, T. M., 1973. Determination of internally consistent thermodynamic data from phase equilibrium experiments. *J. Geol.* **81,** 199–208.
——Greenwood, H. J., 1970. The reaction: dolomite + quartz + water = talc + calcite + carbon dioxide. *Am. J. Sci.* **268,** 225–42.
————1971. The stability of grossularite in H_2O–CO_2 mixtures. *Am. Miner.* **56,** 1674–88.
Graf, D. L., & Goldsmith, J. R., 1955. Dolomite–magnesian calcite relations at elevated temperatures and CO_2 pressures. *Geochim. Cosmochim. Acta,* **7,** 109–28.
Grain, C. F., & Campbell, W. J., 1962. Thermal expansion and phase inversion of six refractory oxides. U.S. Bur. Mines Rep. Invest. 5982, 1–21.
Grattan-Bellew, P. E., 1978. Quartz-tridymite transition under hydrothermal conditions. *Exp. Miner.* **11,** 128–39.
Graziani, G., & Lucchesi, S., 1982. The thermal behavior of scapolites. *Am. Miner.* **67,** 1229–41.
Greenwood, H. J., 1963. The synthesis and stability of anthophyllite. *J. Petrology,* **4,** 317–51.
——1967*a*. Wollastonite stability in H_2O–CO_2 mixtures and occurrence in a contact-metamorphic aureole near Salmo, British Columbia, Canada. *Am. Miner.* **52,** 1669–80.
——1967*b*. The compressibility of gaseous mixtures of carbon dioxide and water between 0 and 500 bars pressure and 45° and 800° centigrade. *Am. J. Sci.* **267A,** 191–208.
——1967*c*. Mineral equilibria in the system MgO–SiO_2–H_2O–CO_2. In: Abelson, P. H., (ed.) *Researches in Geochemistry* II. New York: John Wiley, 542–7.
Gronvold, F., & Samuelson, E. J., 1975. Heat capacity and thermodynamic properties of alpha-Fe_2O_3 in the region 300–1050 K. Antiferromagnetic transition. *J. Phys. Chem. Solids* **36,** 249–56.
Gronvold, F., & Sveen, A., 1974. Heat capacity and thermodynamic properties of synthetic magnetite (Fe_3O_4) from 300 to 1050 K. Ferrimagnetic transition and zero-point entropy. *J. Chem. Therm.* **6,** 859–72.

——Westrum, E. F. Jr., 1959. Alpha-ferric oxide: low temperature heat capacity and thermodynamic functions. *J. Am. Chem. Soc.* **81,** 1780–3.
Grove, T. L., & Burnham, C. W., 1974. Al–Si disorder in calcium Tschermak's pyroxene, $CaAl_2SiO_6$. *Trans. Am. Geophys. Union* **55,** 1202.
Grundy, H. D., & Brown, W. L., 1974. A high temperature X-ray study of low and high plagioclase feldspars. In: MacKenzie, W. S., & Zussman, J., (eds.) *The Feldspars, Proceedings of a NATO Advanced Study Institute.* University of Manchester Press, 162–73.
Guggenheim, S., & Bailey, S. W., 1975. Refinement of the margarite structure in subgroup symmetry. *Am. Miner.* **60,** 1023–9.
——Chang, Y.-H., & Groos, A. F., Koster Van, 1987. Muscovite dehydroxylation: high-temperature studies. *Am. Miner.* **72,** 537–50.
Guven, N., 1971. The structures of $2M_1$ phengite and $2M_1$ muscovite. Z. *Kristallogr.* **134,** 196–212.
Harr, C., Gallagher, J. S., & Kell, G. S., 1984. NBS/NRC Steam Tables. Thermodynamic and transport properties and computer programs for vapor and liquid states of water in SI units. Washington: Hemisphere Publishing Co.
Haas, H., 1972. Diaspore–corundum equilibrium determined by epitaxis of diaspore on corundum. *Am. Miner.* **57,** 1375–85.
——Holdaway, M. J., 1973. Equilibria in the system Al_2O_3–SiO_2–H_2O involving the stability limits of pyrophyllite and thermodynamic data of pyrophyllite. *Am. J. Sci.* **273,** 449–64.
Haas, J. L. Jr., & Fisher, J. R., 1976. Simultaneous evaluation and correlation of thermodynamic data. *Ibid.* **276,** 525–45.
Halbach, H., & Chatterjee, N. D., 1984. An internally consistent set of thermodynamic data for twenty-one CaO–Al_2O_3–SiO_2–H_2O phases by linear parametric programming. *Contr. Miner. Petrol.* **88,** 14–23.
Hariya, Y., & Kennedy, G. C., 1968. Equilibrium study of anorthite under high pressure and high temperature. *Am. J. Sci.* **266,** 193–203.
Harker, R. I., & Tuttle, O. F., 1955. Studies in the system CaO–MgO–CO_2. Part I: The thermal dissociation of calcite, dolomite and magnesite. *Am. J. Sci.* **253,** 209–24.
——1956*a*. Experimental data on the P_{CO_2}–T curve for the reaction: calcite + quartz = wollastonite + carbon dioxide. *Ibid.* **254,** 239–56.
——1956*b*. The lower limit of stability of akermanite ($Ca_2MgSi_2O_7$). *Ibid.* **254,** 468–78.
Haselton, H. T. Jr., 1979. Calorimetry of synthetic pyrope–grossular garnets and calculated stability relations. Ph.D. Thesis University of Chicago.
Haselton, H. T. Jr., Hemingway, B. S., & Robie, R. A., 1984. Low-temperature heat capacities of $CaAl_2SiO_6$ glass and pyroxene and thermal expansion of $CaAl_2SiO_6$ pyroxene. *Am. Miner.* **69,** 481–9.
——Sharp, W. E., & Newton, R. C., 1978. CO_2 fugacity at high temperatures and pressures from experimental decarbonation reactions. *Geophys. Res. Lett.* **5,** 753–6.
——Westrum E. F., Jr., 1980. Low-temperature heat capacities of synthetic pyrope, grossular, and $pyrope_{60}grossular_{40}$. *Geochim. Cosmochim. Acta,* **44,** 701–9.
Hays, J. F., 1966. Lime-alumina-silica. Yb. Carn. Inst., Wash. **65,** 234–9.
——Bell, M., 1973. Albite-jadeite-quartz equilibrium: a hydrostatic determination. *Ibid.* **72,** 706–8.
Hazen, R. M., 1976. Effects of temperature and pressure on the crystal structure of forsterite. *Am. Miner.* **61,** 1280–93.
——1977. Effects of temperature and pressure on the crystal structure of ferromagnesian olivine. *Ibid.* **62,** 286–95.
——Finger, L. W., 1978*a*. The crystal structures and compressibilities of layer minerals at high pressure. II. Phlogopite and chlorite. *Ibid.* **63,** 293–6.
——1978*b*. Crystal structure and compressibilities of pyrope and grossular to 60 kbar. *Ibid.* **63,** 297–303.
——1981. Bulk moduli and high-pressure crystal structures of rutile-type compounds. *J. Phys. Chem. Solids* **42,** 143–51.
——1985. Crystals at high pressure. *Sci. Am.* **252,** 110–7.
Helgeson, H. C., Delany, J. M., Nesbitt, H. W., & Bird, D. K., 1978. Summary and critique of the thermodynamic properties of rock-forming minerals. *Am. J. Sci.* **278A,** 229p.
——Kirkham, D. H., & Flowers, G. C., 1981. Theoretical prediction of the thermodynamic behavior of aqueous electrolytes at high pressures and temperatures: IV. Calculation of activity coefficients, osmotic coefficients, and apparent molal and standard and relative partial molal properties to 600 °C and 5 kb. *Am. J. Sci.* **281,** 1249–516.
Hemingway, B. S., 1987. Quartz: Heat capacities from 340 to 1000 K and revised values for the thermodynamic properties. *Am. Miner.* **72,** 273–9.
——Evans, H. T., Nord, G. L. Jr., Haselton, H. T., Robie, R. A., & Mcgee, J. J., 1986. Akermanite: phase transitions in heat capacity and thermal expansion, and revised thermodynamic data. *Can. Miner.* **24,** 425–34.
——Krupka, K. M., & Robie, R. A., 1981. Heat capacities of the alkali feldspars between 350 and 1000 K from differential scanning calorimetry, the thermodynamic functions of the alkali feldspars from 298·15 to 1400 K, and the reaction quartz + jadeite = analbite. *Am. Miner.* **66,** 1202–15.
——Robie, R. A., 1977. Enthalpies of formation of low albite ($NaAlSi_3O_8$), gibbsite ($Al(OH)_3$) and $NaAlO_2$: revised values for $\Delta H^\circ_{f,298}$ and $\Delta G^\circ_{f,298}$ of some aluminosilicate minerals. *J. Res. U.S. Geol. Surv.* **5,** 413–29.

——1984. Heat capacity and thermodynamic functions for gehlenite and staurolite: with comments on the Schottky anomaly in the heat capacity of staurolite. *Am. Miner.* **69,** 307–18.

——Fisher, J. R., & Wilson, W. H., 1977. Heat capacities of gibbsite, $Al(OH)_3$, between 13 and 480 K and magnesite, $MgCO_3$, between 13 and 380 K and their standard entropies at 298·15 K. *J. Res. U.S. Geol. Surv.* **5,** 797–806.

——Kittrick, J. A. 1978. Revised values for the Gibbs free energy of formation of $[Al(OH)^-_{4aq}]$, diaspore, boehmite, and bayerite at 298·15 K and 1 bar, the thermodynamic properties of kaolinite to 800 K and 1 bar, and the heats of solution of several gibbsite samples. *Geochim. Cosmochim. Acta* **42,** 1533–43.

Hemley, J. J., Montoya, J. W., Christ, C. L., & Hostetler, P. B., 1977*a*. Mineral equilibria in the $MgO–SiO_2–H_2O$ system: I. Talc-chrysotile-forsterite-brucite stability relations. *Am. J. Sci.* **277,** 322–51.

——Marinenko, J. W., & Luce, R. W., 1980. Equilibria in the system $Al_2O_3–SiO_2–H_2O$ and some general implications for alteration/mineralization processes. *Econ. Geol.* **75,** 210–28.

——Shaw, D. R., & Luce, R. W., 1977*b*. Mineral equilibria in the $MgO–SiO_2–H_2O$ system: II. Talc-antigorite-forsterite-anthophyllite-enstatite stability relations and some geologic implications in the system. *Am. J. Sci.* **277,** 353–83.

Hensen, B. J., 1972. Phase relations involving pyrope, enstatite(ss) and sapphirine(ss) in the system $MgO–Al_2O_3–SiO_2$. *Yb. Carn. Inst., Wash.* **71,** 421–7.

Henderson, C. E., Essene, E. J., Anovitz, L. M., Westrum, E. F., Jr., Hemingway, B. S., & Bowman, J. R., 1983. Thermodynamics and phase equilibria of clinochlore, $(Mg_5Al)(Si_3Al)O_{10}(OH)_8$. *Trans. Am. Geophys. Union* **64,** 466.

Herzberg, C. T., 1983. The reaction forsterite + cordierite = aluminous orthopyroxene + spinel in the system $MgO–Al_2O_3–SiO_2$. *Contr. Miner. Petrol.* **84,** 84–90.

Hewitt, D. A., 1973. Stability of the assemblage muscovite-calcite-quartz. *Am. Miner.* **58,** 785–91.

——1975. Stability of the assemblage phlogopite-calcite-quartz. *Ibid.* **60,** 391–97.

——1978. A redetermination of the fayalite-magnetite-quartz equilibrium between 650° and 850 °C. *Am. J. Sci.* **278,** 715–24.

Hochella, M. F. Jr., Brown, G. E. Jr., Ross, F. K., & Gibbs, G. V., 1979. High-temperature crystal chemistry of hydrous Mg- and Fe-cordierites. *Am. Miner.* **64,** 337–51.

Holdaway, M. J., 1971. Stability of andalusite and the aluminum silicate phase diagram. *Am. J. Sci.* **271,** 97–131.

——1972. Thermal stability of Al–Fe epidote as a function of f_{O_2} and Fe content. *Contr. Miner. Petrol.* **37,** 307–40.

Holland, T. J. B., 1979. Experimental determination of the reaction paragonite = jadeite + kyanite + H_2O, and internally consistent thermodynamic data for the part of the system $Na_2O–Al_2O_3–SiO_2–H_2O$, with applications to eclogites and blueschists. *Ibid.* **68,** 293–301.

——1980. The reaction albite = jadeite + quartz determined experimentally in the range 600–1200 °C. *Am. Miner.* **65,** 129–34.

——Powell, R., 1985. An internally consistent thermodynamic dataset with uncertainties and correlations: 2. Data and results. *J. Metamorphic Geol.* **3,** 343–70.

Holm, J. L., & Kleppa, O. J., 1966. The thermodynamic properties of the aluminum silicates. *Am. Miner.* **51,** 1608–22.

——1968. Thermodynamics of the disordering process in albite. *Am. Miner.* **53,** 123–33.

——Westrum, E. F. Jr., 1967. Thermodynamics of polymorphic transformations in silica. Thermal properties from 5 to 1070 K and pressure-temperature stability fields for coesite and stishovite. *Geochim. Cosmochim. Acta,* **31,** 2289–307.

Hoschek, G., 1973. Die Reaktion Phlogopit + Calcit + Quarz = Tremolit + Kalifeldspat + H_2O + CO_2. *Contr. Miner. Petrol.* **39,** 231–7.

——1974. Gehlenite stability in the system $CaO–Al_2O_3–SiO_2–H_2O–CO_2$. *Contr. Miner. Petrol.* **47,** 245–54.

Hosieni, K. R., Reed, A. H., & Scanlon, M. W., 1985. Thermodynamics of the lambda transition and the equation of state of quartz. *Am. Miner.* **70,** 782–93.

Hovis, G. L., 1974. A solution calorimetric and X-ray investigation of Al-Si distribution in monoclinic potassium feldspars. In: MacKenzie, W. S., & Zussman, J., (eds.) *The Feldspars, Proceedings of a NATO Advanced Study Institute.* University of Manchester Press, 114–44.

Huang, W.-L., & Wyllie, P. J., 1975. Melting and subsolidus phase relationships for $CaSiO_3$ to 35 kilobars pressure. *Am. Miner.* **60,** 213–7.

Huckenholz, H. G., Holzl, E., & Lindhuber, W., 1975. Grossularite, its solidus and liquidus relations in the $CaO–Al_2O_3–SiO_2–H_2O$ system up to 10 kbar. *N. Jb. Miner. Abh.* **124,** 1–46.

Irving, A. J., Huang, W.-L., & Wyllie, J., 1977. Phase relations of portlandite, $Ca(OH)_2$ and brucite, $Mg(OH)_2$ to 33 kilobars. *Am. J. Sci.* **277,** 313–21.

Irving, A. J., Wyllie, P. J., 1975. Subsolidus and melting relationships for calcite, magnesite, and the join $CaCO_3–MgCO_3$ to 36 kb. *Geochim. Cosmochim. Acta,* **39,** 35–53.

Isaak, D. G., & Graham, E. K., 1976. The elastic properties of a almandine-spessartine garnet and elasticity in the garnet solid solution series. *J. Geophys. Res.* **81,** 2483–9.

Jackson, I., & Niesler, H., 1982. The elasticity of periclase to 3 GPa and some geophysical implications. In Akimoto, S., & Manghnani, M. H., (eds.) *High-Pressure Research in Geophysics.* Tokyo, Japan., 93–103.

Jacobs, G. K., & Kerrick, D. M., 1981. Devolitilization equilibria in $H_2O–CO_2$ and $H_2O–CO_2–NaCl$ fluids: an

experimental and thermodynamic evaluation at elevated pressures and temperatures. *Am. Miner.* **66,** 1135–53.
Jacobs, G. K., Kerrick, D. M., & Krupka, K. M., 1981. The high temperature heat capacity of natural calcite ($CaCO_3$). *Phys. Chem. Miner.* **7,** 55–9.
Jenkins, D. M., 1981. Experimental phase relations of hydrous peridotites modelled in the system H_2O–CaO–MgO–Al_2O_3–SiO_2. *Contr. Miner. Petrol.* **77,** 166–76.
—— 1983. Stability and composition relations of calcic amphiboles in ultramafic rocks. *Ibid.* **83,** 375–84.
—— 1984. Upper-pressure stability of synthetic margarite plus quartz. *Ibid.* **88,** 332–9.
—— Chernosky, J. V. Jr., 1986. Phase equilibria and crystallochemical properties of Mg-chlorite. *Am. Miner.* **71,** 924–36.
Jenkins, D. M., Newton, R. C., & Goldsmith, J. R., 1985. Relative stability of Fe-free zoisite and clinozoisite. *J. Geol.* **93,** 663–72.
Johannes, W., 1968. Experimental investigation of the reaction forsterite + H_2O = serpentine + brucite. *Contr. Miner. Petrol.* **19,** 309–15.
—— 1969. An experimental investigation of the system MgO–SiO_2–H_2O–CO_2. *Am. J. Sci.* **267,** 1083–104.
—— (1980). Melting and subsolidus reactions in the system K_2O–CaO–Al_2O_3–SiO_2–H_2O. *Contr. Miner. Petrol.* **74,** 29–34.
—— 1984. Beginning of melting in the granite system Qz–Or–Ab–An–H_2O. *Ibid.* **86,** 264–73.
—— Bell, M., Mao, H. K., Boettcher, A. L., Chipman, D. W., Hays, J. F., Newton, R. C., & Seifert, F., 1971. An interlaboratory comparison of piston-cylinder pressure calibration using the albite-breakdown reaction. *Ibid.* **32,** 24–38.
Käse, H.-R., & Metz, P., 1980. Experimental investigation of the metamorphism of silicious dolomites. *Ibid.* **73,** 151–9.
Kalinin, D. V., & Zubkov, M. Y., 1981. Kinetic investigation of the MgO–SiO_2–H_2O system, reaction: serpentine = forsterite + talc + water. *Sov. Geol. Geophys.* **22**(9), 61–68.
Kammer, E. W., Pardue, T. E., & Frissel, H. F., 1948. A determination of the elastic constants for beta quartz. *J. Appl. Phys.* **19,** 265–70.
Karpinskaya, T. B., & Ostrovsky, N. A., 1982. Compressibility of brucite and the reaction of its formation from oxides as related to the possible existence of hydrothermal fluids in the mantle. *Int. Geol. Rev.* **24,** 1071–3.
Kelley, K. K., 1943. Specific heats at low temperatures of magnesium orthosilicate and magnesium metasilicate. *J. Am. Chem. Soc.* **65,** 339–41.
—— 1960. Contributions to the data on theoretical metalurgy. XIII. High temperature heat-content, heat-capacity, and entropy data for the elements and inorganic compounds. *U.S. Bur. Mines Bull.* **584,** 232p.
—— King, E. G., 1961. Contributions to the data on theoretical metallurgy, XIV. Entropies of the elements and inorganic compounds. *Ibid.* **592,** 149p.
—— Todd, S. S., Orr, R. L., King, E. G., & Bonnickson, K. R., 1953. Thermodynamic properties of sodium-aluminum and potassium–aluminum silicates. *U.S. Bur. Mines Rep. Invest.* **4955,** 21p.
Kennedy, G. C., Wasserburg, G. J., Heard, H. C., & Newton, R. C., 1962. The upper three phase region in the system SiO_2–H_2O. *Am. J. Sci.* **260,** 501–21.
Kerrick, D. M., 1968. Experiments on the upper stability limit of pyrophyllite at 1.8 kilobars and 3·9 kilobars water pressure. *Ibid.* **266,** 204–14.
—— 1972. Experimental determination of muscovite + quartz stability with $P_{H_2O} < P_{total}$. *Ibid.* **272,** 946–58.
—— Ghent, E. D., 1979. P-T-X_{CO_2} relations of equilibria in the system: CaO–Al_2O_3–SiO_2–CO_2–H_2O. In: Zharikov, V. A., Fonarev, V. I., Korikovshii, V. A., (eds.) *Problems in Physico-Chemical Petrology, Academy of Sciences of the USSR* **2,** 32–52.
—— Henninger, S. G., 1984. The andalusite–sillimanite equilibrium revisited. *Geol. Soc. Am. Abstr. Prog.* **16,** 558.
—— Jacobs, C. K., 1981. A modified Redlich–Kwong equation for H_2O, CO_2, and H_2O–CO_2 mixtures at elevated pressures and temperatures. *Am. J. Sci.* **281,** 735–67.
King, E. G., 1955. Heat capacities at low temperatures and entropies at 298·16 K of crystalline calcium and magnesium aluminates. *J. Phys. Chem.* **59,** 218–19.
—— 1957. Low-temperature heat capacities and entropies at 298·15 K of some crystalline silicates containing calcium. *J. Am. Chem. Soc.* **79,** 5437–8.
—— Barany, R., Weller, W. W., & Pankratz, L. B., 1967. Thermodynamic properties of forsterite and serpentine. *U.S. Bur Mines Rep. Invest.* **6962,** 19p. 4320–21.
—— Ferrante, M. J., & Pankratz, L. B., 1975. Thermodynamic data for $Mg(OH)_2$ (brucite). *Ibid.* **8041,** 13p.
—— Orr, R. L., & Bonnickson, K. R., 1954. Low temperature heat capacity, entropy at 298·16 K, and high temperature drop calorimetry of sphene ($CaTiSiO_5$). *J. Am. Chem. Soc.* **76,** 4320–21.
—— Weller, W. W., 1961*a*. Low temperature heat capacities and entropies at 298·15 K of diaspore, kaolinite, dickite and halloysite. *U.S. Bur. Mines. Rep. Invest.* **5810,** 6p.
—— 1961*b*. Low temperature heat capacities and entropies at 298·15 K of some sodium- and calcium-aluminum silicates. *Ibid.* **5855,** 8p.
Kiseleva, I. A., Ogorodova, L. P., Topor, N. D., & Chigareva, O. G., 1979. A thermochemical study of the CaO–MgO–SiO_2 system. *Geochem. Int.* 122–34.
Kitihara, S., Takenouchi, S., & Kennedy, G. C., 1966. Phase relations in the system MgO–SiO_2–H_2O at high temperatures and pressures. *Am. J. Sci.* **264,** 223–33.

Kolesnik, Y. N., Nogteva, V. V., Arkhipenko, D. K., Orekhov, B. A., & Paukov, I. Y., 1979. Thermodynamics of pyrope-grossular solid solutions and the specific heat of grossular at 13–300 K. *Geochem. Int.* **16,** 57–64.

Koziol, A., & Newton, R. C., 1986. Definition of anorthite = grossular + kyanite + quartz in the range 650–1250 °C. *Geol. Soc. Am. Abstr. Prog.* **99,** 661.

Kracek, F. C., 1953. Thermochemical properties of minerals. *Yb. Carn. Inst., Wash.* **52,** 69–74.

Krupka, K. M., Robie, R. A., & Hemingway, B. S., 1979. High-temperature heat capacities of corundum, periclase, anorthite, $CaAl_2Si_2O_8$ glass, muscovite, pyrophyllite, $KAlSi_3O_8$ glass, grossular, and $NaAlSi_3O_8$ glass. *Am. Miner.* **64,** 86–101.

——————— Kerrick, D. M., & Ito, J., 1985*a*. Low-temperature heat capacities and derived thermodynamic properties of anthophyllite, diopside, enstatite, bronzite, and wollastonite. *Am. Miner.* **70,** 249–60.

——————————— 1985*b*. High-temperature heat capacities and derived thermodynamic properties of anthophyllite, diopside, dolomite, enstatite, bronzite, talc, tremolite, and wollastonite. *Ibid.* **70,** 261–71.

Kunze, G., 1961. Antigorit: Strukturtheoretische Grundlagen und ihre praktische Bedeutung für die weitere Serpentin-Forschung. *Fortschritte Miner.* **39,** 206–324.

Lager, G. A., & Meagher, E. P., 1978. High-temperature study of six olivines. *Am. Miner.* **63,** 365–77.

Lander, J. J., 1951. Experimental heat contents of SrO, BaO, CaO, $BaCO_3$ and $SrCO_3$ at high temperatures. Dissociation pressures of $BaCO_3$ and $SrCO_3$. *J. Am. Chem. Soc.* **73,** 5794–97.

Leitner, B. J., Weidner, D. J., & Liebermann, R. C., 1980. Elasticity of single crystal pyrope and implications for garnet solid solution series. *Phys. Earth Planet. Int.* **22,** 111–21.

Levien, L., & Prewitt, C. T., 1981. High-pressure crystal structure and compressibility of coesite. *Am. Miner.* **66,** 324–33.

——— Weidner, D. J., 1979*a*. Compression of pyrope. *Ibid.* **64,** 805–8.

——————— 1980. Structure and elastic properties of alpha quartz at pressure. *Ibid.* **65,** 920–30.

——— Weidner, D. J., & Prewitt, C. T., 1979*b*. Elasticity of diopside. *Phys. Chem. Miner.* **4,** 105–13.

Lewis, G. K. Jr., & Drickamer, H. G., 1966. Effect of high pressure on the lattice parameters of Cr_2O_3 and αFe_2O_3. *J. Chem. Phys.* **45,** 224–6.

Lin, C.-Y., & Bailey, S. W., 1984. The crystal structure of paragonite-2M. *Am. Miner.* **69,** 122–7.

Liotta, J. J., & Bohlen, S. R., 1984. A new garnet thermobarometer. *Trans. Am. Geophys. Union.* **65,** p. 291.

Liou, J. G., 1971. Synthesis and stability relations of prehnite, $Ca_2Al_2Si_3O_{10}(OH)_2$. *Am. Miner.* **56,** 507–31.

Markgraf, S. A., & Reeder, R. J., 1985. High-temperature structure refinements of calcite and magnesite. *Ibid.* **70,** 590–600.

Massone, H.-J., Mirwald, P. W., & Schreyer, W., 1981. Experimentelle Überprüfung der Reaktionskurve Chlorit + Quartz = Talk + Disthen im System $MgO–Al_2O_3–SiO_2–H_2O$. *Fortschritte Miner.* **59,** 122–3.

Matsui, T., & Manghnani, M. H., 1985. Thermal expansion of single-crystal forsterite to 1023 K by Fizeau interferometry. *Phys. Chem. Miner.* **12,** 201–10.

Matsushima, S., Kennedy, G. C., Akella, J., & Haygarth, J., 1967. A study of the equilibrium relations in the systems $Al_2O_3–SiO_2–H_2O$ and $Al_2O_3–H_2O$. *Am. J. Sci.* **265,** 28–44. **43,** 861–68.

McPhail, D. C., 1985. The stability of Mg-Chlorite. M.Sc. Thesis Univ. British Columbia, Vancouver, B. C., 45p.

Metz, G. W., Anovitz, L. M., Essene, E. J., Bohlen, S. R., Westrum, E. F. Jr., & Wall, V. J., 1983. The heat capacity and phase equilibria of almandine. *Trans. Am. Geophys. Union* **64,** 346.

Metz, P., 1967. Experimentelle Bildung von Forsterit und Calcit aus Tremolit und Dolomit. *Geochim. Cosmochim. Acta,* **31,** 1517–32.

——1970. Experimentelle Untersuchung der Metamorphose von kieselig dolomitischen Sedimenten: II. Die Bildungsbedingungen des Diopsids. *Contr. Miner. Petrol.* **28,** 221–50.

——1976. Experimental investigation of the metamorphism of siliceous dolomites III. Equilibrium data for the reaction: 1 tremolite + 11 dolomite = 8 forsterite + 13 calcite + $9CO_2$ + 11 H_2O for the total pressure of 3000 and 5000 bars. *Contr. Miner. Petrol.* **58,** 137–48.

——Puhan, D., 1970. Experimentelle Untersuchung der Metamorphose von kieselig dolomitischen Sedimenten. I. Die Gleichgewichtsdaten der Reaktion 3 Dolomit + 4 Quarz + 1 H_2O = 1 Talk + 3 Calcit + 3 CO_2 für die Gesamtgasdrucke von 1000, 3000 und 5000 Bar. *Ibid.* **26,** 302–14.

——1971. Korrektur zur Arbeit 'Experimentelle Untersuchung der Metamorphose von kieselig dolomitischen Sedimenten. I. Die Gleichgewichtsdaten der Reaktion 3 Dolomit + 4 Quarz + 1 H_2O = 1 Talk + Calcit + 3 CO_2 für die Gesamtgasdrucke von 1000, 3000 und 5000 Bar'. *Ibid.* **31,** 169–70.

Mirwald, P. W., 1979. Determination of a high-temperature transition of calcite at 800 °C and one bar CO_2 pressure. *N. Jb. Miner. Monatshefte* **7,** 309–15.

——1981. Thermal expansion of anhydrous Mg-cordierite between 25 and 950 °C. *Phys. Chem. Miner.* **7,** 268–70.

——1982. A high-pressure phase transition in cordierite. *Am. Miner.* **67,** 277–83.

——Malinowski, M., & Schulz, H. 1984. Isothermal compression of low-cordierite to 30 kbar (25 °C). *Phys. Chem. Miner.* **11,** 140–8.

——Maresch, W. V., & Schreyer, W., 1979. Der Wassergehalt von Mg-Cordierit zwischen 500° und 800 °C sowie 0·5 und 11 kbar. *Fortschritte Miner.* **57,** 101–2.

——Massone H.-J., 1980. The low-high quartz and quartz-coesite transition to 40 kbar between 600° and 1600 °C and some reconnaissance data on the effect of $NaAlO_2$ component on the low quartz-coesite transition. *J. Geophys, Res.* **85,** 6983–90.

——Schreyer, W., 1977. Die stabile und metastabile Abbaureaktion von Mg-Cordierit in Talk, Disthen und Quarz und ihre Abhängigkeit vom Gleichgewichtswassergehalt des Cordierits. *Fortschritte Miner.* **55,** 95–97.

Moecher, D. P., Essene, E. J., & Westrum, E. F., 1985. S_{298} of an intermediate scapolite and phase equilibrium constraints on Al–Si disorder. *Trans. Am. Geophys. Union* **66,** 390.

Moore, P. B., & Araki, T., 1972. Atomic arrangement of merwinite, $Ca_3Mg[SiO_4]_2$, an unusual dense-packed structure of geophysical interest. *Am. Miner.* **57,** 1355–74.

Mosesman, M. A., & Pitzer, K. S., 1941. Thermodynamic properties of the crystalline forms of silica. *J. Am. Chem. Soc.* **63,** 2348–56.

Myers, J., & Eugster, H. P., 1983. The system Fe–Si–O: Oxygen buffer calibrations to 1,500 K. *Contr. Miner. Petrol.* **82,** 75–90.

Navrotsky, A., 1986. Cation-distribution energetics and heats of mixing in $MgFe_2O_4$–$MgAl_2O_4$, $ZnFe_2O_4$–$ZnAl_2O_4$, and $NiAl_2O_4$–$ZnAl_2O_4$ spinels: Study by high temperature calorimetry. *Am. Miner.* **71,** 1160–9.

——Loucks, D., 1977. Calculation of subsolidus phase relations in carbonates and pyroxenes. *Phys. Chem. Miner.* **1,** 109–27.

Naylor, B. F., 1946. High-temperature heat contents of TiO, Ti_2O_3, Ti_3O_5, and TiO_2. *J. Am. Chem. Soc.* **68,** 1077–80.

——Cook, O. A., 1946. High temperature heat contents of the metatitanites of calcium, iron, and magnesium. *Ibid.* **68,** 1003–1005.

Neuvonen, K. J., 1952*a*. Thermochemical investigation of the akermanite–gehlenite series. *Fin. geol. Komm. Bull.* **158,** 1–50.

——1952*b*. Heat of formation of merwinite and monticellite. *Am. J. Sci. Bowen* Vol 2, 373–80.

Newton, R. C., 1965. The thermal stability of zoisite. *J. Geol.* **73,** 431–41.

——1966*a*. Kyanite–sillimanite equilibrium at 750 °C. *Sci.* **151,** 1222–25.

——1966*b*. Kyanite–andalusite equilibrium from 700° to 800 °C. *Ibid.* **153,** 170–72.

Newton, R. C., 1966*c*. Some calc-silicate equilibrium relations. *Am. J. Sci.* **264,** 204–22.

——1972. An experimental determination of the high pressure stability limits of magnesian cordierite under wet and dry conditions. *J. Geol.* **80,** 398–420.

——Charlu, T. V., & Kleppa, O. J., 1980. Thermochemistry of the high structural state plagioclases. *Geochim. Cosmochim. Acta,* **44,** 933–41.

——Kennedy, G. C., 1963. Some equilibrium reactions on the join $CaAl_2Si_2O_8$–H_2O. *J. Geophys. Res.* **68,** 2967–83.

——Sharp, W. E., 1975. Stability of forsterite + CO_2 and its bearing on the role of CO_2 in the mantle. *Earth Planet. Sci. Lett.* **26,** 239–44.

——Thompson, A. B., & Krupka, K. M., 1979. Heat capacity of synthetic $Mg_3Al_2Si_3O_{12}$ from 350 to 1000 K and the entropy of pyrope. *Trans. Am. Geophys. Union* **58,** 523.

——Wood, B. J., 1979. Thermodynamics of water in cordierite and some petrologic consequences of cordierite as a hydrous phase. *Contr. Miner. Petrol.* **68,** 391–405.

Nitkiewicz, A., Kerrick, D. M., & Hemingway, B. S., 1984. The effect of particle size on the enthalpy of solution of tremolite: implications for phase equilibria and solution calorimetry. *Geol. Soc. Am. Abstr. Prog.* **16,** 610–11.

Nitsch, K.-H., 1968. Die Stabilität von Lawsonit. *Naturwissenschaften,* **55,** 388.

——1972. Das P–T–X_{CO_2}-Stabilitätsfeld von Lawsonit. *Contr. Miner. Petrol.* **34,** 116–34.

——Storre, B., & Toepfer, U., 1981. Experimentelle Bestimmung der Gleichgewichtsdaten der Reaktion 1 Margarit + 1 Quartz = 1 Anorthit + 1 Andalusit/Disthen + 1 H_2O. *Fortschritte der Miner.* **59,** 139–40.

Okamura, F. P., Ghose, S., & Ohashi, H., 1974. Structure and crystal chemistry of calcium Tschermak's pyroxene, $CaAl_2SiO_6$. *Am. Miner.* **59,** 549–57.

Olinger, B., 1977. Compression studies of forsterite (Mg_2SiO_4) and enstatite ($MgSiO_3$). *High Pressure Research Applications in Geophysics.* 325–34.

O'Neill, H. St. C., 1987. Quartz–fayalite–iron and quartz–fayalite–magnetite equilibria and the free energy of formation of fayalite (Fe_2SiO_4) and magnetite (Fe_3O_4). *Am. Miner.* **72,** 67–75.

Openshaw, R. E., Hemingway, B. S., Robie, R. A., Waldbaum, D. R., & Krupka, K. M., 1976. The heat capacities at low temperature and entropies at 298·15 K of low albite, analbite, microcline, and sanidine. *J. Res. U.S. Geol. Surv.* **4,** 195–204.

Orr, R. L., 1953. High temperature heat contents of magnesium orthosilicate and ferrous orthosilicate. *J. Am. Chem. Soc.* **75,** 528–9.

Osborn, E. F., & Schairer, J. F., 1941. The ternary system pseudowollastonite-akermanite-gehlenite. *Am. J. Sci.* **239,** 713–63.

Ostrovsky, I. A., 1966. PT-diagram of the system SiO_2–H_2O. *Geol. J.* **5,** 127–34.

Oterdoom, W. H., & Gunter, W. D., 1983. Activity models for plagioclase and CO_3-scapolites—an analysis of field and laboratory data. *Am. J. Sci.* **283A,** 255–82.

——Wenk, H.-R., 1983. Ordering and composition of scapolite: Field observations and structural interpretations. *Contr. Miner. Petrol.* **83,** 330–41.

Pankratz, L. B., & Kelley, K. K., 1963. Thermodynamic data for magnesium oxide (periclase). *U.S. Bur. Mines Rep. Invest.* **6295,** 5p.

——— 1964*a*. High-temperature heat contents and entropies of andalusite, kyanite, and sillimanite. *Ibid.* **6370,** 7p.

——— 1964*b*. High-temperature heat contents and entropies of akermanite, cordierite, gehlenite, and merwinite. *Ibid.* **6555,** 7p.

Perkins, III D., 1983. The stability of Mg-rich garnet in the system $CaO–MgO–Al_2O_3–SiO_2$ at 1000–1300 °C and high pressure. *Am. Miner.* **68,** 355–64.

Perkins, III D., Essene, E. J., Westrum, E. F. Jr., & Wall, V. J., 1977. Application of new thermodynamic data to grossular phase relations. *Contr. Miner. Petrol.* **64,** 137–47.

——— ——— ——— 1979. New thermodynamic data for diaspore and their application to the system $Al_2O_3–SiO_2–H_2O$. *Am. Miner.* **64,** 1080–90.

—— Holland, T. J. B., & Newton, R. C., 1981. The Al_2O_3 contents of enstatite in equilibrium with garnet in the system $MgO–Al_2O_3–SiO_2$ at 15–40 kbar and 900°–1600 °C. *Contr. Miner. Petrol.* **78,** 99–109.

—— Westrum, E. F., Jr., & Essene, E. J., 1980. The thermodynamic properties and phase relations of some minerals in the system $CaO–Al_2O_3–SiO_2–H_2O$. *Geochim. Cosmochim. Acta.* **44,** 61–84.

Perkins, E. H., Brown, T. H., & Berman, R. G., 1986. *PT*-SYSTEM, *TX*-SYSTEM, *PX*-SYSTEM: three programs which calculate pressure-temperature-composition phase diagrams. *Comp. Geosci.* **12,** 749–55.

Powell, R., & Holland, T. J. B., 1985. An internally consistent thermodynamic dataset with uncertainties and correlations: 1. Methods and a worked example. *J. Metamorphic Geol.* **3,** 327–42.

Prewitt, C. T., Sueno, S., & Papike, J. J. 1976. The crystal structures of high albite and monalbite at high temperatures. *Am. Miner.* **61,** 1213–25.

Prunier, A. R., & Hewitt, D. A., 1985. Experimental observations on coexisting zoisite-clinozoisite. *Ibid.* **70,** 375–8.

Puhan, D., 1978. Experimental study of the reaction: dolomite + K-feldspar + H_2O = phlogopite + calcite + CO_2 at the total gas pressures of 4000 and 6000 bars. *N Jb. Miner. Monatshefte* **1978,** 110–27.

—— Johannes, W., 1974. Experimentelle Untersuchung der Reaktion Dolomit + Kalifeldpat + H_2O = Phlogopit + Calcit + CO_2. Ein Method-envergleich. *Contr. Miner. Petrol.* **48,** 23–31.

Ragnarsdottir, K. V., & Walther, J. V., 1983. Pressure sensitive silica geothermometer determined from quartz solubility experiments at 250 °C. *Geochim. Cosmochim. Acta* **47,** 941–6.

Ralph, R. L., Finger, L. W., Hazen, R. M., & Ghose, S., 1984. Compressibility and crystal structure of andalusite at high pressure. *Am. Miner.* **69,** 513–9.

Ralph, R. L., Hazen, R. M., & Finger, L. W., 1981. Cell parameters of orthoenstatite at high temperature and pressure. *Yb Carn. Inst., Wash.* **1980,** 376–79.

Raz, U., 1983. Thermal and volumetric measurements on quartz and other substances at pressures up to 6 kbars and temperatures up to 700 °C. Ph.D. Thesis, ETH, 7386, 127.

Reeder, R. J., & Markgraf, S. A., 1986. High-temperature crystal chemistry of dolomite. *Am. Miner.* **71,** 775–804.

—— Wenk, H.-R., 1983. Structure refinements of some thermally disordered dolomites. *Ibid.* **68,** 769–76.

Richardson, S. W., Gilbert, M. C., & Bell, M., 1968. Kyanite–sillimanite equilibrium between 700 and 1500 °C. *Am. J. Sci.* **266,** 513–41.

——— ——— ——— 1969. Experimental determination of kyanite-andalusite and andalusite-sillimanite equilibria: the aluminum silicate triple point. *Ibid.* **267,** 259–72.

Richet, P., Bottinga, Y., Denielou, L., Petitet, J. P., & Tequi, C., 1982. Thermodynamic properties of quartz, cristobalite and amorphous SiO_2: drop calorimetry measurements between 1000 and 1800 K and a review from 0 to 2000 K. *Geochim. Cosmochim. Acta*, **46,** 2639–58.

Robie, R., 1965. Heat and free energy of formation of herzenbergite, troilite, magnesite, and rhodochrosite calculated from equilibrium data. U. S. Geol. Surv. Prof. Paper 525D, D65-D72.

—— Bethke, P. M., & Beardsley, K. M., 1967. Selected X-ray crystallographic data, molar volumes, and densities of minerals and related substances. *U. S. Geol. Surv. Bull.* **1248,** 87p.

—— Finch, C. B., & Hemingway, B. S., 1982*a*. Heat capacity and entropy of fayalite (Fe_2SiO_4) between 5·1 and 383 K: comparison of calorimetric and equilibrium values for the QFM buffer reaction. *Am. Miner.* **67,** 463–469.

—— Hemingway, B. S., 1984*a*. Entropies of kyanite, andalusite, and sillimanite: additional constraints on the pressure and temperature and Al_2SiO_5 triple point. *Ibid.* **69,** 298–306.

——— ——— 1984*b*. Heat capacities and entropies of phlogopite ($KMg_3[AlSi_3O_{10}](OH)_2$) and paragonite ($NaAl_2[AlSi_3O_{10}](OH)_2$) between 5 and 900 K and estimates of the enthalpies and Gibbs free energies of formation. *Ibid.* **69,** 858–68.

——— ——— Fisher, J. R., 1979. Thermodynamic Properties of Minerals and Related Substances at 298·15 K and 1 bar (10^5 Pascals) Pressure and at Higher Temperatures. *U. S. Geol. Surv. Bull.* **1452,** 456p.

——— ——— Takei, H., 1982*b*. Heat capacities and entropies of Mg_2SiO_4, Mn_2SiO_4 and Co_2SiO_4 between 5 and 380 K. *Am. Miner.* **67,** 470–82.

——— ——— Wilson, W. H., 1976. The heat capacities of calorimetry conference copper and of muscovite $KAl_2(AlSi_3)O_{10}(OH)_2$, pyrophyllite $Al_2Si_4O_{10}(OH)_2$, and illite $K_3(Al_7Mg)(Si_{14}Al_2)O_{40}(OH)_8$ between 15 and 375 K and their standard entropies at 298·15 K. *J. Res. U. S. Geol. Surv.* **4,** 631–44.

——— ——— ——— 1978. Low-temperature heat capacities and entropies of feldspar glasses and of anorthite. *Am. Miner.* **63,** 109–23.

——Stout, J. W., 1963. Heat capacity from 12 to 305 K and entropy of talc and tremolite. *J. Phys. Chem.* **67,** 2252–6.

Robinson, G. R. Jr., Haas, J. L. Jr., Schafer, C. M., & Haselton, H. T., Jr., 1982. Thermodynamic and thermophysical properties of selected phases in the MgO–SiO_2–H_2O–CO_2, CaO–Al_2O_3–SiO_2–H_2O–CO_2, and Fe–FeO–Fe_2O_3–SiO_2 chemical systems, with special emphasis on the properties of basalt. *U.S. Geol. Surv. Open-file Rep.* 83–79, 429p.

Salje, E., 1985. Thermodynamics of sodium feldspar I: order parameter treatment and strain induced coupling effects. *Phys. Chem. Miner.* **12,** 93–8.

——1986. Heat capacities and entropies of andalusite and sillimanite: the influence of fibrolitization on the phase diagram of the Al_2SiO_5 polymorphs. *Am. Miner.* **71,** 1366–71.

——Kuscholke, B., Wruck, B., & Kroll, H., 1985. Thermodynamics of sodium feldspar II: experimental results and numerical calculations. *Phys. Chem. Miner.* **12,** 99–107.

Sato, Y., Akaogi, M., & Akimoto, S., 1978. Hydrostatic compression of the synthetic garnets pyrope and almandine. *J. Geophys. Res.* **83,** 335–8.

Scarfe, C. M., & Wyllie, P. J., 1967. Experimental redetermination of the upper stability limit of serpentine up to 3-kb pressure. *Trans. Am. Geophys. Union* **48,** 255.

Schauer, A., 1965. Thermal expansion, grueneisen parameter, and temperature dependence of lattice vibration frequencies of aluminum oxide. *Can. J. Phys.* **43,** 523–31.

Schlenker, J. L., Gibbs, G. V., Hill, E. G., Crews, S. S., & Myers, R. H., 1977. Thermal expansion coefficients for indialite, emerald, and beryl. *Phys. Chem. Miner.* **1,** 243–55.

Schramke, J. A., Kerrick, D. M., & Blencoe, J. G., 1982. The experimental determination of the brucite = periclase + water equilibrium with a new volumetric technique. *Am. Miner.* **67,** 269–76.

Seifert, F., 1970. Low temperature compatibility relations of cordierite in haplopelites of the system K_2O–MgO–Al_2O_3–SiO_2–H_2O. *J. Petrology* **11,** 73–99.

——1973. Stability of the assemblage cordierite-corundum in the system MgO–Al_2O_3–SiO_2–H_2O. *Contr. Miner. Petrol.* **41,** 171–8.

——1974. Stability of sapphirine: a study of the aluminous part of the system MgO–Al_2O_3–SiO_2–H_2O. *J. Geol.* **82,** 173–204.

——1976. Stability of the assemblage cordierite + K feldspar + quartz. *Contr. Miner. Petrol.* **57,** 179–85.

——Schreyer, W., 1970. Lower temperature stability limit of Mg cordierite in the range 1–7 kb water pressure: a redetermination. *Ibid.* **27,** 225–38.

Seki, Y., 1959. Relation between chemical composition and lattice constraints of epidote. *Am. Miner.* **44,** 720–30.

Sharp, A. D., Essene, L. M., Metz, G. W., Westrum, E. F. Jr., Hemingway, B. S., & Valley, J. W., 1986. The heat capacity of a natural monticellite and phase equilibria in the system CaO–MgO–SiO–CO_2. *Geochim. Cosmochim. Acta,* **50,** 1475–84.

——Hazen, R. M., & Finger, L. W., 1987. High-pressure crystal chemistry of monticellite, CaMgSiO¡sub4¿. *Am. Miner.* **72,** 748–55.

Shearer, J. S., & Kleppa, O. J., 1973. The enthalpies of formation of $MgAl_2O_4$, $MgSiO_3$, Mg_2SiO_4 and Al_2SiO_5 by oxide melt solution calorimetry. *J. Inorg. Nucl. Chem.* **35,** 1073–8.

Shmulovich, K. I., 1974. Phase equilibria in the CaO–Al_2O_3–SiO_2–CO_2. *Geochem. Int.* **11,** 883–7.

——1978. Stability limits of grossular and wollastonite in the H_2O–CO_2 system up to 6 kbar. *Ibid.* **14,** 126–34.

Shomate, C. H., 1946. Heat capacities at low temperatures of the metatitanates of iron, calcium and magnesium. *J. Am. Chem. Soc.* **68,** 964–6.

——1947. Heat capacities at low temperatures of titanium dioxide (rutile and anatase). *J. Am. Chem. Soc.* **69,** 218–9.

Shvedenkov, G. Y., Shvedenkova, S. V., Dashevskii, Y. A., Kalinin, D. V., 1983. Phase equilibria in the system containing muscovite, paragonite, alkaline feldspars, H_2O, and CO_2. *Sov. Geol. Geophys.* **24,** 73–9.

Skinner, B. J., 1956. Physical properties of end-members of the garnet group. *Am. Miner.* **41,** 428–36.

——1966. Thermal expansion. In: S. P. Clark (ed.) *Handbook of Physical Constants, Geol. Soc. Amer. Memoirs* **97,** 75–96.

——Clark, S. P. Jr., & Appleman, D. E., 1961. Molar volumes and thermal expansions of andalusite, kyanite and sillimanite. *Am. J. Sci.* **259,** 651–68.

Skippen, G. B., 1971. Experimental data for reactions in siliceous marbles. *J. Geol.* **79,** 457–81.

——1974. An experimental model for low pressure metamorphism of siliceous dolomitic marble. *Am. J. Sci.* **274,** 487–509.

Slaughter, J., Kerrick, D. M., & Wall, V. J., 1975. Experimental and thermodynamic study of equilibria in the system CaO–MgO–SiO_2–H_2O–CO_2. *Ibid.* **275,** 143–62.

Smith, D., 1971. Stability of the assemblage iron-rich orthopyroxene–olivine–quartz. *Am. J. Sci.* **271,** 370–82.

Smyth, F. H., & Adams, L. H., 1923. The system calcium oxide–carbon dioxide. *J. Am. Chem. Soc.* **45,** 1167–84.

Southard, J. C., 1941. A modified calorimeter for high temperatures. The heat content of silica, wollastonite and thorium dioxide above 25°C. *Ibid.* **63,** 3142–6.

Staudigel, H., & Schreyer, W., 1977. The upper thermal stability of clinochlore, $Mg_5Al[AlSi_3O_{10}](OH)_8$, at 10–35 kb PH_2O. *Contr. Miner. Petrol.* **61,** 187–98.

Staveley, L. A. K., & Linford, R. G., 1969. The heat capacity and entropy of calcite and aragonite, and their interpretation. *J. Chem. Therm.* **1,** 1–11.

Stephenson, D. A., Sclar, C. B., & Smith, J. V., 1966. Unit cell volumes of synthetic orthoenstatite and low clinoenstatite. *Miner. Mag.* **35,** 838–46.

Storre, B., & Nitsch, K.-H., 1972. Die Reaktion 2 Zoisit + 1 CO_2 = 3 Anorthit + 1 Calcit + 1 H_2O. *Contr. Miner. Petrol.* **35,** 1–10.

——— 1974. Zur Stabilität von Margarit im System CaO–Al_2O_3–SiO_2–H_2O. *Ibid.* **43,** 1–24.

Stout, J. W., Robie, R. A., 1963. Heat capacity from 11 to 300 K, entropy and heat of formation of dolomite. *J. Phys. Chem.* **67,** 2248–52.

Strens, R. G. J., 1968. Reconnaissance of the prehnite stability field. *Miner. Mag.* **36,** 864–7.

Stull, D. R., & Prophet, H., 1971. JANAF thermochemical tables. Nat. Stand. Ref. Data Ser. 37, 1141 p.

Sueno, S., Cameron, M., Papike, J. J., & Prewitt, C. T., 1973. The high temperature crystal chemistry of tremolite. *Am. Miner.* **58,** 649–64.

——— Prewitt, C. T., 1976. Orthoferrosilite: High temperature crystal chemistry. *Ibid.* **61,** 38–53.

Sumino, Y., 1979. The elastic constants of Mn_2SiO_4, Fe_2SiO_4 and Co_2SiO_4, and the elastic properties of olivine group minerals at high temperature. *J. Phys. Earth* **27,** 209–38.

—— Anderson, O. L., 1984. Elastic constants of minerals. In: Carmichael, R. S., (ed.) *Handbook of Physical Properties of Rocks.* Boca Raton, Florida: CRC Press, 39–138.

Suzuki, I., & Anderson, L., 1983. Elasticity and thermal expansion of a natural garnet up to 1000 K. *J. Phys. Earth* **31,** 125–38.

—— Seya, H. T., & Sumino, Y., 1981. Thermal expansion of fayalite Fe_2SiO_4. *Phys. Chem. Miner.* **7,** 60–63.

Symmes, G. H., 1986. The thermal expansion of natural muscovite, paragonite, margarite, pyrophyllite, phologopite, and two chlorites: the significance of high T/P volume studies on calculated phase equilibria. B.A. Thesis, Amherst College, Amherst, Massachusetts.

Takeda, H., & Morosin, B., 1975. Comparison of observed and predicted structural parameters of mica at high temperature. *Acta Crystal.* **B31,** 2444–52.

Taylor, L. A., & Bell, P. M., 1970. Thermal expansion of pyrophyllite. *Yb. Carn. Inst. Wash.* **1969,** 193–4.

Thanh, D., Vo, and Lacam, A., 1984. Experimental study of the elasticity of single crystalline calcite under high pressure (the calcite I-calcite II transition at 14·6 kbar). *Phys. Earth Planet. Int.* **34,** 195–203.

Thierry, P., Chatillon-Colinet, C., Mathieu, J. C., Regnard, J. R., & Amosse, J., 1981. Thermodynamic properties of the forsterite-fayalite (Mg_2SiO_4–Fe_2SiO_4) solid solution. Determination of heat of formation. *Phys. Chem. Miner.* **7,** 43–6.

Thompson, A. B., 1970. A note on the kaolinite-pyrophyllite equilibrium. *Am. J. Sci.* **268,** 454–58.

—— Wennemer, M., 1979. Heat capacities and inversions in tridymite, cristobalite, and tridymite-cristobalite mixed phases. *Am. Miner.* **64,** 1018–26.

Thompson, J. B. Jr., Waldbaum, D. R., Hovis, G. L., 1974. Thermodynamic properties related to ordering in end-member alkali feldspars. In: MacKenzie, W. S., & Zussman, J., (eds.) *The Feldspars, Proceedings of a NATO Advanced Study Institute.* University of Manchester Press, 218–48.

Todd, S. S., 1950. Heat capacities at low temperatures and entropies at 298·16 K of andalusite, kyanite, and sillimanite. *J. Am. Chem. Soc.* **72,** 4742–3.

Tombs, N. C., & Rooksby, H. P., 1951. Structure and antiferromagnetism in magnetite. *Acta Crystal.* **4,** 474–5.

Torgeson, D. R., & Sahama, T. G., 1948. A hydrofluoric acid solution calorimeter and the determination of the heats of formation of Mg_2SiO_4, $MgSiO_3$, and $CaSiO_3$. *J. Am. Chem. Soc.* **70,** 2156–60.

Vaidya, S. N., Bailey, S., Pasternack, T., & Kennedy, G. C., 1973. Compressibility of fifteen minerals to 45 kilobars. *J. Geophys. Res.* **78,** 6893–8.

Vaughan, M. T., & Guggenheim, S., 1986. Elasticity of muscovite and its relationship to crystal structure. *Ibid.* **91,** 4657–64.

—— Weidner, D. J., 1978. The relationship of elasticity and crystal structure in andalusite and sillimanite. *Phys. Chem. Miner.* **3,** 133–44.

Velde, B., 1966. Upper stability of muscovite. *Am. Miner.* **51,** 924–9.

Victor, A. C., & Douglas, T. B., 1963. Thermodynamic properties of magnesium oxide and beryllium oxide from 298 to 1200 K. *J. Res. Nat. Bur. Standards* **67A,** 325–9.

Wagner, V. H., 1932. Zur Thermochemie der Metasilikate des Calciums und Magnesiums und des Diopsids. *Z. Anorg. Allgemeine Chemie* **208,** 1–22.

Waldbaum, D. R., 1968. High-temperature thermodynamic properties of alkali feldspars. *Contr. Miner. Petrol.* **17,** 71–7.

Walter, L. S., 1963*a*. Experimental studies on Bowen's decarbonation series: I: P–T univariant equilibria of the 'monticellite' and 'akermanite' reactions. *Am. J. Sci.* **261,** 488–500.

—— 1963*b*. Experimental studies on Bowen's decarbonation series: II: P-T univariant equilibria of the reaction: forsterite + calcite = monticellite + periclase + CO_2. *Am. J. Sci.* **261,** 773–9.

Wang, H. F., 1978. Elastic constant systematics. *Phys. Chem. Miner.* **3,** 251–61.

Watanabe, H., 1982. Thermochemical properties of synthetic high-pressure compounds relevant to the earth's mantle. In: Akimoto, S., & Manghnani, M. H., (eds.) *High-Pressure Research in Geophysics,* Tokyo, Japan, 441–64.

Watt, J. P., & Ahrens, T. J., 1986. Shock wave equation of enstatite. *J. Geophys. Res.* **91,** 7495–503.

Weaver, J. S., Chipman, D. W., & Takahashi, T., 1979. Comparison between thermochemical and phase stability data for the quartz–coesite–stishovite transformations. *Am. Miner.* **64,** 604–14.

Wechsler, B. A., & Prewitt, C. T., 1984. Crystal structure of ilmenite ($FeTiO_3$) at high temperature and at high pressure. *Am. Miner.* **69,** 176–85.
Weeks, W. F., 1955. Heats of formation of metamorphic minerals in the system CaO–MgO–SiO_2–H_2O and their petrological significance. *J. Geol.* **64,** 456–73.
Weir, C. E., 1956. Isothermal compressibilities of alkaline earth oxides at 21 °C. *J. Res. Natl. Bur. Standards* **56,** 187–9.
Weller, W. W., & Kelley, K. K., 1963. Low-temperature heat capacities and entropies at 298·15 K of akermanite, cordierite, gehlenite, and merwinite. *U.S. Bur. Mines Rep. Invest.* **6343,** 7 p.
Westrum, E. F., Jr., Essene, E. J., & Perkins, III D., 1979. Thermophysical properties of the garnet, grossular: $Ca_3Al_2Si_3O_{12}$. *J. Chem. Therm.* **11,** 57–66.
—— Gronvold, F., 1969. Magnetite (Fe_3O_4). Heat capacity and thermodynamic properties from 5 to 350 K, low-temperature transition. *Ibid.* **1,** 543–57.
White, W. P., 1919. Silicate specific heats. *Am. J. Sci.* **47,** 1–21.
Widmark, E. T., 1980. The reaction chlorite + dolomite = spinel + forsterite + calcite + carbon dioxide + water. *Contr. Miner. Petrol.* **72,** 175–9.
Wilburn, D. R., & Bassett, W. A., 1977. Isothermal compression of magnetite (Fe_3O_4) up to 70 kbar under hydrostatic conditions. *High Pressure–High Temp.* **9,** 3539–43.
—— —— Sato, Y., & Akimoto, S., 1978. X-ray diffraction compression studies of hematite under hydrostatic, isothermal conditions. *J. Geophys. Res.* **83,** 3509–12.
Windom, K. E., & Boettcher, A. L., 1976. The effect of reduced activity of anorthite on the reaction grossular + quartz = anorthite + wollastonite: a model for plagioclase in the earth's lower crust and upper mantle. *Am. Miner.* **61,** 889–96.
Winter, J. K., & Ghose, S., 1979. Thermal expansion and high temperature crystal chemistry of the Al_2SiO_5 polymorphs. *Ibid.* **64,** 573–86.
—— Okamura, F. P., & Ghose, S., 1979. A high-temperature structural study of high albite, monalbite, and the albite–monalbite phase transition. *Ibid.* **64,** 409–23.
Wones, D. R., & Dodge, F. C. W., 1977. The stability of phlogopite in the presence of quartz and diopside. In: Fraser, D. G., (ed.) *Thermodynamics in Geology.* Dordrecht: Reidel Publishing Company, 229–47.
Wood, B. J., 1976. The reaction phlogopite + quartz = enstatite + sanidine + H_2O. *Prog. Exp. Petrol. Nat. Env. Res. Council* **11,** 17–9.
—— 1978. Reactions involving anorthite and $CaAl_2SiO_6$ pyroxene at high pressures and temperatures. *Am. J. Sci.* **278,** 930–42.
—— Holloway, J. R., 1984. A thermodynamic model for subsolidus equilibria in the system CaO–MgO–Al_2O_3–SiO_2. *Geochim. Cosmochim. Acta* **48,** 159–76.
Wood, B. J., Kirkpatrick, R. J., & Montez, B., 1986. Order–disorder phenomena in $MgAl_2O_4$ spinel. *Am. Miner.* **71,** 999–1006.
Yagi, T., Yoshiaki, I., Sato, Y., & Akimoto, S., 1975. Effect of hydrostatic pressure on the lattice parameters of Fe_2SiO_4 olivine up to 70 kbar. *Phys. Earth Planet. Int.* **10,** 348–54.
Yin, H.-A., & Greenwood, H. J., 1983. Displacement of equilibria of OH-tremolite and F-tremolite solid solution. I. Determination of the equilibrium *P–T* curve of OH-tremolite. *Trans. Amer. Geophys. Union* **64,** 347.
Yoder, H. S. Jr., 1968. Akermanite and related melilite-bearing assemblages. *Yb. Carn. Inst. Wash.* **66,** 471–7.
Yoder, H. S., & Weir, C. E., 1951. Change of free energy with pressure of reaction nepheline + albite = 2 jadeite. *Am. J. Sci.* **249,** 683–94.
Zharikov, V. A., Shmulovich, K. I., & Bulatov, V. K., 1977. Experimental studies in the system CaO–MgO–Al_2O_3–SiO_2–CO_2–H_2O and conditions of high temperature metamorphism. *Tectonophysics,* **43,** 145–62.
Ziegenbein, D., & Johannes, W., 1974. Wollastonitbildung aus Quartz und Calcit bei Pf = 2, 4 und 6 kb. *Fortschritte der Miner.* **44,** 77–79.

APPENDIX

Summary of calorimetric and volumetric data at 1 bar, 298·15 K*

Phase	$\Delta_f H^{P_r,T_r}$	S^{P_r,T_r}	V^{P_r,T_r}
Akermanite	−3863·77 ± 3·16(1)	212·50 ± 1·00(4)	9·254 ± ·004(4)
	−3876·46 ± 2·86(2)	209·20 ± 2·09(5)	
	−3865·37 ± 2·93(3)		
Albite	−3935·10 ± 3·40(6)	207·40 ± 0·40(8)	10·043 ± ·009(7)
Albite (high)			10·083 ± ·009(7)
Albite (low)	−3935·10 ± 3·40(6)	207·40 ± 0·40(8)	10·043 ± ·009(7)
Almandine	−5269·20 ± 5·49(9)	339·70 ± 0·50(10)	11·511 ± ·002(11)

APPENDIX (*Continued*)

Phase	$\Delta_f H^{P_r,T_r}$	S^{P_r,T_r}	V^{P_r,T_r}
Andalusite	−2592·58 ± 1·79(12)	91·39 ± 0·14(14)	5·147 ± ·003(13)
		93·22 ± 0·42(15)	
Anorthite	−4228·02 ± 2·86(16)	199·30 ± 0·30(20)	10·079 ± ·004(7)
	−4224·17 ± 3·17(17)		
	−4227·48 ± 3·25(17)		
	−4223·44 ± 3·41(18)		
	−4254·91 ± 2·55(19)		
Anthophyllite	−12086·00 ± 7·53(21)	537·00 ± 2·70(22)	26·540 ± ·042(23)
Antigorite		3598·53 ± 26·78(24)	174·913 ± ·867(25)
Brucite	−924·54 ± 1·40(6)	63·18 ± 0·13(6)	2·463 ± ·007(7)
Ca–Al pyroxene	−3296·28 ± 2·48(17)	135·30 ± 1·00(26)	6·356 ± ·001(26)
Calcite	−1207·37 ± 1·40(6)	91·71 ± 0·20(28)	3·689 ± ·001(27)
Chrysotile	−4364·33 ± 3·39(24)	221·33 ± 1·67(24)	10·746 ± ·042(29)
Clinochlore		397·60 ± 2·00(30)	21·152 ± ·008(31)
			21·090 ± ·010(32)
Coesite	−905·58 ± 2·09(6)	40·38 ± 0·42(33)	2·064 ± ·002(34)
Cordierite	−9160·43 ± 6·01(35)	407·10 ± 3·70(5)	23·322 ± ·013(7)
	−9158·71 ± 5·81(35)		
Corundum	−1675·70 ± 1·30(36)	50·92 ± 0·10(36)	2·557 ± ·001(7)
Cristobalite (alpha)	−908·35 ± 2·09(6)	43·40 ± 0·13(6)	2·573 ± ·004(7)
Cristobalite (beta)			
Diaspore	−1000·59 ± 5·00(6)	35·31 ± 0·17(37)	1·776 ± ·003(7)
Diopside	−3197·29 ± 2·96(38)	142·70 ± 0·20(22)	6·619 ± ·002(22)
	−3201·16 ± 2·80(17)		
Dolomite	−2324·49 ± 1·67(6)	155·18 ± 0·42(39)	6·434 ± ·003(7)
Enstatite (clino)		67·78 ± 0·84(40)	3·132 ± ·001(41)
Enstatite (ortho)	−1546·63 ± 2·04(1)	66·27 ± 0·10(22)	3·134 ± ·002(23)
Enstatite (proto)			3·238 ± ·008(7)
Fayalite	−1479·99 ± 6·30(42)	151·00 ± 0·30(44)	4·630 ± ·004(9)
	−1479·36 ± 2·40(43)		
Ferrosilite		94·60 ± 1·00(11)	3·296 ± ·001(45)
Forsterite	2171·56 ± 2·22(1)	94·11 ± 0·10(48)	4·379 ± ·003(7)
	−2176·96 ± 1·46(46)		4·366 ± ·001(35)
	−2176·20 ± 1·32(47)		
	−2174·25 ± 1·62(35)		
	−2171·69 ± 1·71(24)		
	−2172·32 ± 1·81(38)		
	−2171·86 ± 1·81(38)		
Gehlenite	−3978·60 ± 2·76(3)	198·60 ± 0·60(50)	9·024 ± ·009(7)
	−3986·74 ± 3·24(49)	198·32 ± 1·67(5)	9·005 ± ·002(3)
	−3999·51 ± 2·84(2)		
Grossular	−6630·15 ± 5·08(17)	256·48 ± 1·30(51)	12·535 ± ·004(54)
		254·72 ± 1·50(52)	
		260·12 ± 1·50(53)	
Hematite	−824·60 ± 1·26(6)	87·40 ± 0·08(55)	3·027 ± ·001(7)
Ilmenite	−1236·62 ± 1·59(6)	108·90 ± 0·50(56)	3·169 ± ·008(7)
Jadeite	−3029·40 ± 3·40(6)	133·47 ± 1·25(57)	6·040 ± ·010(7)
Kaolinite	−4120·12 ± 3·98(43)	203·70 ± 1·30(58)	9·952 ± ·026(7)
Kyanite	−2594·58 ± 1·76(12)	82·30 ± 0·13(14)	4·414 ± ·004(59)
		83·76 ± 0·33(15)	
Lawsonite	−4879·07 ± 3·96(43)	230·04 ± 2·00(60)	10·132 ± ·012(7)
Lime	−635·09 ± 0·90(36)	38·10 ± 0·40(36)	1·676 ± ·001(7)
Magnesite	−1113·28 ± 1·34(61)	65·09 ± 0·13(62)	2·803 ± ·002(27)
Magnetite	−1115·70 ± 2·09(6)	146·14 ± 0·42(63)	4·452 ± ·001(64)
Margarite		263·63 ± 2·09(60)	12·960 ± ·004(65)
Meionite		701·11 ± 5·00(66)	34·036 ± ·002(67)
Merwinite	−4535·62 ± 3·95(1)	253·13 ± 2·09(5)	9·847 ± ·002(69)
	−4566·74 ± 3·73(68)		
Monticellite	−2250·25 ± 2·20(1)	108·10 ± 0·20(70)	5·148 ± ·001(70)
	−2262·60 ± 1·50(68)		
Muscovite	−5976·74 ± 4·51(43)	287·70 ± 0·60(71)	14·083 ± ·006(72)

APPENDIX (*Continued*)

Phase	$\Delta_f H^{P_r,T_r}$	S^{P_r,T_r}	V^{P_r,T_r}
Paragonite		277·10 ± 0·90(73)	13·211 ± ·009(74)
			13·247 ± ·092(75)
Periclase	−601·50 ± 0·30(36)	26·95 ± 0·15(36)	1·125 ± ·001(7)
Phlogopite	−6215·30 ± 6·30(77)	315·90 ± 1·00(73)	14·964 ± ·005(76)
			14·991 ± ·036(7)
Potassium feldspar	−3967·70 ± 3·30(6)	214·20 ± 0·40(8)	10·872 ± ·010(7)
Sanidine		232·90 ± 0·40(8)	10·898 ± ·002(8)
Microcline	−3967·70 ± 3·30(6)	214·20 ± 0·40(8)	10·872 ± ·010(7)
Prehnite		292·75 ± 2·09(60)	14·026 ± ·019(60)
Pyrope	−6291·51 ± 3·75(35)	266·27 ± 3·00(53)	11·318 ± ·002(78)
			11·312 ± ·002(35)
Pyrophyllite		239·40 ± 0·40(71)	12·761 ± ·010(71)
Quartz (alpha)	−910·70 ± 1·00(36)	41·46 ± 0·20(36)	2·269 ± ·001(7)
Quartz (beta)			
Rutile	−944·75 ± 1·26(6)	50·25 ± 0·21(79)	1·882 ± ·001(7)
Sillimanite	−2583·34 ± 1·97(47)	95·79 ± 0·14(14)	5·003 ± ·001(80)
	−2589·49 ± 1·76(12)	96·11 ± 0·42(15)	4·983 ± ·003(59)
		129·29 ± 0·84(81)	5·565 ± ·017(7)
Sphene	−2302·00 ± 2·70(47)	80·58 ± 0·42(82)	3·978 ± ·001(35)
Spinel	−5915·93 ± 4·35(43)	260·79 ± 0·42(39)	13·626 ± ·022(23)
Talc	−12355·00 ± 17·30(21)	549·07 ± 2·09(39)	27·270 ± ·009(76)
Tremolite	−907·49 ± 2·39(6)	44·02 ± 0·42(83)	2·665 ± ·020(7)
Tridymite (low)			
Tridymite (high)			
Wollastonite	−1633·55 ± 2·02(17)	81·69 ± 0·12(22)	3·993 ± ·010(7)
	−1632·68 ± 1·70(38)	82·01 ± 0·84(84)	
Pseudowollastonite	−1626·50 ± 1·87(17)	87·45 ± 0·84(84)	4·008 ± ·014(7)
Zoisite (ortho)		295·85 ± 2·09(60)	13·588 ± ·008(60)
Zoisite (clino)			13·659 ± ·004(85)
			13·685 ± ·010(86)
Carbon dioxide (gas)	−393·510 ± 0·40(36)	213·68 ± 0·40(36)	
Water (liquid)	−285·830 ± 0·30(36)	69·915 ± 0·04(36)	

* All enthalpies of formation measured above 298·15 K have been corrected to 298·15 K using the *Cp* functions given in Table 3.

References: (1) Brousse *et al.* (1984); (2) Neuvonen (1952*a*); (3) Charlu *et al.* (1981); (4) Hemingway *et al.* (1986); (5) Weller & Kelley (1963); (6) Robie *et al.* (1979); (7) Robie *et al.* (1967); (8) Openshaw *et al.* (1976); (9) Chatillon-Colinet *et al.* (1983); (10) Metz *et al.* (1983); (11) Bohlen *et al.* (1983*b*); (12) Holm & Kleppa (1966); (13) Holdaway (1971); (14) Robie & Hemingway (1984*a*); (15) Todd (1950); (16) Newton *et al.* (1980); (17) Charlu *et al.* (1978); (18) Barany (1962); (19) Kracek (1953); (20) Robie *et al.* (1978); (21) Weeks (1955); (22) Krupka *et al.* (1985*a*); (23) Chernosky *et al.* (1985); (24) King *et al.* (1967); (25) Kunze (1961); (26) Haselton *et al.* (1984); (27) Markgraf & Reeder (1985); (28) Staveley & Linford (1969); (29) Chernosky (1975); (30) Henderson *et al.* (1983); (31) Chernosky (1978); (32) Jenkins & Chernosky (1986); (33) Holm *et al.* (1967); (34) Weaver *et al.* (1979); (35) Charlu *et al.* (1975); (36) CODATA (1978); (37) Perkins III *et al.* (1979); (38) Kiseleva *et al.* (1979); (39) Stout & Robie (1963); (40) Kelley (1943); (41) Stephenson *et al.* (1966); (42) Thierry *et al.* (1981); (43) Hemingway & Robie (1977); (44) Robie *et al.* (1982*a*); (45) Sueno *et al.* (1976); (46) Torgeson & Sahama (1948); (47) Shearer & Kleppa (1973); (48) Robie *et al.* (1982*b*); (49) Barany (1963); (50) Hemingway & Robie (1984); (51) Kolesnik *et al.* (1979); (52) Westrum *et al.* (1979); (53) Haselton & Westrum (1980); (54) Krupka *et al.* (1979); (55) Gronvold & Westrum (1959); (56) Anovitz *et al.* (1985); (57) Kelley *et al.* (1953); (58) Hemingway *et al.* (1978); (59) Skinner *et al.* (1961); (60) Perkins III *et al.* (1980); (61) Robie (1965); (62) Hemingway *et al.* (1977); (63) Westrum & Gronvold (1969); (64) Tombs & Rooksby (1951); (65) Chatterjee (1974); (66) Moecher *et al.* (1985); (67) Oterdoom & Wenk (1983); (68) Neuvonen (1952*b*); (69) Moore & Araki (1972); (70) Sharp *et al.* (1986); (71) Robie *et al.* (1976); (72) Chatterjee & Johannes (1974); (73) Robie & Hemingway (1984*b*); (74) Lin & Bailey (1984); (75) Chatterjee (1970); (76) Hewitt (1975); (77) Clemens *et al.* (1987); (78) Hazen & Finger (1978*b*); (79) Shomate (1947); (80) Winter & Ghose (1979); (81) King *et al.* (1954); (82) King (1955); (83) Anderson (1936); (84) Kelley & King (1961); (85) Chatterjee *et al.* (1984); (86) Seki (1959).